


Dr Alex Burton-Johnson  
British Antarctic Survey  
Natural Environment Research Council  
High Cross, Madingley Road  
Cambridge  
CB3 0ET

E-mail: [alerto@bas.ac.uk](mailto:alerto@bas.ac.uk)

Dear Alexander Robinson,

Thank you for reviewing our revisions as Editor. We have addressed your point regarding terminology and include our comments and the manuscript with track changes below.

All the best,

A handwritten signature in black ink, appearing to read 'Alex Burton-Johnson', with a horizontal line drawn above it.

Dr Alex Burton-Johnson

**Editor Decision:** Publish subject to minor revisions (review by editor) (19 Aug 2020) by Alexander Robinson

**Comments to the Author:**

The reviewer comments have been thoroughly addressed, so I believe the manuscript is near-ready for publication. At the moment, I would only suggest the following minor further revision below.

Heat flow versus heat flux (response to Brice Van Liefferinge): It is now clear why you use the term heat flow throughout, which you have justified well. To increase the chances of broad adaption of the 'correct' term, I would suggest adding a footnote, or comment when the term is introduced that explicitly states why you use heat flow. This will hopefully help to encourage others to adapt it in the future.

- A paragraph has been added as a new section (1.2.) discussing the terminology and the justifying the use of "flow" rather than "flux", as in the reply to Reviewer Brice Van Liefferinge.

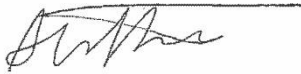
Dr Alex Burton-Johnson  
British Antarctic Survey  
Natural Environment Research Council  
High Cross, Madingley Road  
Cambridge  
CB3 0ET

E-mail: [alerto@bas.ac.uk](mailto:alerto@bas.ac.uk)

Dear Brice Van Liefferinge,

Thank you for taking the time to provide such a helpful and thorough review. You provided many pertinent comments, and their implementation has greatly improved our manuscript. We have addressed all of your points, and list them below alongside your review.

All the best,

A handwritten signature in black ink, appearing to read 'Alex Burton-Johnson', written over a horizontal line.

Dr Alex Burton-Johnson

Brice Van Liefferinge (Referee)

bvlieffe@gmail.com

Received and published: 13 April 2020

Dear Authors,

I enjoyed reading your paper on the comparison of the different GHF estimate methods. This paper provides a great overview of the work done on GHF reconstructions and provides key future directions. All known methods are described and are well supported by explicit examples and references in the manuscript. I really liked section 4 on GHF derived estimates. I think that all the key references are included. I added a few and strongly suggest to add and describe the work of Rezvanbehbahani et al. (2017) on machine learning techniques as done in Greenland. The introduction and conclusion support well the manuscript as do the figures (see specific comments).

The language used is appropriate. However, I would suggest the following general changes: a) In the title you use “flow” but I would suggest to use “flux”, as well as for the whole manuscript (see specific comments). b) The manuscript is qualitative in a few paragraphs. More quantitative descriptions could be provided such as maximum and minimum GHF of the different data sets, discuss the representativeness of point GHF values, . . . where possible. c) The limitations of the different methods to estimate GHF (ice borehole measurements, model estimates, . . .) are not always discussed. A sentence could be provided for each. E.g. ice borehole measurements provide a minimum GHF value when the base is at the pressure melting point. d) Figure 6 needs to be discussed in more detail in the text. A description of the different data sets used is lacking (see specific comments). e) Section 4.5 is quite long compared to the other subsections, and describes in a lot of details a technique that is not widely in Antarctica because of the lack of measurements. It seems therefore that including specific equations is superfluous, and perhaps the paragraph on its application in Antarctica could then be extended. I attach a detailed review of the paper for the specific line-by-line comments, see attached PDF. All the best, Brice Van Liefferinge

#### **Reply to Main Comments:**

a) In the title you use “flow” but I would suggest to use “flux”, as well as for the whole manuscript (see specific comments).

- This was a topic of discussion when drafting the SCAR-SERCE White Paper on geothermal heat flow (Burton-Johnson *et al.*, 2020). The community consensus was that “flow” is the correct terminology. “Heat flow” is not limited to the movement of material, but the mechanism of heat transfer (dominantly by conduction when near the Earth’s surface). It was highlighted that the two terms are used interchangeably within the scientific literature, but “heat flow” has been established for decades to describe the rate of heat transferred across the surface of Earth per unit area, and is the term used by the International Heat Flow Commission. The most important consideration is to state the units ( $\text{mw}/\text{m}^2$ ), as we have done. A very important and worthwhile discussion and consideration though, and we thank you for raising it. Hopefully this will bring us closer to a more consistent use of the terms.

b) The manuscript is qualitative in a few paragraphs. More quantitative descriptions could be provided such as maximum and minimum GHF of the different data sets, discuss the representativeness of point GHF values, . . . where possible.

- Maximum and minimum values are not the best way to represent these datasets. Following Burton-Johnson *et al.* (2017), to be more quantitative we have added probability density plots of the GHF estimates in East and West Antarctica, and added maps of mean and SD for the different geophysically-derived GHF estimates.

c) The limitations of the different methods to estimate GHF (ice borehole measurements, model estimates, . . .) are not always discussed. A sentence could be provided for each. E.g. ice borehole measurements provide a minimum GHF value when the base is at the pressure melting point.

- The advantages and limitations are now summarised in a table.

d) Figure 6 needs to be discussed in more detail in the text. A description of the different data sets used is lacking (see specific comments).

- The section where each model is discussed has been added to the legend. All of the data coverage shown is discussed in detail in each section.

e) Section 4.5 is quite long compared to the other subsections, and describes in a lot of details a technique that is not widely in Antarctica because of the lack of measurements. It seems therefore that including specific equations is superfluous, and perhaps the paragraph on its application in Antarctica could then be extended.

- Section significantly shortened.

Please also note the supplement to this comment:

<https://www.the-cryosphere-discuss.net/tc-2020-59/tc-2020-59-RC1-supplement.pdf>

### Replies to specific comments

Supplemental comments, ordered by "Page. Number." E.g. "3.2." is comment two on page three of the supplement.

1.1. This might seem to be a picky comment but it is important to be precise. I would suggest to use "flux" than "flow": heat flow should be reserved for the movement of material while heat flux is a transport of a quantity of energy over time. As in this paper you focus more on the GHF beneath the Ice Sheet (bedrock surface), I would use "flux". Otherwise can you explain the use of "flow"?

- See reply above (Main comments (a) )

1.2. "estimate" (extract sounds like by effort or force)

- Changed.

2.1. present and

- Text added.

2.2. See comment on the Title

- See reply to earlier comment (1.1.)

- 4.1. I would suggest to add somewhere that ice sheet temperature is also influenced by the ice thickness: as ice acts as an insulator, the greater the ice thickness, the warmer the ice at the base. This is counterbalanced by cold temperature advecting from the surface, itself influenced the accumulation rate.
- Both points now added to this section.
- 4.2. Whole
- To avoid the confusion with an equal temperature effect through the whole ice sheet thickness, we have decided to exclude this addition.
- 4.3. Basal
- Added.
- 4.4. Cross-Out
- Changed
- 4.5. "increase" ==> from -13°C to 7°C
- Changed.
- 4.6. and expands the surface area of the bed at the pressure point from 16% to more than 50%.
- Details added.
- 4.7. Cross-Out
- "Non-uniform" is the correct spelling.
- 4.8. As you mention surface temperature in this paragraph, I suggest to add a sentence on surface accumulation which can have a strong influence on the basal conditions even in the interior of the ice sheet, and counteract the effect of the GHF (see Fig. 2 Van Liefferinge and Pattyn 2013)
- Accumulation rate now mentioned.
- 5.1. You should also add the work of Rezvanbehbahani et al. (2017) : Rezvanbehbahani et al. (2017) use for the first time machine learning techniques to derive GHF from relevant geologic features (gravity measurements, magnetic anomaly) and GHF measurements (derived from crustal thickness, rock composition and active thermal feature). S. Rezvanbehbahani, L. A. Stearns, A. Kadivar, J. D. Walker, and C. J. van der Veen. Predicting the geothermal heat flux in Greenland: a machine learning approach. Geophysical Research Letters, 2017. ISSN 1944-8007. doi: 10.1002/2017GL075661.
- Reference added in reply to comment 29.3 (below).
- 5.2. Cit: Fischer 2013, Climate of the past paper. <https://www.clim-past.net/9/2489/2013/>
- Citation added.
- 5.3. Van Liefferinge and not Liefferinge
- Changed
- 6.1. Curie Point Depth (CPD as in section 4.1 L311)
- Changed
- 6.2. I suggest to develop in one or two sentences the implications of the Antarctic Ice Sheet like in section 2.3.2
- Apologies, we do not understand this request. This section is discussing how GHF studies inform mantle dynamics research.
- 6.3. It is a simple suggestion but why not provide a table presenting all the methods used to estimate the GHF with the advantages and disadvantages, to have an overview of all the methods together. This sentence could be extended as well to give an overview of the section's content.
- Summary table of methods added.
- 7.1. GHF
- Changed

8.1. In the xlsx supplementary material, I guess that in the row "method", borehole means "Boreholes into bedrock" ? If yes can you provide the exhaustive (or estimation) of the number of boreholes into bedrock in Antarctica and cite the SOM.

- Number of data points of each type now added to the "Existing Data" section.

8.2. A key point that is not explained here, is that, when the base of the ice sheet is at the pressure melting point (presence of water), the GHF estimate is a minimum GHF estimate, which means that the GHF can be higher! See also section 5, 5.1

- We agree with the reviewer that if the base of the ice sheet is at the pressure melting point, GHF cannot be estimated from the gradient of temperature alone and only a minimum value of GHF can be estimated. We believe that is clearer to refer in this Section only with studies estimating GHF and we have explicitly stated that one of the requirements is "that the ice sheet has been unequivocally frozen to the bed for long enough that the bedrock and overlying ice sheet have thermally equilibrated"

8.3. add citation

- Citations added

11.1. A: Fox Maule et al., did you use the 2005 version of the data set or the updated one from Purucker ? Based on the figure, you are using the Purucker et al update so please cite: M. Purucker. Geothermal heat flux data set based on low resolution observations collected by the champ satellite between 2000 and 2010, and produced from the mf-6 model following the technique described in fox maule et al.(2005). See [http://websrv. cs. umt. edu/isis/index. php](http://websrv.cs. umt. edu/isis/index. php), 2013.

- The updated reference is added to the figure and where appropriate in the rest of the manuscript.

12.1. I would suggest to be very explicit about what each data set is in that figure. e.g. Passalacqua et al., 2017: "radar reflectivity and inverse modelling". Provide a table with the links to the data sets ? (see general comments)

- The section where each model is discussed has been added to the legend.

12.2. derived estimates (to be consistent with the other sub-section title )

- Changed.

13.1. CPD

- Changed.

14.1. . B)

- (B) is used as a reference to the illustration whilst explaining (A) rather than a separate description.

14.2. Cross-Out

- See 14.1

14.3. Highlighted

- See 14.1

15.1. CPD

- Added.

15.2. Cross-Out

- Corrected.

15.3. :

- Corrected.

15.4. bottom of the magnetic source

- Corrected.

- 15.5. As is, to me, this figure illustrates more the difference between Martos et al. (2017) and the two methods than between seismic and gravity modeling. Why not simply plot the difference between the two methods you describe?
- Whilst the difference between the figures is due to the difference between the two Moho estimates, the figure is to show that there are regions where the Curie depth is deeper than the Moho estimate regardless of the Moho estimation method. Consequently, this is the most appropriate way to present the data.
- 16.1. derived estimates (see 4.1)
- Reworded.
- 17.1. Thanks for pointing this difference out !
- Thank you.
- 17.2. model derived estimates (e.g)
- Reworded.
- 17.3. as before for the sub-title.
- Reworded.
- 18.1. Can you provide some numbers on the maximum and minimum GHF ?
- This is dependent on the borehole estimates used.
- 18.2. Section 4.5 is quite long compared to the other subsections, and describes in a lot of detail a technique that is not widely used in Antarctica because of the lack of measurements. It seems therefore that including specific equations is superfluous, and perhaps the paragraph on its application in Antarctica could then be extended.
- Section significantly shortened.
- 21.1. Simplify in one sentence.
- Section re-worded and shortened.
- 23.1. You use whilst several times, you could remove some of them.
- Alternatives are now used here and elsewhere in the document.
- 23.2. Underline
- See preceding comment.
- 23.3. you can also cite: J. W. Goodge, C. M. Fanning, C. M. Fisher, and J. D. Vervoort. Proterozoic crustal evolution of central East Antarctica: Age and isotopic evidence from glacial igneous clasts, and links with Australia and Laurentia. *Precambrian Research*, 299:151–176, 2017.
- This paper precedes the Goodge (2018) paper, but discusses what can be determined of the age and composition of the unexposed crust, but does not discuss the heat production implications. To avoid confusion for the reader and to direct them to the relevant paper, we have chosen not to include the earlier paper.
- 24.1. (Van Liefferinge and Pattyn, 2013).
- Corrected
- 24.2. As it is difficult to know the melt rate, I would say that this is not the GHF estimate but the minimum value of the GHF estimate or the minimum GHF to reach the pressure melting point.
- We agree with the reviewer that if ice is melting at the base only a minimum value of GHF can be estimated. However, all the methods referred in Sections 5.1 and 5.3 use additional constraints to estimate GHF. In Section 5.2 we explicitly state that only a minimum value of the GHF can be estimated.
- 25.1. Van
- Corrected
- 25.2. Van
- Corrected



- 25.3. ,  
- Corrected
- 25.4. more than  
- Added "at least"
- 25.5. cite: A. P. Wright and M. J. Siegert. A fourth inventory of Antarctic subglacial lakes. Antarctic Science, 24:659–664, 2012.  
- Reference added
- 26.1. again if at the PMP, for me it is more a minimum GHF as we don't know whether there is melt or not. If the melt is low, both values are very closed to each other  
- See response to 24.2
- 27.1. Van  
- Corrected.
- 29.1. You should include the new TCD paper of Talalay 2020: <https://www.the-cryosphere-discuss.net/tc-2020-32/tc-2020-32.pdf>
- 29.2. Dome Fuji is not frozen to the bed, so it is a minimum GHF  
- Text added.
- 29.3. I strongly suggest to add a few words on machine learning techniques as done in Greenland by Rezvanbehbahani et al. (2017). See before and something like: "Machine learning techniques used to determine the GHF over the Greenland Ice Sheet (Rezvanbehbahani et al., 2017) could be developed for the Antarctic Ice sheet. Up until now, we provide a statistical analysis of basal temperatures and GHF based on the use of different data sets. The use of a Monte Carlo approach, which is based on repeated random sampling to calculate GHF, could bring new perspectives on the data, and in particular on associated uncertainties which would allow us to critically assess our results."  
- Text added
- 30.1. and only where the bed is frozen.  
- Text added ("where the basal ice is frozen to the bedrock").
- 33.1. Van  
- Corrected.
- 33.2. I would add that up until now, thermodynamical models are still dependent of GHF estimates (large GHF data sets, borehole temperature measurements, ...)  
- Text added.
- 33.3. for local measurements  
- Added "for local estimates".
- 38.1. Please also mention the updated version of this data set by Purucker 2013 which is the available data set now
- 39.1. Cross-Out  
- Corrected.
- 41.1. Van Liefferinge, B., and Pattyn, F.: ...  
- Corrected.
- 41.2. Van  
- Corrected.

Dr Alex Burton-Johnson  
British Antarctic Survey  
Natural Environment Research Council  
High Cross, Madingley Road  
Cambridge  
CB3 0ET

E-mail: [alerto@bas.ac.uk](mailto:alerto@bas.ac.uk)

Dear Anonymous Reviewer,

Thank you for taking the time to provide such a helpful and thorough review. You provided many pertinent comments, and their implementation has greatly improved our manuscript. We have addressed all of your points, and list them below alongside your review.

All the best,

A handwritten signature in black ink, appearing to read 'Alex Burton-Johnson', written over a horizontal line.

Dr Alex Burton-Johnson

Anonymous Referee #2

Received and published: 20 April 2020

Review of Burton-Johnson et al. Geothermal heat flow in Antarctica: current and future directions

Burton-Johnsen et al. review the geological and glaciologic methods for inferring the geothermal flux of Antarctica. This is an important question for a variety of glaciological applications and the understanding of Antarctic geology. The paper is well written and informative. Probably the best description of its utility is that I've already sent it to 3 of my students to help them understand the different methods used to infer geothermal flux.

What I've found most interesting about the paper is the description of the geologic methods. As a glaciologist, these techniques have been difficult to understand and evaluate in the primary papers and I found this paper helpful, but given my specialty, I am also unable to critically review the geology-based content. It might be worth ensuring that a geologist/geophysicist provides assessment as well.

My only major concern of this manuscript centers on the table of compiled geothermal flux estimates. There has been no significant evaluation of the estimates provided, despite a column entitled "DataQuality". Some sites having multiple different estimates, such as WAIS Divide, with no explanation or evaluation of the difference. To be truly useful, this table needs to be better curated with commentary on why the measurements should or should not be accepted. Because of the huge uncertainties in many (if not all) of the methods, many authors have unwisely justified their own results with erroneous or preliminary interpretations of others. It would be a great service to help remove the confusion about the quality of the different measurements. I realize this is a considerable exercise and understanding the details of each and every measurement is likely beyond what is reasonable for the authors, but even a cursory classification of the confidence in each measurement is hugely helpful. And discrimination/unification of multiple estimates for the same sites seems like a reasonable request.

Minor Comment: The authors are very optimistic about long-wavelength microwave emissivity, which I do not believe is yet warranted. In reviewing Macelloni et al, the authors acknowledge that there was little actual verification, so it is not clear that this technique has added useful information. While a discussion of this technique is useful, it needs a fuller description of the limitations and how difficult they will be to overcome. The sentence on L922-924 reads like a direct funding plea and should be avoided.

**Reply to main comments above:**

a) "a cursory classification of the confidence in each measurement is hugely helpful. And discrimination/unification of multiple estimates for the same sites seems like a reasonable request."

- A qualitative classification of each estimate in the supplementary table has now been added along with a table of the qualifiers for each classification. These qualifiers are based on literature in the manuscript, so although likely controversial in some instances, are not arbitrarily determined (e.g. 90m as a qualifier for bedrock boreholes is based on the observed depth of surface temperature effects in the DVDP boreholes; Decker, 1974; Decker et al., 1975; Pruss et al., 1974).

b) "The authors are very optimistic about long-wavelength microwave emissivity, which I do not believe is yet warranted."

- Discussion of the caveats of this technique have been expanded.

### Replies to specific comments

Specific comments: L9: I know I'm tilting at windmills here, but "geothermal heat" is redundant. Just "geothermal" is enough.

- Whilst "heat" is implicit in "geothermal", "geothermal heat flow" is the full standard terminology used in the literature, and we inherit that convention.

L13: provide at least one sentence on what you found by reviewing methods and compiling estimates before jumping into future directions

- Text added.

L15: Be specific about how the EAIS is the most sensitive to geothermal flux. The EAIS is not uniformly the most sensitive. For instance, the flux of ice in the Ross Ice Streams is incredibly sensitive to geothermal flux and basal water which is not true of the vast majority of EAIS.

- With the removal of the specific comment on microwave emissivity, the EAIS is no longer mentioned.

L16: long-wavelength microwave emissivity has not been sufficiently demonstrated to be useful to warrant a specific bullet point

- Point removed.

L25-27: This seems like an overstatement. I would argue the ice-bedrock friction which controls the basal sliding rate is far less constrained and much more important.

- Emphasis reduced.

L30-33: Provide references

- References added.

L52: change "lower" to "smaller" that size and position are not confused

- Changed.

L76: I don't think the equation came through in the correction form, or else something else is wrong. There is no integral and lamda is never defined. This whole section is therefore very confusing.

- Correct, most of the equation seems to have got lost – Quite embarrassing! This is fixed now.

L85: Geothermal flux is actually not that important to the ice temperature. The accumulation rate and surface temperature are much more important. Once the geothermal flux is sufficient to cause basal melting, the temperature profile is only minorly impacted even for large variations in geotherm flux.

- Sentence reworded. The scale and sensitivity of the ice sheet temperature to GHF variation is discussed in the following paragraphs of this section.

L99: flip -7 and -13 to be consistent with text and ordering

- Corrected.

L99: Reword this sentence because an increase from -13 to -7 would not change the basal melt rate since it would still be below freezing. So be more specific about the threshold behavior of variations in geothermal flux.

- -7°C is the mean temperature (already stated). That the basal melt rate increases is shown by the increase 16% to more than 50% of the basal area exceeding the PMP.

L106: The PMP effect is incredibly small. The PMP decreases the basal temperature by ~2C from the thin ice at the coast to the thick ice in the interior whereas the surface temperature decreases by ~30C. This just isn't a big effect.

- We agree with the reviewer that the effect of pmp on basal temperature is small. However we are discussing here the sensitivity of basal conditions to GHF. Both references cited show that the sensitivity is larger in the interior of East Antarctica and the reason is that the basal temperature is closer to the PMP. In areas where basal temperature is near PMP, small changes in GHF affects the extension of basal melting and has a stronger effect on the ice sheet. We have rewritten the sentence for clarity.

L121: change "are" to "can be" because some ice streams, like the Ross ice streams, with very low driving stress don't produce a lot of melt and appear to be freezing at the bed (Joughin et al., 2004, Melting and freezing beneath the Ross ice streams, Antarctica).

- Text changed.

L122-125: This is a subtle concept, so please articulate what is happening in more detail.

- Text added. As with all points in this summary paper, the reader is forwarded to the correct reference.

L137-138: Frozen beds are not a prerequisite for deep coring operations. Dome C, Dome Fuji, NGRIP and NEEM are examples of drilling to temperate beds. Potential melting may necessitate clean access or a buffer, but the language should be clear.

- We agree with the reviewer our comment is focussed on 'Oldest Ice challenge' and not true for every ice core location. We have written the sentence.

L243: Fig 3: This seems like a really strange example to choose. First, there is nothing in the figure which shows what the geothermal flux is. Second, where is the bed? Third, this appears to be a high accumulation rate and shallow ice thickness site, where the temperature profile is dominated by advection, and the confidence in the geothermal flux is low. I'd recommend using either Law Dome (Dahl-Jensen et al., 1999) or Siple Dome (Engelhardt, 2004) as better examples.

- Replaced with the Dahl-Jensen (1999) example from Law Dome.

Paragraph starting at L247: Maybe I'm just confused, but where is advection in this? This seems appropriate for a material that doesn't flow. If I'm wrong and advection is being considered, please articulate how it fits into the circular frequency.

- As stated at the start of this section, the method is applicable where the ice sheet is stationary (frozen to the bed) and thermally equilibrated; hence horizontal advection is minimal. For clarity, this point is now repeated at the start of this section.

L267: These three references are all abstracts. I don't think this method will actually work because there is too much memory of past temperature, too much uncertainty in the vertical velocity profile,

and too much uncertainty in the thermal conductivity of ice. (also, this will really only provide an lower limit since increasing the geothermal flux will cause basal melting at some point and then the temperature profile because relative insensitive to variations in geothermal flux)

- The debate over an estimation of a simplified model ‘working’ or ‘not working’ is futile. There is no way around the uncertainties that the reviewer is mentioning and we will only say here that in any study they should be propagated into the estimation uncertainty. In any case, we agree with the reviewer that the estimations rely on a simplified models and this need to be clearer in the paper. We have rewritten the sentence.

I don’t feel qualified to comment on section 4.

L661: I don’t like the forward vs. inverse model distinction since many of the “forward” methods are based on inverse methods.

- Good point; reworded.

L665: change “ground” to “ice”

- Reworded.

L711: Section 5.2. This makes a compelling case for inferring minimum geothermal flux. I’d suggest adding to this section the reverse case: that is, the maximum geothermal flux can be estimated if the ice is known to be frozen to the bed. Raymond Arches are compelling evidence of a frozen bed, which Fudge et al. (2019) used to estimate maximum geothermal flux for two Siple Coast ice rises. Together, the minimum and maximum inferences can be more useful than either alone.

- Text added.

L728: Describe how far from South Pole. There’s a lot of discussion of the South Pole lake, which is ~100km away, so the work of Jordan et al. is actually pretty far removed from South Pole.

- Distance added.

L736: I think the authors are overly optimistic about this method. In reviewing Macelloni et al., it seems like they were able to infer little besides the ice being warmer with depth. The authors acknowledge that there was little actual verification. While the section should be included, it needs a fuller description of the limitations and how difficult they will be to overcome.

- The limitations of the method and the challenges in developing the approach are now expanded in the section on current challenges, Section 7.3 (also responding to comment “L915-924” below).

L767: I think you should add a section on using englacial attenuation to determine ice sheet temperature. While published literature has mostly focused on depth-age average values (MacGregor et al., 2015, doi:10.1002/2014JF003418; Schroeder et al., 2016, doi: 10.1017/jog.2016.100), there has been considerable progress with obtaining depth profiles, particularly as multiple radar systems can be cross-compared.

- The studies on temperature-dependent attenuation by Carter et al (2009) and Schroeder et al (2016) are already discussed in Section 5.1.

L852: This sentence underestimates what is known about Dome C geothermal flux. The geothermal flux is actually quite well constrained by glaciological modeling (see Parenin et al., 2007). The de

Mendoze retracted paper is an incredibly strange reference that is completely outside of the glaciological and ice core communities. I think this is very misleading.

- Sentence removed.

L857: Figure 16: would a log scale make more sense since the 30mW/m<sup>2</sup> cutoff seems too small

- Scale expanded to 60 mW/m<sup>2</sup>

L861-874: Thank you for this paragraph. It is wonderful to read an insightful critique of the Cure depth technique. I think you are too diplomatic when you write “without being critical of the model itself”.

- Thank you.

L915-924: I think this section is too optimistic. The last sentence in particular is inappropriate.

- The last sentence has been removed and the limitations of the method expanded (also addressing point “L736”)

L960: “sliding” not “slide”

- Changed.

Dr Alex Burton-Johnson  
British Antarctic Survey  
Natural Environment Research Council  
High Cross, Madingley Road  
Cambridge  
CB3 0ET

E-mail: [alerto@bas.ac.uk](mailto:alerto@bas.ac.uk)

Dear John Goodge,

Thank you for taking the time to provide comments on our manuscript. Whilst these were largely structural, we agree that they will make a large improvement to the coherence of the manuscript in light of its length and the diversity of work included. Our comments are provided below alongside your review.

All the best,

A handwritten signature in black ink, appearing to read 'Alex Burton-Johnson', with a horizontal line extending to the right across the top of the signature.

Dr Alex Burton-Johnson



J. Goodge

jgoodge@d.umn.edu

Received and published: 25 March 2020

Nice paper and worthwhile compilation of ideas as well as a look forward. I have a few suggestions, mainly to help improve organization of topics.

I wonder about the overall organization of section 4.6, which is about how we make GHF estimates in heterogeneous crust. The opening section 4.6.1 goes into determining heat production from rock samples obtained from exposure, but does not discuss interpretations of GHF offered in these papers. On the other hand, GHF is discussed in sections 4.6.3 and 4.6.4, building on other ways to get at heat production. Seems perhaps better to comment on the implications for GHF from the heat production studies and how this reflects heterogeneities?

- The implications of the studies are now included as a new paragraph at the end of Section 4.6.1.

Further, I understand the distinction between rock outcrop and sampling rocks from moraines, but I wonder if it would make more sense to move up the discussion of glacial moraine materials from the CTM either into section 4.6.1 or perhaps changing that clast section to follow the other as new section 4.6.2? They both relate to determining heat production in rocks.

- Paragraph moved to follow the section on HPE measurement from bedrock.

Also, I suggest changing the title of section 4.6.4 from 'Detrital material' to 'Glacially- derived rock clasts' or something along those lines. For better or worse, 'detrital material' to many people will conjure up detrital minerals from sedimentary deposits or sedimentary rocks, or even sediment itself. In this case, it's an important distinction because we sampled large rock clasts that can be treated analytically just like any rock samples taken from exposure.

- Reworded as suggested.

John Goodge

1 **Geothermal heat flow in Antarctica: current and future**  
2 **directions**

3 Alex Burton-Johnson<sup>1</sup>, Ricarda Dziadek<sup>2</sup>, and Carlos Martin<sup>1</sup>

4 <sup>1</sup>British Antarctic Survey, High Cross, Madingley Road, Cambridge, CB3 0ET, UK

5 <sup>2</sup>Alfred Wegener Institute - Helmholtz Centre for Polar and Marine Research, Am Alten Hafen, Bremerhaven,  
6 Germany

7 *Correspondence to:* Alex Burton-Johnson (alerto@bas.ac.uk)

8 **1. Abstract**

9 Antarctic geothermal heat flow (GHF) affects the temperature of the ice sheet, determining its ability to slide and  
10 internally deform, as well as the behaviour of the continental crust. However, GHF remains poorly constrained,  
11 with few and sparse local, borehole-derived estimates, and large discrepancies in the magnitude and distribution  
12 of existing continent-scale estimates from geophysical models. We review the methods to estimate GHF,  
13 discussing the strengths and limitations of each approach, compile borehole and probe-derived estimates from  
14 measured temperature profiles, and recommend the following future directions: 1) Obtain more borehole-derived  
15 estimates from the subglacial bedrock and englacial temperature profiles. 2) Estimate GHF from inverse  
16 glaciological modelling, constrained by evidence for basal melting and englacial temperatures (e.g. using  
17 microwave emissivity). 3) Revise geophysically-derived GHF estimates using a combination of Curie depth,  
18 seismic, and thermal isostasy models. 4) Integrate in these geophysical approaches a more accurate model of the  
19 structure and distribution of heat production elements within the crust, and considering heterogeneities in the  
20 underlying mantle. And 5) continue international interdisciplinary communication and data access.

21

Deleted: extract

Deleted: ,

Deleted: 2) Estimate GHF beneath the interior of the East Antarctic Ice Sheet (the region most sensitive to GHF variation) via long-wavelength microwave emissivity. 3

Deleted: 4

Deleted: 5

Deleted: 6

## 30 1. Introduction

31 The Antarctic ice sheet is the world's largest potential driver of sea level rise, and accurately modelling its  
32 dynamics relies, amongst others, on constraining conditions at the ice-bedrock interface. Measuring these basal  
33 conditions is inherently challenging and, of all the parameters affecting ice sheet dynamics, subglacial geothermal  
34 heat flow (GHF) is one of the least constrained (Larour et al., 2012; Llubes et al., 2006). Despite this uncertainty,  
35 GHF affects (1) ice temperature and, as a consequence, ice mechanical properties (rheology), (2) basal melting  
36 and sliding, and (3) the development of unconsolidated water-saturated sediments; all of which can promote ice  
37 flow (Greve and Hutter, 1995; Larour et al., 2012; Siegert, 2000; Winsborrow et al., 2010). Beyond ice dynamics,  
38 our knowledge of GHF allows us to model past and present basal melt rates in our exploration for old ice core  
39 climate records (Van Liefferinge et al., 2018), constrain models of glacial isostatic adjustment (GIA; van der Wal  
40 et al., 2013, 2015), and inform on the geological and tectonic development of Antarctica (McKenzie et al., 2005).

41 In recognition of the ambiguity and importance of Antarctic GHF, an increasing number of studies in geology,  
42 geophysics, and glaciology have sought to constrain this parameter, with a developing dedicated multinational  
43 interdisciplinary community (Burton-Johnson et al., 2019; Halpin and Reading, 2018). However, with an  
44 expanding research base and a requirement for multidisciplinary science, the necessity for a multidisciplinary  
45 review of current approaches and future directions was highlighted by the GHF sub-group of SERCE (Solid Earth  
46 Response and influence on Cryospheric Evolution) and the Scientific Committee on Antarctic Research (SCAR)  
47 (Burton-Johnson et al., 2019). This paper also provides the background material for a SCAR-commissioned White  
48 Paper on future research directions (Burton-Johnson et al., 2020).

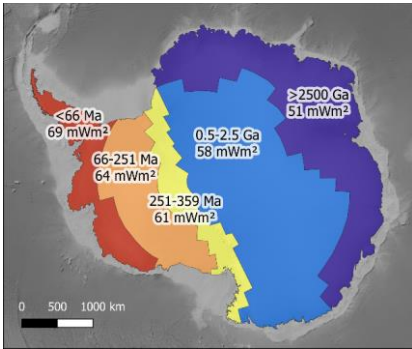
### 49 1.1. What is geothermal heat flow (GHF)?

50 GHF describes the transport of heat energy from the interior of the Earth to the surface (Gutenberg, 1959; Pollack  
51 et al., 1993). This heat originates from two primary sources: 1) The primordial heat remaining from the formation  
52 of the Earth, when the kinetic energy of celestial collisions was transformed into heat energy; and 2) the  
53 radioactive decay of heat-producing elements (HPEs) and their isotopes; 98% of which is derived from Uranium,  
54 Thorium, and Potassium (Beardmore and Cull, 2001; Lowrie, 2007). The HPEs are incompatible with the mineral  
55 structures of the mantle, so are concentrated into the crust (Boden, 2016; McDonough and Sun, 1995). Other  
56 sources of possible contributions to GHF are: 1) geoneutrino emission from the mantle (Huang et al., 2013;  
57 Korenaga, 2011), and 2) gravitational pressure (Elbeze, 2013; Morgan et al., 2016).

58 The estimated average heat flow of continental crust is  $67.1 \text{ mW m}^{-2}$ , whilst for oceanic crust it is  $78.8 \text{ mW m}^{-2}$   
59 (Lucazeau, 2019; although estimates vary according to sampling strategy and the number of observations). The  
60 difference between continental and oceanic heat flow reflects the smaller thickness of oceanic crust, with hot  
61 mantle rocks at comparatively shallow depths. Continental GHF varies significantly, primarily in response to  
62 variations in crustal heat production, age, composition, tectonic history, and thickness of crust and mantle  
63 (Mareschal and Jaupart, 2013). This results from the geological complexity of composite continental crust  
64 compared with oceanic crust. GHF is generally lower in stable crust away from convergent and divergent  
65 continental margins and rift basins, and higher in these magmatically active provinces (Lucazeau, 2019; Pollack  
66 et al., 1993). On a broad regional scale, continental GHF correlates negatively with age, allowing first order  
67 empirical estimation of Antarctic GHF based on its range of crustal ages (Fig. 1; Llubes et al., 2006; Sclater et al.,

Deleted: lower

69 1980). However, Antarctic crustal heat production estimates show high variability across sampled age ranges  
 70 (Gard et al., 2019), with lithology and tectonic setting being important controls on the heat production distribution  
 71 (Carson et al., 2014; Halpin et al., 2019).



72  
 73 **Fig. 1. Empirical estimation of GHF based on generalised Antarctic crustal ages and mean global GHF values of**  
 74 **continental crust of similar age (adapted from Llubes et al., 2006). Basemap bathymetry from ETOPO1 (Amante and**  
 75 **Eakins, 2009).**

76 The rate of heat flow,  $Q$ , can be approximated by the Fourier's Law (Baron Fourier, 1822). In the simple model  
 77 of a homogenous material with a constant thermal gradient, this equates to:

$$78 \quad Q = -\kappa \partial T / \partial z$$

79 (1)

80 Where  $Q$  has the units  $\text{mW m}^{-2}$  (i.e. power per unit area);  $T$  is the temperature (K),  $z$  is the vertical distance (m);  
 81 and  $\kappa$  is the thermal conductivity of the material ( $\text{mW m}^{-1} \text{K}^{-1}$ ). When considering the basal conditions of the  
 82 Antarctic ice sheet, we are interested in the heat flow at bedrock surface. We also need to consider internal heat  
 83 production,  $A$  ( $\mu\text{W m}^{-3}$ ). For a simple case of constant thermal conductivity and heat production, surface heat flow  
 84 can be described by:

$$85 \quad Q = \kappa_d [\partial T / \partial z]_d + \int A(z) \delta z$$

86 (2)

87 Where the integral is measured from the surface to a depth,  $d$  (equation 1.13 in Beardsmore and Cull, 2001).

88 We would like to highlight here that most methods to estimate GHF derive it from the temperature gradient, as in  
 89 Equations 1 and 2. However, these equations are a simplification, as temperature variation over time, surface  
 90 topography, internal heat production, and variation in the properties of the material all affect the observed  
 91 temperature gradient.

Deleted:  $Q = \lambda_d \nabla T$

Field Code Changed

93 **1.2. A note on terminology: Heat “Flow” vs Heat “Flux”**

Formatted: Heading 2

94 In the scientific literature, heat “flow” and heat “flux” are used interchangeably. The consensus from the SCAR-  
95 SERCE White Paper authorship (Burton-Johnson et al., 2020) is that “flow” is the correct terminology. “Heat  
96 flow” is not limited to the movement of material, but the mechanism of heat transfer (dominantly by conduction  
97 when near the Earth’s surface). Although the two terms are used interchangeably, heat “flow” has been established  
98 for decades to describe the rate of heat transferred across the surface of Earth per unit area, is the term used by the  
99 International Heat Flow Commission, and is thus the term used here. We recommend adopting this term in  
100 preference in the future, although the most important consideration is to state the correct units (mW m<sup>2</sup>).

Formatted: Superscript

101 **2. Motivation: What is the importance of GHF in Antarctica?**

102 **2.1. Glaciology**

103 GHF can strongly influence the basal temperature of the ice sheet. As a consequence, it is a key contributor to  
104 basal meltwater production, ice rheology, basal friction, basal sliding velocity, and erosion (Fahnestock et al.,  
105 2001; Goelzer et al., 2017; Hughes, 2009).

Deleted: s

Deleted: temperature

106 The heat budget at the base of an ice sheet can be described (Vieli et al., 2018):

$$Q_g + Q_s + Q_w + Q_p + Q_f + Q_c = 0$$

108 (3)

109 Where  $Q_g$  is the GHF,  $Q_s$  is the heat generated by sliding,  $Q_w$  is the heat generated by subglacial water flow,  $Q_p$   
110 is the heat required to maintain the flowing water at pressure melting point, and  $Q_f$  is the heat released by freezing  
111 or used by melting; and  $Q_c$  is the heat conducted away in the ice towards the ice surface. Of the positive  
112 contributions to basal heat, that generated by sliding ( $Q_s$ ) can be orders of magnitude greater than that from GHF  
113 ( $Q_g$ ), but in slow flowing areas  $Q_s$  is negligible and GHF plays a key role in the heat budget (Larour et al., 2012;  
114 Pittard et al., 2016a).

115 To illustrate this point, Llubes et al. (2006) modelled a 20 mW m<sup>-2</sup> increase in GHF across the Antarctic continent  
116 (from uniform values of 40 to 60 mW m<sup>-2</sup>). This resulted in a 6°C increase in the mean basal temperature, from  
117 13°C to -7°C, and expanded the proportion of the basal ice area above the pressure melting point (PMP) from  
118 16% to more than 50%. This variation directly affects the basal melt rates, with a uniform 40 mW m<sup>-2</sup> generating  
119 6.7 km<sup>3</sup> yr<sup>-1</sup> of basal melting across Antarctica, whilst 60 mW m<sup>-2</sup> would generate 18 km<sup>3</sup> yr<sup>-1</sup>. However, unlike  
120 the GHF values used, the resultant basal temperature variation is non-uniform: Although the two heat flow models  
121 produce only a few °C difference in basal temperature near the coast, they generate up to 15°C difference in  
122 central East Antarctica. This is because horizontal advection and frictional basal heating are negligible beneath  
123 the thick, slow moving ice of East Antarctica, and surface temperatures have a reduced effect on basal conditions  
124 (Llubes et al., 2006; Pollard et al., 2005). In these regions of thick ice, the increased pressure brings the basal ice  
125 temperature closer to its PMP (Pollard et al., 2005), and the thicker ice has a greater insulating effect. Although  
126 the effect of pressure of basal temperature is much smaller than surface temperature variation, in areas where of  
127 thick ice where the basal temperature is close to the PMP, even small variation in GHF can determine whether

Deleted: -7°C to

Deleted:

Deleted: Whilst

Deleted: Also, i

Deleted: pressure melting point

Deleted: PMP;

Deleted: V

Deleted: thus

Deleted: s

139 basal melting occurs. ~~This has~~ a resultant effect on the basal friction and sliding of the ice sheet (Pollard et al.,  
140 2005). In addition, the increased ice temperature makes it more susceptible to internal deformation, which also  
141 enhances its ability to flow (Llubes et al., 2006).

Deleted: ,

Deleted: with

142 Even beneath the comparatively thinner ice of West Antarctica, the sensitivity of basal temperature to heat flow  
143 is enhanced (Llubes et al., 2006). There is evidence that this region, dominated tectonically by the West Antarctic  
144 Rift System (Jordan et al., 2020), exhibits very high values of basal heat flow and resultant basal melting  
145 (Schroeder et al., 2014). Above  $85 \text{ mW m}^{-2}$ , the basal temperature of much of the West Antarctic Ice Sheet will  
146 pass its pressure melting point (in agreement with radar evidence for extensive basal melting; Llubes et al., 2006;  
147 Rémy and Legresy, 2004; Schroeder et al., 2014). Consequently, enhanced basal heat flow in West Antarctica can  
148 have a large effect on its basal melt rates, although the thinner ice sheet in West Antarctica compared to East  
149 Antarctica makes it more sensitive to surface parameters (~~advection and conduction of the~~ surface temperature,  
150 ~~itself influenced by the accumulation rate~~; Llubes et al., 2006).

Deleted: accumulation and

151 In addition to enhancing basal melting and reducing basal friction, increased GHF enhances ice flow by increasing  
152 the englacial temperature and thus reducing the ice stiffness (Larour et al., 2012). Because the heat produced by  
153 basal friction and viscous deformation ~~can be~~ orders of magnitude greater than from GHF in fast-flowing ice  
154 streams, this effect is only significant in upstream, slow-flowing areas (Larour et al., 2012). In these regions of  
155 thick, slow-flowing ice, even local high heat flow anomalies of insufficient heat for basal melting can result in the  
156 development of accelerated, channelised flow for hundreds of kilometres upstream and downstream of the GHF  
157 anomaly ~~through the effect of GHF on the ice rheology~~ (Pittard et al., 2016a). Regions along ice divides and  
158 adjacent to ice streams are particularly sensitive to enhanced GHF (Pittard et al., 2016b).

Deleted: are

159 Whilst the points above highlight the necessity of estimating Antarctic GHF, it is very important that the accuracy  
160 of these estimates can be verified. The impact of inaccurate GHF constraints on models of ice sheet dynamics  
161 have been shown by comparing GHF estimates for Greenland. Ice sheet modelling controlled by spatially variable  
162 GHF forcing reproduces the observed state to only a limited degree, and fails to reproduce either the topography  
163 or the low basal temperatures measured in southern Greenland (Rogozhina et al., 2012). Instead, an unrealistic  
164 spatially uniform GHF forcing produces a considerably better fit. If the much larger Antarctic ice sheet is to be  
165 accurately modelled, the accuracy of the GHF estimates used must be well constrained by multiple independent  
166 methodologies, sensitivity tests, and comparison of different models.

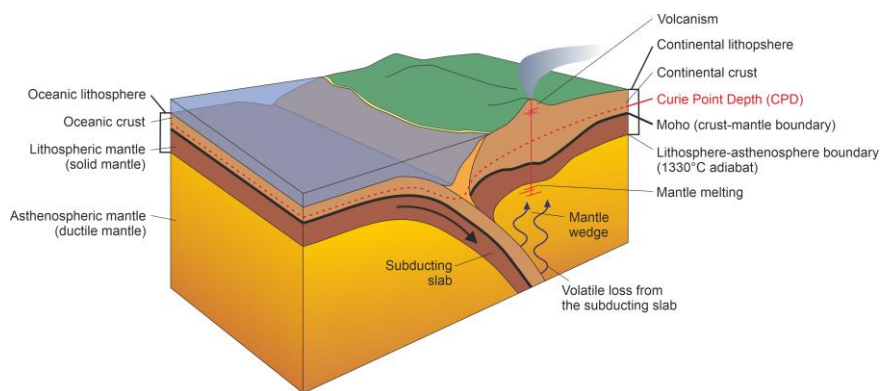
167 Recently, there has been increasing interest in the exploration of suitable locations for coring Antarctica's oldest  
168 continuous ice record (Fischer et al., 2013). This problem requires accurate knowledge of GHF, as basal melt rates  
169 limit the maximum possible age of recoverable ice (Van Liefferinge et al., 2018). Additionally, due to  
170 environmental concerns around possible drilling fluid contamination, frozen bed conditions are a prerequisite for  
171 deep coring operations ~~for recovery of the oldest ice records~~.

## 172 2.2. Glacial Isostatic Adjustment (GIA)

173 The temperature of the lithosphere and upper mantle are important parameters for modelling the isostatic response  
174 to changes in the volume of the overlying ice sheet (i.e. glacial isostatic adjustment, GIA). This is because the  
175 (visco-)elastic properties of the lithosphere and mantle directly relate to its thermal properties (Chen et al., 2018;

180 Kuchar and Milne, 2015). GIA is a critical component of the long-term evolution of ice sheets and could  
181 potentially stabilise retreating ice streams in submarine settings (Barletta et al., 2018; Kingslake et al., 2018). Of  
182 particular importance here is that the temperature-dependant viscosity that controls GIA can be modelled using  
183 surface heat flow estimates (van der Wal et al., 2013, 2015).

### 184 2.3. Geology and tectonics



185  
186 **Fig. 2. Basic illustration of a subduction zone at a convergent margin between oceanic and continental lithosphere to**  
187 **clarify the geological concepts and terms used in this paper.**

#### 188 2.3.1. Mantle dynamics

189 Heat flow variation and its isostatic effects (i.e. the buoyancy control on crustal elevation, resulting from the  
190 different densities of the dense mantle and less dense overlying crust) provide evidence for mantle dynamics  
191 beneath a continent. For example, high heat flow anomalies have been proposed as evidence for sub-lithospheric  
192 heating by present and past mantle plumes (regional hot spots of warm mantle upwelling beneath the lithosphere;  
193 e.g. Courtney and White, 1986; Martos et al., 2018), and the absence of enhanced heat flow where mantle ascent  
194 is proposed has been used to argue against such processes (e.g. Stein and Stein, 2003). Also, because of the  
195 relationship between surface heat flow and isostatic elevation, heat flow studies can reveal thermal or  
196 compositional variation of the sub-continental mantle, as a reduction in its density can increase the isostatic  
197 elevation of the surface topography (Hasterok and Gard, 2016).

#### 198 2.3.2. Development of the lithosphere

199 The thermal properties of the lithosphere control its response to tectonic deformation (e.g. Sandiford and Hand,  
200 1998), such as the development of crustal shear zones and earthquakes. The lithosphere's thermal properties also  
201 affect the relative density of lithosphere and underlying mantle, and (as a result of this buoyancy effect) the  
202 isostatic surface elevation. This in turn influences the heights of Antarctica's mountain ranges and the depths of  
203 its sedimentary basins (McKenzie et al., 2005). For these reasons, understanding the continent's GHF will inform  
204 on the development of many of Antarctica's largest tectonic features. For example, the lithospheric extension of

205 the West Antarctic Rift System, the prominent elevation of the Transantarctic Mountains, the deep topographic  
206 depression of the Wilkes subglacial basin, and the extensive Palmer Land Shear Zone of the Antarctic Peninsula.

|207



Section	Method	Description	Advantages	Disadvantages
<b>3. Measured Temperature Gradients</b>				
3.1.	Bedrock boreholes	GHF estimated from measured temperature gradient into bedrock boreholes.	- Local estimates of GHF derived directly from the bedrock.	- Only point estimates. - Affected by local variation. - Requires drilling through the ice sheet and deep enough into the rock.
3.2.	Ice boreholes	Temperature gradient measured in ice boreholes, and GHF estimated from the basal temperature gradient or models of the temperature profile.	- Provides local estimates of GHF beneath the ice sheet without drilling into bedrock.	- The ice sheet must be frozen to the bed and thermally equilibrated. - Limited by modelling accuracy of the ice sheet thermal history - Hot water drilling requires 2 years for thermal equilibration after drilling.
3.3.	Marine/onshore sediment temperature probes	GHF estimated from shallow (<10m) temperature gradient measured using gravity-driven probes.	- Faster acquisition than borehole estimates, as no drilling required.	- Requires deep water without long-period temperature variation.
<b>4. Geophysical and geological methods</b>				
4.1.	Magnetic-derived estimates	Temperature gradient calculated by estimating the depth of the Curie isotherm from magnetic anomalies.	- Allows continent-scale estimates. - Does not require models of the crust and mantle structure.	- Assumes that the depth to the bottom of the magnetic source is temperature controlled (i.e. it represents the Curie isotherm), despite possible other geological controls. - Spatial resolution limited by altitude of sensor and depth of magnetic source.
4.2.	Seismic-derived estimates	Calculate GHF empirically or via forward modelling using the relationship of mantle seismic velocity and temperature, and estimation of lithospheric thickness.	- Allows continent-scale estimates. - Empirical models utilise well-constrained regions. - Forward models estimate the geological source of GHF.	- Empirical estimates assume global comparison is valid. - Forward models assume mantle and crustal composition. - Limited spatial resolution.
4.3.	Gravity model-derived estimates	Calculates GHF from models of crust and mantle structure derived from gravity estimates of crustal thickness.	- Allows large-scale GHF estimates. - Incorporates constraints on crustal composition.	- Models are non-unique, requiring further constraints. - Assumes values of crustal and mantle composition.
4.4.	Conjugate margin-derived estimates	Reconstruct the Gondwana supercontinent, interpolating Antarctic GHF from better constrained adjacent continents.	- Utilises regions where GHF is better constrained. - Should be most accurate around continental margins.	- Poor constraints away from continental margins. - Affected by choice of input data and interpolation method.
4.5.	Isostatic elevation	Calculates GHF from topography using a compositional correction.	- The topographical input is a well constrained variable.	- Requires assumptions of crustal thickness, density, heat production, and thermophysical properties. - Low spatial resolution.
4.6.	Incorporating heterogeneous crustal compositions.	Incorporating measurements of crustal heat production and models of heterogeneous crustal structure into geophysical GHF models.	- A more realistic representation of the geological sources of GHF. - Reflects the concentration of heat production in the crust.	- Requires assumptions of the subglacial geology away from outcrops. - The 3D structure and composition of the crust and mantle is ambiguous.
<b>5. Glaciological methods</b>				
5.1.	Subglacial water	Radar evidence for subglacial water used to model the required GHF distribution for required basal melting and hydrology.	- Based on observable effects of GHF.	- Requires accurate ice sheet thermal models. - Subglacial water only accumulates in appropriate topographic depressions.
5.2.	Subglacial lakes	Lakes identified by enhanced radar reflectivity, and the minimum GHF required for basal melting estimated from ice sheet thermal models.	- Based on observable effects of GHE. - Where the ice sheet is frozen to the bed, maximum GHF can be calculated.	- Requires accurate ice sheet thermal models. - Subglacial water only accumulates in appropriate topographic depressions.
5.3.	Englacial stratigraphy	Melt rates and required GHF calculated from englacial layers identified in radar data.	- Based on observable effects of GHE. - Identifies high GHF anomalies.	- Requires accurate data and interpolation from ice cores. - Requires accurate ice sheet thermal models.
5.4.	Microwave emissivity	Englacial temperatures modelled with variable GHF to simulate observed satellite-derived, temperature dependent microwave radiation.	- Derives more extensive englacial temperature profiles than can be achieved by boreholes.	- Only applicable to areas of thick, slow flowing ice. - Method requires further validation.

Formatted Table

Formatted: Indent: Left: 0 cm, Hanging: 0.21 cm

Formatted: Font: 8 pt

**Table 1. Summary of methods to estimate GHF and their section in the manuscript.**

209 **3. GHF estimates from measured temperature gradients**

210 Having highlighted the importance of constraining Antarctica’s GHF, the following sections discuss current  
211 approaches to its estimation. The methods discussed are summarised in Table 1.

212 Local heat flow estimates can be derived by measuring the temperature at various depths below the surface (either  
213 in the bedrock, overlying sediments, or within the ice sheet) and deriving a temperature gradient. In Antarctica,  
214 GHF has been derived through temperature measurements from boreholes into the bedrock or into the ice sheet,  
215 and also from probes into unconsolidated sediments. It is important to recognise that these are “estimates” not  
216 “measurements” of GHF, particularly when using them to verify the accuracy of geophysical or inverse GHF  
217 estimates. This is because the measured thermal gradient can be affected by processes other than GHF, including  
218 surface temperature variation and hydrothermal circulation. When evaluating a specific local estimate, its  
219 derivation, local geology, and other regional GHF estimates must be considered. Thermal gradients and surface  
220 heat flow may vary significantly over 10 km lateral spatial resolutions (Carson et al., 2014) with variations in  
221 geology (affecting heat production and conductivity; Carson et al., 2014; Hasterok and Chapman, 2011),  
222 hydrothermal circulation (affecting local heat convection and redistribution; Fisher and Harris, 2010), and  
223 topography (affecting heat diffusion pathways to the surface; Bullard, 1938; Lees, 1910).

**Deleted:** geothermal heat flow

224 **3.1. Boreholes into bedrock**

225 The thermal gradient can be determined by measuring the temperature variation at different depths in the crust.  
226 Away from Antarctica, these measurements are from boreholes (commonly those drilled for mineral or  
227 hydrocarbon exploration), mineshafts, caves, or other cavities. The temperature gradient of the crust’s uppermost  
228 10-50 m is dominantly affected by downward conduction of the surface temperature rather than GHF. To address  
229 this, temperature measurements are made over the largest depth range possible (typically 100-1000 m).

230 Borehole temperature measurements are made using wire-line temperature probes, with a thermistor at the leading  
231 tip and measurements made progressively downwards to minimise disturbance of the borehole fluids prior to  
232 temperature measurement. The temperature is measured from the bore fluid, not the surrounding rock, so an  
233 important consideration is the need for thermal equilibration of the wall rock and the borehole fluids following  
234 drilling and prior to measurement. In addition, the heat produced during drilling needs to be dissipated from the  
235 borehole. As a guide, 10-20 times the drilling time is required before a borehole is equilibrated to within  
236 instrument accuracy (Bullard, 1947; Jaeger, 1956), although observations show that after 3 times the drilling time,  
237 borehole fluids are within 0.05°C of equilibrium values (Lachenbruch and Brewer, 1959). As an example of the  
238 time required for bedrock drilling, drilling of the multiple Cape Roberts Project boreholes averaged 16-31 m day  
239 <sup>-1</sup> (Talalay and Pyne, 2017). For the low water flows used in small-core (<4 cm diameter) diamond drilling  
240 (compared with the high water flows of wider core diameter rotary drilling), heat exchange is negligible except  
241 for the upper and lowermost ~20 % of the borehole, and full temperature profile measurements can be taken about  
242 two days after drilling cessation (Jaeger, 1961, 1965).

**Deleted:** measurements can be taken about two days after drilling cessation, except from

**Deleted:**

**Deleted:** As an example, drilling of the multiple Cape Roberts Project boreholes averaged 16-31 m day<sup>-1</sup> (Talalay and Pyne, 2017). (Davis et al., 1997; Fisher et al., 2007) (Hyndman et al., 1987)

243 Depth below the bedrock surface must be considered when taking borehole temperature measurements. Where  
244 terrestrial bedrock is exposed, atmospheric temperature and seasonal variation perturbs the thermal gradient in the  
245 upper >100 m of the crust. In Antarctica, temperatures from Hole 3 of the Dry Valley Drilling Project provided  
246 estimates of “equilibrium” gradient only when deeper than 90 m (Decker, 1974; Decker et al., 1975; Pruss et al.,

255 1974). It may be possible to compensate for seasonal variation in shallower boreholes using long-term  
256 observations of the temperature gradient (>1 year), although the previous attempt (from a 7.6 m borehole at  
257 McMurdo Station; Risk and Hochstein, 1974) derived an anomalously high GHF estimate ( $164 \text{ mW m}^{-2}$ , compared  
258 to  $66 \text{ mW m}^{-2}$  from a 260 m deep borehole; Decker and Bucher, 1982).

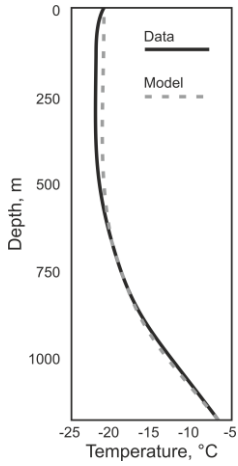
259 Subglacial bedrock is not exposed to atmospheric temperature variation, so the geothermal gradient can be  
260 measured from shallower depths. However, it is affected by heat derived from the overlying ice sheet: internal  
261 and basal frictional shear heating from the ice sheet, heat advection, basal water, and seasonal temperature  
262 variation (e.g. Ritz, 1987). In the absence of a deep, borehole-derived, subglacial bedrock temperature profile, the  
263 depth required to accurately measure the unperturbed geothermal temperature gradient is currently unknown.  
264 Thermal diffusion modelling over timescales of low frequency climate variation may constrain this.

### 265 3.2. Ice boreholes

266 Subglacial GHF can be estimated from the temperature gradient from boreholes into the ice sheet (e.g. Engelhardt,  
267 2004; Fudge et al., 2019; Nicholls and Paren, 1993). This requires that there is no additional heating from basal  
268 shear or horizontal advection, and that the ice sheet has been unequivocally frozen to the bed for long enough that  
269 the bedrock and overlying ice sheet have thermally equilibrated. To meet this requirement, the temperature profile  
270 is best measured from cores into the summits of ice domes where the ice sheet is stationary (Engelhardt, 2004).  
271 As applies to bedrock boreholes, a delay between drilling and temperature measurement is required for the thermal  
272 disturbance from the drilling to dissipate. For hot-water drilling, this can take 2 years (Barrett et al., 2009;  
273 Engelhardt, 2004). The temperature profile is typically measured using thermistors, recording the temperature  
274 through changes in resistivity to electrical currents. Either a string of thermistors is deployed into the borehole  
275 prior to freezing, and the temperature recorded over time, or the hole can be kept open with drill fluid and  
276 downhole temperature measured with a moving thermistor. More recently, temperature has been recorded also  
277 using distributed temperature systems (DTS; [Suárez et al., 2011](#); [Ukil et al., 2011](#)). The temperature is derived  
278 from the travel time of a laser beam within an optical fibre. All of these methods require thermal equilibration.

279 Once the englacial temperature profile is obtained, GHF estimation can be achieved through three methods.  
280 Firstly, if the borehole reaches the ice-bedrock interface, and the bedrock and overlying ice are in thermal  
281 equilibrium, then the GHF can be estimated in the same way as for bedrock boreholes (e.g. Engelhardt, 2004).  
282 That is, using the temperature gradient in the ice near the ice-bedrock interface but using the thermal conductivity  
283 of ice rather than rock (Equation 1). Secondly, rather than measuring a temperature profile above the bed, the  
284 basal temperature at the ice-bedrock interface can be measured, and temperature modelled through time to  
285 constrain the required GHF (e.g. Fudge et al., 2019). Thirdly, if the borehole doesn't reach bedrock, and similarly  
286 to the previous method, a thermal model is required to constrain GHF (e.g. Zagorodnov et al., 2012). In the  
287 methods where modelling is required, the variables are modified within constraints determined for the location  
288 until the modelled temperature profile best fits the measurements (Fig. 3), and the modelled temperature gradient  
289 within the bedrock used for GHF calculation.

Formatted: Font: 10 pt



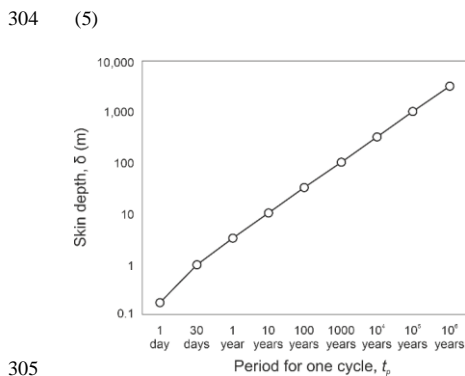
290  
 291 **Fig. 3. An example of temperature measurements (solid black line) and steady state model (dashed grey line) from**  
 292 **which GHF can be estimated. Adapted from (Dahl-Jensen et al., 1999) for Law Dome ice borehole temperature profile.**  
 293 **Note that it is the deeper temperature gradient that is modelled rather than the shallower temperature variation.**

294 **In regions where the ice sheet is frozen to the bed and thermally equilibrated,** GHF can be estimated from  
 295 boreholes that do not reach the bedrock providing that the temperature profile is obtained below the penetration  
 296 depth (or skin depth,  $\delta$ ) of surface temperature variation into the ice sheet. This depth is defined by the circular  
 297 frequency of the variation ( $\omega$ ), and the thermal diffusivity of the material ( $k$ ) according to Equation 4 (Fig. 4;  
 298 Carslaw and Jaeger, 1959; Wangen, 2010).

$$\delta = \sqrt{2k/\omega}$$

300 (4)  
 301 Where circular frequency ( $\omega$ ) is defined by Equation 5, where  $t_p$  is the time for one period (or cycle) of the  
 302 temperature variation (Wangen, 2010).

$$\omega = 2\pi/t_p$$



305  
 11

- Deleted: crosses
- Deleted: the LARISSA Site Beta
- Field Code Changed
- Deleted: Zagorodnov et al. (2012)
- Deleted: from the Bruce Plateau, Antarctic Peninsula
- Deleted: the

311 **Fig. 4. Relationship between skin depth and periodicity of temperature variation through a material of thermal**  
312 **diffusivity,  $k$ , of  $10^{-6} \text{ m}^2 \text{ s}^{-1}$ . This diffusivity is comparable to ice at  $-10^\circ\text{C}$  (James, 1968), or average values of a range**  
313 **of rock types at  $-50^\circ\text{C}$  (Vosteen and Schellschmidt, 2003), and increases with decreasing temperature for both**  
314 **materials.**

315 The deepest significant perturbations of the englacial temperature profile are from glacial-interglacial cycles, and  
316 GHF is best estimated from the englacial temperature profile below the depth at which this effect becomes  
317 negligible. In Greenland, this is the bottom 20 % of the ice sheet, but in areas of low-accumulation in Antarctica  
318 this can extend to much shallower depths. With sufficiently accurate temperature measurements, the full  
319 temperature profile of the ice sheet and the subglacial GHF may be estimated from boreholes penetrating only the  
320 upper 600 m or 20 % of the total ice sheet thickness (Hindmarsh and Ritz, 2012; Mulvaney et al., 2019; Rix et al.,  
321 2019). However, use of shallow boreholes to estimate GHF use simplified thermal models and assumptions on  
322 ice sheet evolution, and so require further validation.

323 However, poorly-constrained thermal effects within the ice sheet propagate uncertainties in GHF estimates from  
324 ice sheet boreholes (Cuffey and Paterson, 2010, Chapter 9). This is a particular problem if there is any ambiguity  
325 as to whether the ice sheet is frozen to the bed. The englacial temperature profile depends on heat sources at the  
326 surface, base, and within the ice (i.e. internal deformation-derived frictional heating). Heat sources that act at the  
327 base of the ice, such as frictional heating by basal motion, are impossible to differentiate from GHF.

### 328 3.3. Marine and onshore unconsolidated sediments

329 Shallow ( $<10$  m) temperature gradients in unconsolidated sediments can be recorded using gravity-driven probes  
330 rather than drilled boreholes. They carry multiple thermistors along the length of the probe that provide a  
331 temperature profile. These measurements can be taken from unconsolidated sediments offshore (e.g. Dziadek et  
332 al., 2019, 2017), in subglacial lakes (Fisher et al., 2015) or below ice shelves (Begeman et al., 2017).

333 As applies to borehole measurements, temperature gradients in unconsolidated sediments must be taken at  
334 sufficient depth to represent the crustal temperature gradient and not be perturbed by temperature variation in the  
335 overlying water or ice (i.e. they must be representative of steady-state conditions). The penetration depth of  
336 temperature variation is dependent on its frequency (Equation 4 and Fig. 4; Carslaw and Jaeger, 1959).  
337 Consequently, diurnal or annual cycles only affect the upper few centimetres to couple of metres of the surface  
338 temperature profile, whilst variations over the last 200-300 years will affect the upper 200 m, and post-glacial  
339 warming can be observed down to 2500 m. These effects are dampened by an overlying water column or ice sheet,  
340 but temperature variation over 10 kyr can still affect basal ice sheet temperatures (Engelhardt, 2004). Although  
341 large ( $>10^\circ\text{C}$ ) seasonal temperature variations are dampened by  $\sim 90\%$  at water depths of 3-5 m (Müller et al.,  
342 2016), long-term variations (e.g. climate-controlled variations in Circumpolar Deep Water over the last  $\sim 12$  kyr;  
343 Hillenbrand et al., 2017) are likely recorded in the upper 3 m at 400 m water depth, 2 m at 700 m depth, and even  
344 the upper  $\sim 1$  m at 1000 m depth (Dziadek et al., 2019).

345 Similarly to borehole temperature measurements, a time delay must be considered between penetration of the  
346 sediments and temperature measurement. A ten minute delay between sediment penetration and measurement is

Deleted: Whilst

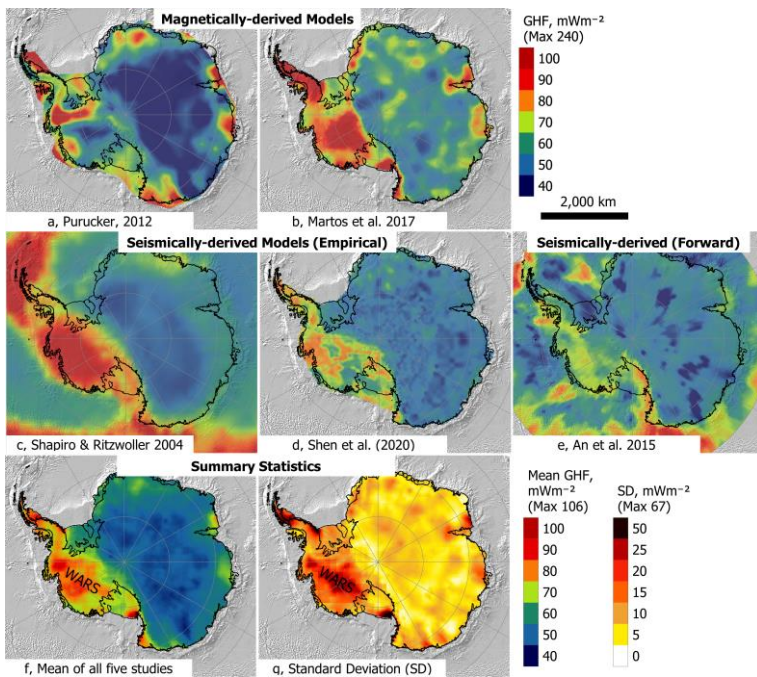
348 sufficient to allow decay of frictional heating, as the temperature decay takes ~100 s (Dziadek et al., 2019; Pfender  
349 and Villingner, 2002).

350 Unconsolidated temperature measurements can also be taken from marine boreholes (e.g. IODP boreholes). For  
351 bedrock boreholes, a delay is required between drilling and measurement for thermal equilibration of the wall  
352 rock and the borehole fluids, which would be problematic for marine boreholes where a drill ship cannot remain  
353 on site. Instead, for boreholes into unconsolidated sediments, a probe is deployed into the borehole bottom  
354 sediments shortly after drilling. Although technology has improved (Davis et al., 1997; Heesemann et al., 2006),  
355 measurements can be affected by frictional heating during and after probe deployment, or by movement of water  
356 and sediments within the hole. Only measurements that exhibit the expected temperature decay rate after  
357 penetration are thus reliable (Hyndman et al., 1987).

#### 358 4. Geophysical and geological methods to estimate GHF

359 In addition to the few and sparse penetrative GHF estimates in Antarctica, continental (Fig. 5) and regional (Fig.  
360 6) estimates have been derived from both solid Earth (geophysical/geological), and glaciological data and models.

Deleted: ¶

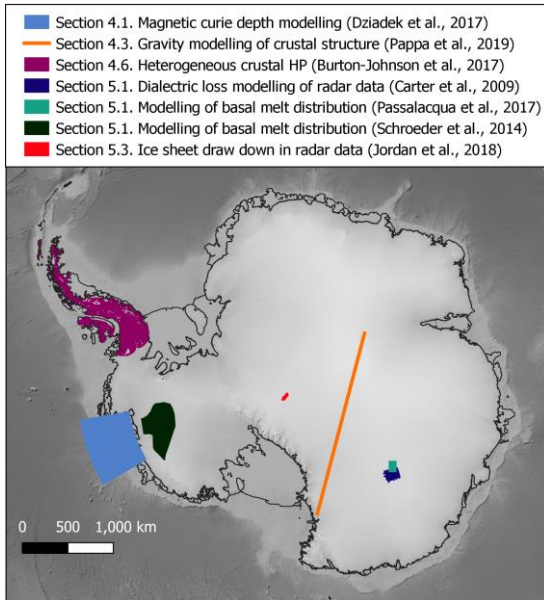


361  
362 **Fig. 5. Continent-scale geophysical estimates of GHF derived from magnetic Curie depth estimates (a and b; Martos et**  
363 **al., 2017, and Purucker, 2012 - an update of Fox Maule et al. 2005), and seismic models (c to e; An et al., 2015b; Shapiro**  
364 **and Ritzwoller, 2004; Shen et al., 2020). The mean and standard deviation of the combined studies are given in f and**  
365 **g, (available in the Supplementary Material), highlighting the large disparities in West Antarctica. WARS – West**  
366 **Antarctic Rift System.**

Field Code Changed

Deleted: (a and b; Fox Maule et al., 2005; Martos et al., 2017a)

Deleted: e



371

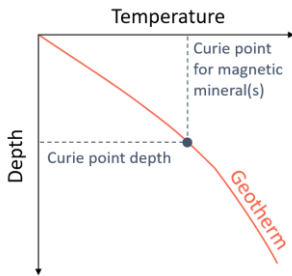
372 **Fig. 6. Coverage of sub-continental scale regional estimates of GHF, with reference to the section where the data is**  
 373 **discussed.**

374 **4.1. Magnetic-derived estimates**

375 As for the penetrative methods of GHF estimation described above (Section 3), geophysical methods also derive  
 376 GHF from a temperature gradient. In this case, magnetic survey data is used to determine the depth at which the  
 377 maximum temperature of ferromagnetic magnetisation is exceeded (the Curie temperature; Haggerty, 1978). This  
 378 Curie temperature is different for different minerals, but is assumed in these studies to be the Curie temperature  
 379 of magnetite (580 °C) as this mineral is most commonly the dominant contributor to crustal magnetisation (Bansal  
 380 et al., 2011; Fox Maule et al., 2005; Langel and Hinze, 1998).

381 Above the Curie temperature, rocks lose their ability to maintain ferromagnetic magnetisation (e.g. Haggerty,  
 382 1978). The depth of this isotherm in the crust (the Curie Point Depth, CPD; Fig. 7 and Fig. 2) is thus assumed to  
 383 be the depth to the bottom of the magnetic source (DBMS) determined from magnetic survey data. The DBMS  
 384 maps a transition zone, rather than an exact depth (Haggerty, 1978), and can provide information on crustal  
 385 temperatures at depths not accessible by other means (Andrés et al., 2018; Okubo et al., 1985). Regions found to  
 386 have a shallower DBMS (and thus an assumed shallower CPD) are expected to have higher average temperature  
 387 gradients, and, therefore, higher GHF (e.g. Aboud et al., 2011; Andrés et al., 2018; Arnaiz-Rodríguez and  
 388 Orihuela, 2013; Bansal et al., 2013, 2011; Bhattacharyya and Leu, 1975; Guimarães et al., 2013; Li et al., 2017;  
 389 Obande et al., 2014; Okubo et al., 1985; Ross et al., 2006; Salem et al., 2014; Tanaka et al., 1999; Trifonova et  
 390 al., 2009).

**Deleted: methods deriving GHF from Curie depth**



392

393 Fig. 7. Approximation of the geothermal gradient from the Curie point depth (CPD). The CPD is assumed to mark the  
 394 base of the magnetic crust (DBMS).

Deleted: Curie point depth

395 The first Antarctic-wide magnetically-derived GHF map (Fox Maule et al., 2005; updated by Purucker, 2012, Fig.  
 396 5a) used the “equivalent source magnetic dipole method” (Mayhew, 1979) to map magnetic anomalies from  
 397 multiple satellites at different altitudes as evenly distributed magnetic dipoles on the Earth’s surface (Dyment and  
 398 Arkani-Hamed, 1998). Due to filtering of the data during processing, this magnetic anomaly distribution is only  
 399 susceptible to shallow, short-wavelength magnetic variation. To calculate the CPD, a long-wavelength CPD model  
 400 was modified until it reproduced the determined short-wavelength anomalies. The temperature gradient  
 401 represented by this CPD was combined with assumed homogenous crustal properties (heat production and  
 402 conductivity) to model the surface heat flow. Due to the high altitude of the satellite data, the horizontal resolution  
 403 of this approach was limited to at least a few hundred kilometres.

Field Code Changed

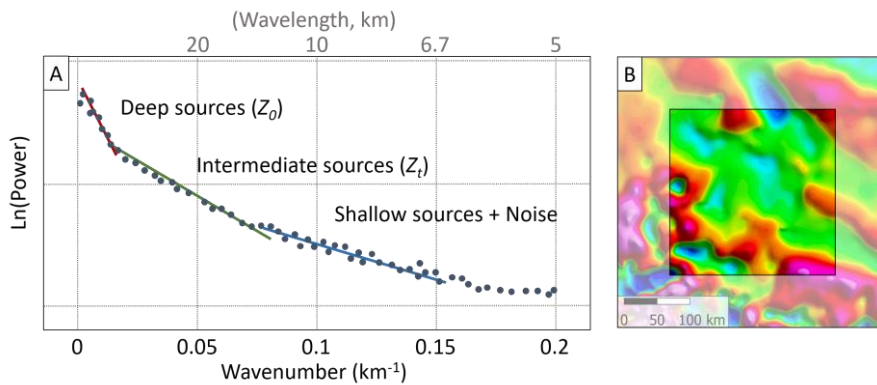
Deleted: (Fox Maule et al., 2005; Fig. 5a)

404 Spectral methods are the alternative and more commonly applied approach to estimating the DBMS, analysing  
 405 the spectrum of wavelengths in magnetic profiles or gridded data (e.g. Blakely, 1996; Okubo et al., 1985; Spector  
 406 and Grant, 1970). These methods depend on the implicit assumption that long wavelength features result from  
 407 deep sources. The depth of this source is calculated from a “power spectrum” (Fig. 8) of wavenumber (the inverse  
 408 of the wavelength) against the logarithm of each wavenumber’s “power” (the square of each wavelength’s  
 409 magnitude after conversion by a Fast Fourier Transformation to describe the spectrum of wavelengths in the  
 410 signal). From this power spectrum (Fig. 8) the top ( $Z_t$ ) and centre ( $Z_0$ ) of the deepest magnetic layer are inferred  
 411 from the slope of the intermediate and long wavelength zone of the spectra derived from magnetic anomaly data.  
 412 The DBMS ( $Z_{DBMS}$ ) stems from the simple geometric relationship between these depths:

413 
$$Z_{DBMS} = 2Z_0 - Z_t$$

414 (6)





417  
 418 **Fig. 8. A) Identification of the slopes of the intermediate and long wavelength magnetic anomalies from the power**  
 419 **spectrum of magnetic anomalies within a single magnetic window (B). For illustration, small circular anomalies in the**  
 420 **magnetic window (B) would correspond to shallow sources in the power spectrum, whilst larger anomalies would**  
 421 **correspond to intermediate and deep sources.**

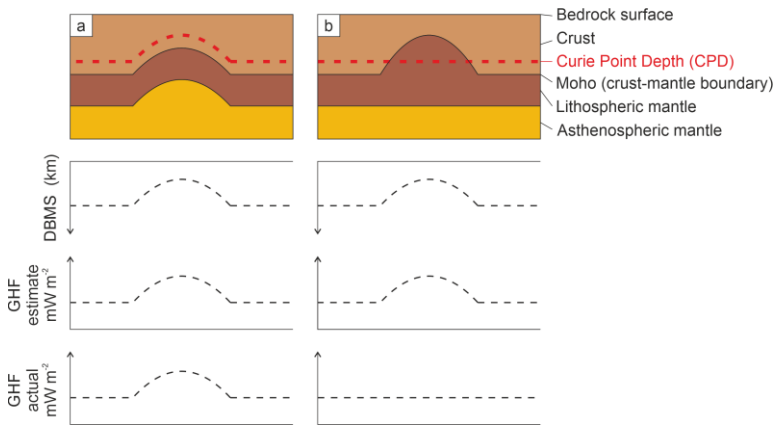
422 To map the DBMS across a study area, the spectra of magnetic anomalies are computed within overlapping  
 423 rectangular windows regularly spaced over the aeromagnetic map. Particularly for gridded data, the dimensions  
 424 of the region chosen to analyse the long wavelength frequencies must be sufficiently large to capture the DBMS.  
 425 Ravat et al. (2007) elaborate that the dimension of the region analysed may need to be (in some cases) up to 10  
 426 times the DBMS, but that dimensions exceeding 200 to 300 km may average different large-scale crustal  
 427 structures. This suggests that satellite data, which typically detects magnetic anomalies in that wavelength, may  
 428 not be suitable for this spectral method of CPD estimation. Choosing the window size therefore forces a trade-off  
 429 between accurately determining the DBMS within each sub-region and resolving small changes in DBMS between  
 430 sub-regions (Ross et al., 2006).

431 Spectral methods have been applied in Antarctica (Dziadek et al., 2017; Martos et al., 2017a; Purucker and  
 432 Whaler, 2007; Fig. 5b and Fig. 6) to combined satellite and airborne magnetic anomaly data (e.g. ADMAP;  
 433 Golynsky et al., 2006; Maus, 2010). The results show a general agreement at a continental scale, but vary  
 434 significantly on a regional scale (Fig. 5). This is related to the resolution of the magnetic anomaly data, particularly  
 435 in regions where only satellite magnetic data are available. Furthermore, regional-scale magnetic anomaly  
 436 databases are usually a mosaic of individual aeromagnetic surveys. Ross et al. (2006) emphasise that subtle  
 437 discontinuities along survey boundaries are caused by differences in survey specifications, such as flight line  
 438 spacing, flight altitude, regional field removal, or the quality of data acquisition. These, for instance, may  
 439 contaminate the long-wavelength signal caused by deep magnetic sources (Grauch, 1993). Long wavelength  
 440 features can also result from shallow but spatially extensive sources, such as volcanic provinces, and can lead to  
 441 an underestimation of the DBMS.

442 CPD estimates assume a homogenous magnetic mineralogy of magnetite, and thus a Curie temperature of 580 °C  
 443 (Bansal et al., 2011; Fox Maule et al., 2005; Langel and Hinze, 1998). This assumption neglects the compositional  
 444 variability in plutonic rocks that lead to Curie temperature ranges between 300 °C and 680 °C, and in cases of

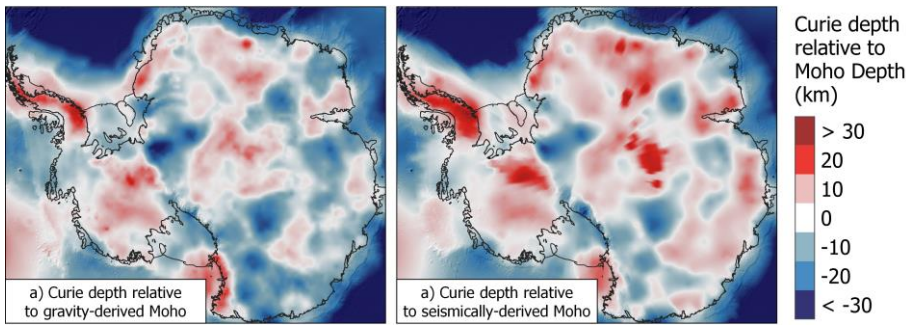
445 magnetic assemblages of Fe-Ni-Co-Cu metal alloys up to 620 °C to 1084 °C (Haggerty, 1978). Without further  
 446 constraints and validations, these assumptions remain the best approach, especially in sparsely sampled regions  
 447 like Antarctica, but introduce uncertainties of several kilometres in Curie depths and consequent uncertainties in  
 448 GHF estimates (Bansal et al., 2011; Ravat et al., 2007). Similarly, in areas of thin crust, non-magnetic mantle  
 449 rocks can be shallower than the Curie depth. In these regions, the calculated CPD will appear shallower due to a  
 450 lack of magnetic minerals in the mantle rocks (Fig. 9; Frost and Shive, 1986; Wasilewski and Mayhew, 1992).  
 451 This can be investigated through comparison of the Antarctic Curie depth estimates with the seismically- or  
 452 gravitationally-derived depth of the crust-mantle boundary (the Moho depth; Fig. 10 and Fig. 2). For example,  
 453 thermal modelling of seismic, gravity, and magnetic data showed the DBMS of the Norwegian margin reflected  
 454 the basement geometry, not the CPD, and that surface heat flow estimates using magnetic CPD models were thus  
 455 unreasonably high (Ebbing et al., 2009).

Deleted: Curie isotherm



456  
 457 **Fig. 9.** Two scenarios illustrating the ambiguity in estimating Curie point depth (CPD) and GHF. a) Estimates from a  
 458 region with a shallow CPD over an area of thin crust. b) Similar but incorrectly interpreted estimates from a region of  
 459 shallow non-magnetic mantle rocks. In scenario (b), the DBMS is shallower despite there being no deviation in the CPD  
 460 depth. DBMS, Depth to the bottom of the magnetic source (assumed to represent the CPD in the GHF estimates  
 461 discussed).

Deleted: Curie isotherm  
 Deleted: Curie isotherm  
 Deleted: Curie isotherm  
 Deleted: -  
 Deleted: B  
 Deleted: M  
 Deleted: S  
 Deleted: Curie depth



462

472 **Fig. 10. Comparison of Curie depth (Martos et al., 2017) and depth of the crust-mantle boundary (the Moho depth)**  
473 **derived from a) gravity modelling (Pappa et al., 2019b), and b) seismic modelling (An et al., 2015a). Negative values**  
474 **show areas where the estimated Curie depth is deeper than the estimated Moho depth, and positive values are where**  
475 **the Curie depth is shallower than the Moho depth.**

476 However, whilst in general the Earth's mantle does not contribute to the magnetic signal (due to its weak  
477 magnetisation and high temperature conditions), in some cases the Curie depth may indeed lie within the mantle.  
478 This occurs where metallic magnetic phases in the mantle beneath old, tectonically stable crust ("cratons"; Ferré  
479 et al., 2013) or subduction regions (e.g. Blakely et al., 2005) contribute to mantle magnetisation. In these settings  
480 the crust-mantle boundary should not be considered an absolute magnetic boundary (Ferré et al., 2013). This  
481 implies that if in a given region the Moho depths are shallower than the deepest magnetic layer, a magnetic mantle  
482 at temperatures below the Curie temperature may be considered. However, even in these cases the upper mantle  
483 susceptibility will be more than 1-2 magnitudes smaller than the overlying crust. This is not considered in current  
484 spectral methods assuming constant susceptibility. Consequently, Curie depth methods yield non-unique  
485 solutions, and further available constraints and observations need to be considered, when interpreting the Curie  
486 temperature distribution (e.g. geological evidence, borehole measurements, and Moho depth estimates).

#### 487 4.2. Seismic-derived estimates

488 Temperature is the dominant control on seismic velocity in the mantle (e.g. Carlson et al., 2005), and hence the  
489 mantle heat flow at the base of the Antarctic crust can be determined from seismic data. By determining the change  
490 in seismic velocities marking the density discontinuity at the lithosphere-asthenosphere boundary (Fig. 2) the  
491 depth of the 1330°C isotherm can be estimated. This is the "mantle adiabat" marking the top of the seismic low-  
492 velocity zone, and the change from a solid to ductile mantle (Fig. 2). The continental-scale GHF can then be  
493 estimated by assuming the heat production and conductivity of the lithosphere above this boundary, and  
494 integrating this with the seismically-derived mantle heat flow (An et al., 2015b; Fig. 5d). However, the  
495 seismically-derived, continent-scale Antarctic GHF model of An et al. (2015a) (Fig. 5d) is limited to a lateral  
496 spatial resolution of >120 km, assumes a laterally uniform crustal structure, and is insensitive to the lithospheric  
497 geotherm (instead it inversely correlates with crustal thickness).

498 Composition also affects seismic velocities. For example, a 2% increase in velocity can be explained either by a  
499 120°C decrease in temperature, a 7.5% depletion in iron, or a 15% depletion in aluminium (Godey et al., 2004).  
500 Slow mantle velocities at subduction zones can also be caused by water or hydrous fluids serpentinising the mantle  
501 wedge (Fig. 2; Kawakatsu and Watada, 2007). However, velocity in the Antarctic seismic model (An et al., 2015b)  
502 does not account for variability of mantle compositions, mineralogy, grain size, or water content of the mantle or  
503 crust. An uncertainty in the lithospheric thickness of 15-30 km was assumed by (An et al., 2015b) based on the  
504 150°C temperature uncertainty, but ~50 km uncertainty for ~200 km thick lithosphere may be more accurate  
505 (Artemieva, 2011; Godey et al., 2004). In addition, seismological models suffer from limited and inconsistent  
506 spatial coverage, which can lead to discrepancies in upper mantle velocities and differences in Moho depths (Fig.  
507 2) up to 10 km, even for the same receiving station (An et al., 2015b supporting information; Pappa et al., 2019).

508 Some constraints on the mantle and lithosphere composition can be determined from xenoliths (rock fragments  
509 of the deep crust or mantle entrained in magma rising from depth) or exposed deep crustal sections, where

Deleted: estimates

511 variation in temperature and composition with depth can be determined from the metamorphic minerals present.  
512 Constraints can also be derived empirically by comparing the seismic velocity with similar regions. Shapiro and  
513 Ritzwoller (2004) (Fig. 5c) extrapolated global heat flow measurements to Antarctica based on the assumption  
514 that structurally similar regions have similar magnitudes of GHF. This was achieved by calculating a spatially  
515 variable “similarity functional” determined from the differences between the seismic velocity and seismic Moho  
516 depth between a location of interest and a comparable location elsewhere. A histogram of heat flow measurements  
517 could then be assigned to the location of interest in Antarctica based on the similarity-weighted sum of  
518 measurements from structurally similar regions, and the mean values of these distributions mapped as continental  
519 heat flow. Spatial resolution was limited to the lateral resolution of the global shear velocity model across  
520 Antarctica (600-1000 km; Shapiro and Ritzwoller, 2002). Although the studies of Shapiro and Ritzwoller (2004)  
521 and An et al. (2015a) both used seismic data and are thus frequently compared, it is important to highlight that  
522 they use very different approaches in deriving heat flow (the former employing a probabilistic approach and the  
523 latter using forward modelling).

524 The empirical seismically-derived model for Antarctica has recently been revised (Fig. 5d; Shen et al., 2020).  
525 Rather than the low-resolution global database used by Shapiro and Ritzwoller (2004), an Antarctic seismic model  
526 was derived and compared with the high-resolution seismic model and GHF measurements of the USA; again  
527 calculating spatially variable similarity functionals to compare the data. Recognising the non-unique solutions  
528 provided by this method, Shen et al. (2020) also map the associated uncertainties of their model.

#### 529 4.3. Gravity model-derived estimates

530 Satellite gravity data has been used as an alternative to seismic modelling to determine crustal thickness. Pappa  
531 et al. (2019b) used satellite gravity data, a model of global gravity variation (the “geoid”), surface and bedrock  
532 topography, and assumed rock and ice densities to calculate the topographically-corrected variation of gravity in  
533 Antarctica (the “Bouguer anomaly”), from which the depth of the crust-mantle boundary could be calculated. This  
534 approach to calculate crustal thickness is sensitive to long-wavelength (>150 km) features representing deep  
535 structures, rather than short-wavelength, near surface density changes. However, gravity-modelling solutions are  
536 non-unique, and require additional constraints on the density contrast between the crust and mantle at a reference  
537 depth, and/or seismic depth constraints on crustal thickness.

538 Using the gravity-derived crustal thickness estimates, cross-sectional models of the mantle and lithospheric  
539 structure were calculated, with adjustments made to crustal density and crustal thickness until the models reflected  
540 the observed variation in gravity and elevation (Pappa et al., 2019b). By assigning assumed values of heat  
541 productivity and thermal conductivity values to the modelled cross-sections, surface heat flow was calculated  
542 along the line of the modelled cross-section (Fig. 6) ↓

#### 543 4.4. Conjugate margin-derived estimates

544 An alternative approach to constrain the probable GHF of East Antarctica is to compare it with its Gondwanan  
545 conjugate margins, reconstructed prior to the breakup of the supercontinent (Fig. 11). Plate tectonic  
546 reconstructions indicate that the subglacial geology of East Antarctica is comparable to the margins of Australia,  
547 Africa, and India (Aitken et al., 2016; Daczko et al., 2018; Ferraccioli et al., 2011; Flowerdew et al., 2013; Mulder

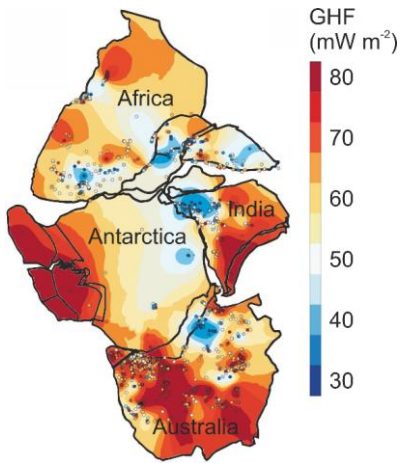
Deleted: modelling

Commented [BA1]: I have been informed that there is no current plan to publish a surface heat flow map from the crustal model, so this has been removed.

Deleted: A 3D lithospheric model has since been published (Pappa et al., 2019a), and a map of Antarctica’s resultant estimated GHF is in preparation for publication (pers. comms.).

Deleted: s

554 et al., 2019). By kriging the heat flow measurements of the continents in their pre-Gondwana breakup  
555 arrangement, Pollett et al. (2019) interpolated a heat flow surface through Antarctica and its conjugate margins  
556 (Fig. 11). This method highlighted similarities and differences between the most recent seismic and magnetically  
557 derived geophysical models of Antarctic heat flow (An et al., 2015b; Martos et al., 2017) with the better  
558 constrained heat flow of the conjugate margins. In particular, this approach showed reasonable agreement along  
559 the margin with Africa, but an absence in either the magnetic or seismic models of high heat flow provinces in  
560 East Antarctica comparable with south Australia; an absence of the low heat flow of SW Australia in the  
561 magnetically-derived model of East Antarctica (Martos et al., 2017); and an absence of the high heat flow of  
562 northern India in the seismically-derived model of East Antarctica (An et al., 2015b). However, when  
563 extrapolating heat flow away from the conjugate margins into the interior of Antarctica, this approach is  
564 susceptible to the method of interpolation used and the quality and scarcity of the borehole-derived GHF estimates  
565 in the interior of Antarctica (Section 3).



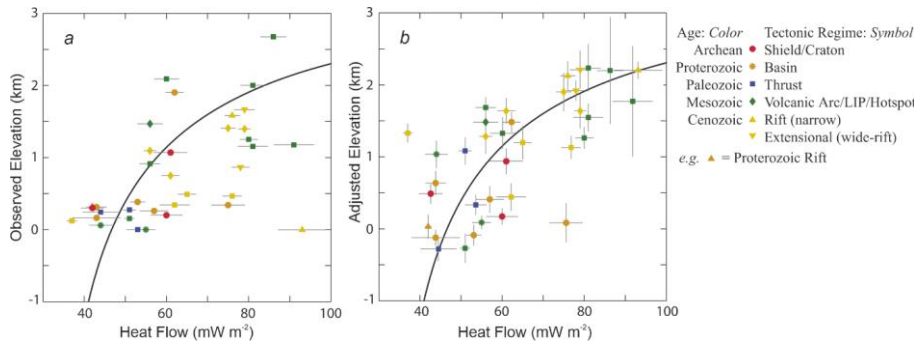
566  
567 **Fig. 11. Interpolated heat flow map of Gondwana, showing the derivation of Antarctic GHF from the reconstructed**  
568 **conjugate margins of the supercontinent. Terrestrial heat flow data shown by points. Adapted from Pollett et al. (2019).**

#### 569 4.5. Isostatic elevation

570 In addition to crustal thickness and density, the thermal state of the lithosphere also contributes to its isostasy and  
571 observed surface elevation. The effect of thermal isostasy on the bathymetry of oceanic crust is well recognised:  
572 as oceanic crust migrates from the spreading ridge it cools, thickens, contracts, and subsides (Stein and Stein,  
573 1992). However, the effect of thermal isostasy on continents is masked by compositional contributions to isostatic  
574 elevation (i.e. lateral variations in crustal thickness and density, Fig. 12a; Hasterok and Chapman, 2007b, 2007a).

Deleted:

Deleted:



577  
 578 **Fig. 12. Relationship of the median observed (a) and adjusted (b) elevation and median compiled heat flow values of 36**  
 579 **geological provinces on the land and continental shelves of North America, ranging from 30 - 2082 x 10<sup>3</sup> km<sup>2</sup>. Compiled**  
 580 **heat flow data excluded values outside of the range 20 - 120 mW m<sup>-2</sup> as these values were most likely affected by near**  
 581 **surface processes (e.g. hydrothermal circulation) or shallow magmatism, and do not reflect the lithosphere's thermal**  
 582 **state. Observed elevations are converted to adjusted elevation by normalising according to their seismically-derived**  
 583 **crustal thickness and crustal density and an equation for thickness and density-based isostasy. The black curve shows**  
 584 **the best-fitting thermal-isostatic model for North American adjusted elevation and heat flow. Adapted from Hasterok**  
 585 **and Chapman (2007a).**

586 Hasterok and Chapman (2007b, 2007a) developed a methodology for investigating thermal isostasy in the  
 587 continental lithosphere by normalising the observed elevation using an isostatic correction. The calculated  
 588 compositionally-corrected elevation generally increases with increasing surface heat flow (Fig. 12b). This  
 589 approach was used to derive the thermal contribution to isostatic elevation of Australia and North America, and  
 590 estimate the continental sub-lithospheric and radiogenic heat flow (Hasterok and Chapman, 2007b; Hasterok and  
 591 Gard, 2016). Whilst in general, the compositionally-corrected elevation and surface heat flow values followed the  
 592 modelled curve for thermal isostatic equilibrium (Fig. 12b), anomalous regions lie away from this curve. These  
 593 anomalies result from: 1) additional sources of buoyancy and/or dynamic support (e.g. anomalously buoyant  
 594 mantle lithosphere); 2) anomalous surface heat flow, not representative of the deeper thermal regime (e.g. high  
 595 concentration of heat producing elements in the shallow crust); 3) deviations from the thermal properties of the  
 596 reference crustal model (e.g. heat production); or 4) combinations of these properties (Hasterok and Gard, 2016).

597 Although developed for regions of known heat flow, application of this approach to Antarctica (Hasterok et al.,  
 598 2019) may provide an alternative estimate of heat flow based largely on two well-constrained variables: surface  
 599 and bedrock topography. However, it is dependent on the quality of constraints on crustal thickness, density, heat  
 600 production, and thermophysical properties of the upper crust (of which uncertainty in upper crustal heat production  
 601 has the largest effect; Hasterok and Chapman, 2007b). For example, regions where high surface heat flow is  
 602 dominantly from anomalously high upper crustal heat production will have lower elevations than regions of  
 603 similar surface heat flow but with lower upper crustal heat production. Crust that has experienced tectonic and  
 604 magmatic activity in the Cenozoic (i.e. <66 Ma) may be in a transient rather steady-state thermal regime, so this  
 605 approach may have challenges in West Antarctica. Steady-state thermal modelling is thus more applicable to the  
 606 old, stable crust of East Antarctica; particularly if the heat flow and isostasy of the conjugate margins are  
 607 considered (Hasterok and Gard, 2016; Pollett et al., 2019). However, differences between the crustal thickness

**Deleted:** The normalised elevation ( $\epsilon'$ ) is calculated from Equation 7 (Han and Chapman, 1995):  

$$\epsilon' = \epsilon + h'_c \left(1 - \frac{\rho'_c}{\rho_m}\right) - h_c \left(1 - \frac{\rho_c}{\rho_m}\right) \quad (7)$$

Where  $\epsilon$  is the observed elevation;  $h_c$  and  $\rho_c$  are respectively the seismically-derived crustal thickness and density of the study area;  $h'_c$  and  $\rho'_c$  are the thickness and density respectively of a standard crustal column; and  $\rho_m$  is the mantle density. When the crust is below sea level, an additional term including bathymetric water depth ( $\epsilon_{obs}$ ) and seawater density ( $\rho_w$ ) are included (Equation 8; Han and Chapman, 1995):

$$\epsilon' = \epsilon + h'_c \left(1 - \frac{\rho'_c}{\rho_m}\right) - h_c \left(1 - \frac{\rho_c}{\rho_m}\right) - \left(\frac{\epsilon_{obs} \rho_w}{\rho_m}\right) \quad (8)$$

**Deleted:** C

**Deleted:**

**Deleted:** By differentiating the different contributions to isostatic elevation, it was shown that crustal thickness and density contribute ~3 km of the observed elevation range of North America, and thermal isostasy contributes a further ~3 km; similar in magnitude to the effect of thermal isostasy on oceanic lithosphere (Hasterok and Chapman, 2007a, 2007b). However, there are uncertainties in the thermal isostasy model associated with the assumed properties, including thermal conductivity, thermal expansion, and heat production in the upper and lower crust, of which uncertainty in upper crustal heat production has the largest effect (Hasterok and Chapman, 2007b). Uncertainties in the seismic data used for calculating crustal thickness and density affect the uncertainty of the compositional isostatic correction (Equations 7 and 8; Hasterok and Chapman, 2007b).

**Deleted:**

**Deleted:** seismic

**Deleted:** and

**Deleted:** as well as constraints on the

643 based on gravity modelling and isostatic elevation modelling may indicate variable densities and/or compositions  
644 of the underlying mantle (Pappa et al., 2019b, 2019a).

#### 645 4.6. Enhancement of GHF estimates by incorporation of heterogeneous crustal compositions

646 The geophysical approaches described above assume laterally homogenous heat production in the crust. However,  
647 given the geologically heterogeneous composition of the crust, it is important to consider the effects of variable  
648 lithospheric heat production and incorporate this into forward models of GHF.

649 Radiogenic heat production in the upper crust contributes an estimated 26-40 % of the total continental GHF  
650 (Artemieva and Mooney, 2001; Hasterok and Chapman, 2007b, 2011; Pollack and Chapman, 1977; Vitorello and  
651 Pollack, 1980). Radioactive isotopes of the heat producing elements (HPEs) uranium, thorium, and potassium (U,  
652 Th, and K) are responsible for ~98% of lithospheric heat production (Beardsmore and Cull, 2001). These elements  
653 are incompatible with mineral structures in the mantle and lower crust, so concentrate in the upper crust and  
654 decrease in abundance with depth during planetary differentiation (the chemical and physical separation of an  
655 initially homogenous planetary body into one with an iron-rich core, magnesium-silicate-rich mantle, and a thin  
656 silicate-rich crust; Roy et al., 1968; Rudnick and Fountain, 1995).

657 The upper crust itself is highly heterogeneous in composition. HPE distribution is determined by their  
658 compatibility in different minerals, concentrating them in Si-rich silicic rocks (e.g. granite or rhyolite) relative to  
659 Fe-rich mafic rocks (e.g. gabbro or basalt). Immature sediments inherit the HPE abundance of their eroded source  
660 rocks, but decrease in HPE abundance with increasing maturity and the consequent decrease in their lithic contents  
661 (Burton-Johnson et al., 2017; Rybach, 1986). Crustal heat production is thus heterogeneous, and the most  
662 significant control of HPE abundance and resultant heat production in the lithosphere is the distribution of the  
663 composite lithologies of the upper crust (Lachenbruch, 1968; Sandiford and McLaren, 2002; Taylor and  
664 McLennan, 1985).

##### 665 4.6.1. Whole rock geochemical analysis of heat production

666 Heat production of exposed lithologies can be determined from their concentrations of HPE (U, Th, and K)  
667 determined by geochemical analysis, or by airborne or ground-based gamma ray surveys. Radiogenic heat  
668 production for each sample ( $H$ ,  $\mu\text{Wm}^{-3}$ ) for the present day ( $t=0$ ) can be determined from Equation 7 (Turcotte  
669 and Schubert, 2014):

$$670 \quad H = (0.9928C_0^U H^{U238} + 0.0071C_0^U H^{U235} + C_0^{Th} H^{Th232} + 0.000119C_0^K H^{K40})D$$

671 (7)

672 Where  $C_0^U$ ,  $C_0^{Th}$  and  $C_0^K$  are the measured concentrations (ppm) of U, Th and K respectively;  $H^{U238}$ ,  $H^{U235}$ ,  $H^{Th232}$   
673 and  $H^{K40}$  are the heat productivities of the respective isotopes  $^{238}\text{U}$  ( $9.37 \times 10^{-5} \text{ Wkg}^{-1}$ ),  $^{235}\text{U}$  ( $5.69 \times 10^{-4} \text{ Wkg}^{-1}$ ),  
674  $^{232}\text{Th}$  ( $2.69 \times 10^{-5} \text{ Wkg}^{-1}$ ) and  $^{40}\text{K}$  ( $2.79 \times 10^{-5} \text{ Wkg}^{-1}$ ); and  $D$  is the assumed density of the rock (e.g. 2800, 2850,  
675 and  $3000 \text{ kg m}^{-3}$  for felsic, intermediate, and mafic granulites, respectively; Hasterok and Chapman, 2011). When  
676 using geochemical data to calculate heat production, this allows new and archive data to be used to calculate the  
677 heat production of the sampled outcrop. However, many archive analyses occurred prior to the development of

Deleted: 9

Deleted: 9

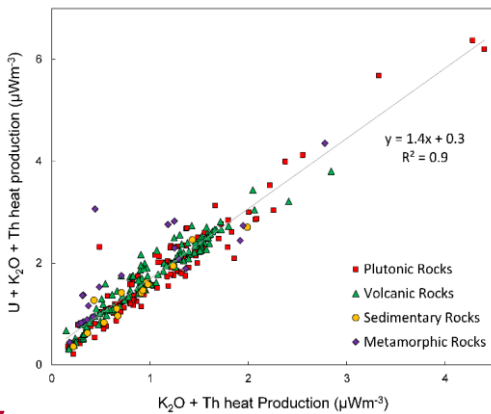
680 accurate U quantification (e.g. by high resolution XRF or ICP-MS). An empirical relationship (Equation 8;  
 681 Burton-Johnson et al., 2017) allows calculation of total U, Th, and K heat production ( $H$ ) from samples possessing  
 682 only Th and K data ( $H_{K,Th}$ ; correlation coefficient,  $R^2 = 0.9$ ; Fig. 13).

$$H = 1.4H_{K,Th} + 0.3$$

684 (8)

685 Heat production values can be assigned to bedrock geology either by interpolation of the point values or by  
 686 assigning the point values to the mapped geology and assigning their average value to the geological unit; the  
 687 average being either the mean (Veikkolainen and Kukkonen, 2019), area weighted mean (Slagstad, 2008), or  
 688 median value (Burton-Johnson et al., 2017). Interpolation shows spatial variability within a unit, but is affected  
 689 by the interpolation method used, requires sufficient and evenly distributed data coverage, and is affected by  
 690 anomalous values. For these reasons, the median values were used for the unevenly distributed archive data of the  
 691 Antarctic Peninsula (Burton-Johnson et al., 2017). In Antarctica, maps of median (Antarctic Peninsula, Fig. 6;  
 692 Burton-Johnson et al., 2017) and transects of mean (coastal East Antarctica; Carson et al., 2014; Carson and  
 693 Pittard, 2012) heat production data have been integrated with geophysical models of the deeper heat flow to  
 694 estimate the total GHF at the bedrock surface.

695 Integrating spatially variable upper crustal heat production into the geophysical models of Antarctic GHF resulted  
 696 in increased estimated spatial GHF variability, including local regions of high GHF above HPE-enriched granitic  
 697 intrusions (Carson et al., 2014; Leat et al., 2018). The relative concentration of the HPE into the upper crust may  
 698 result in it contributing a highly variable 6-70% of the total GHF, although 3D crustal modelling is required to  
 699 constrain its thickness (Burton-Johnson et al., 2017). This modelling also showed the impact of sedimentary basins  
 700 on GHF distribution, as thick, extensive units of immature, clay-rich sediments may form extensive regions of  
 701 enhanced GHF, even though more mature, quartz-rich sediments are associated with low GHF (Burton-Johnson  
 702 et al., 2017). This highlights the importance of accurately constraining the upper crustal geology and its chemistry  
 703 when estimating GHF from geophysical data.



704

Deleted: ly

Deleted: 10

Deleted: 10

Deleted: this approach has been applied to the Antarctic Peninsula (Burton-Johnson et al., 2017; Fig. 6) and along coastal outcrops in East Antarctica (Carson et al., 2014; Carson and Pittard, 2012). These studies

Deleted: their maps of variable lithospheric heat production

Deleted: (Carson et al., 2014; Leat et al., 2018)¶



714 **Fig. 13. The relationship between total calculated heat production from U, K<sub>2</sub>O and Th decay and the heat production**  
715 **values from K<sub>2</sub>O and Th only for different broad lithologies, enabling total heat production calculation from incomplete**  
716 **archive data (n = 319; Burton-Johnson et al., 2017).**

#### 717 **4.6.2. Glacially-derived rock clasts**

718 Although heat production can be determined for exposed bedrock, the likely heat production of the rocks beneath  
719 the Antarctic ice sheet is harder to constrain. To investigate East Antarctica, glacial clasts were sampled from  
720 moraines adjacent to the Transantarctic Mountains (Goodge, 2018). Granitic samples older than 500 Ma (Ross  
721 Orogen) were selected as likely lithologies of the interior of East Antarctica, as these are the dominant lithologies  
722 of other Precambrian cratons (>542 Ma regions of tectonically-stable continental crust; e.g. central Canada). These  
723 clasts were analysed for their HPE abundance and attributed to their likely source area (the drainage basin of their  
724 associated glaciers). A probable range of subglacial heat flow values was estimated by assuming mantle and lower  
725 crustal GHF values and a thickness for the upper crust based on other Precambrian shields. This indicates that  
726 East Antarctic heat flow is comparable to other Precambrian cratons, and comparable to geophysical models of  
727 East Antarctic heat flow (Van Liefferinge and Pattyn, 2013). However, broader application of this approach is  
728 biased towards more erosion resistant rock types, whilst less competent lithologies will not be preserved after  
729 glacial transport and deposition.

#### 730 **4.6.3. Gamma ray spectrometry**

731 Rather than whole rock geochemical analysis, the gamma ray spectrum can be used to determine the  
732 concentrations of radioactive isotopes, including those of K, Th, and U, and was first used for U exploration.  
733 Gamma ray spectrometry can be surveyed in the field, on samples, or from the air. Airborne surveys can cover  
734 large areas, and have been used to survey Western Australia, SW England, and all of Finland (Beamish and Busby,  
735 2016; Bodorkos et al., 2004; Hyvönen et al., 1972). However, the data requires multiple corrections, and the  
736 recorded data integrates the radiation from the bedrock, surface cover (including soil and vegetation), the  
737 atmosphere, cosmic radiation, and the aircraft, making the data less accurate than ground measurements or sample  
738 analysis (Veikkolainen and Kukkonen, 2019). The technique is only sensitive to the upper 25cm of the land  
739 surface, with overlying sediments and water bodies masking the radiation and leading to underestimates of heat  
740 production (Phaneuf and Mareschal, 2014). However, if the signal could be linked to mapped geological units and  
741 other evidence for subglacial geology (e.g. aeromagnetic and gravity anomalies) it may be feasible to extrapolate  
742 the calculated heat production beneath the ice sheet. Hand-held gamma ray spectrometry studies, where heat  
743 production can be correlated with lithology along exhumed crustal profiles, show promise in this regard elsewhere  
744 (Alessio et al., 2018).

#### 745 **4.6.4. Crustal structure**

746 Whilst surface HPE distribution can be constrained by measurements, the vertical distribution is more ambiguous.  
747 In heat flow models, heat production is often assumed to decrease exponentially with depth (e.g. Fox Maule et al.,  
748 2005; Martos et al., 2017). This exponential model was developed to explain observations from exposures of  
749 large, thick composite granite bodies (batholiths) where magma was initially emplaced at different depths in the  
750 crust (Lachenbruch, 1968, 1970; Swanberg, 1972) and reflects a proposed decrease in HPE abundance with

Deleted: ¶

752 increasing metamorphic grade (Lachenbruch, 1968; Sandiford and McLaren, 2002). However, this relationship  
753 has been challenged by other studies comparing HPE abundance and metamorphic grade (Alessio et al., 2018;  
754 Veikkolainen and Kukkonen, 2019), showing that the lithological change from the largely silicic upper crust to  
755 the mafic lower crust has a larger influence on HPE abundance than metamorphic grade (Bea, 2012; Bea and  
756 Montero, 1999). Deep (9-12 km) boreholes also show a correlation of heat production with lithology, but not with  
757 depth (Clauser et al., 1997; Popov et al., 1999). In fact, heat production *increased* for the first 2 km of the 12 km  
758 superdeep well of the Kola Peninsula, Russia, then remained variable but high with increasing depth (Popov et  
759 al., 1999). Similarly, heat production increases below 3 km in the recent 5 km UD-1 well of the Cornubian  
760 Batholith, UK (Dalby et al., 2020). As such, the available evidence indicates that the first-order HPE distribution  
761 is controlled by the HPE abundance of the crust prior to metamorphism and the vertical distribution of the crust's  
762 composite rock types. Inversely, it indicates that HPE distribution is not controlled by depth in the crust or the  
763 degree of metamorphism resulting from the increase in pressure and temperature.

764 Without evidence for the deeper structure of the crustal column, the lithological and HPE distribution of the  
765 lithosphere can instead be modelled as layers of variable thickness and heat production: the upper crust, middle  
766 crust, lower crust, and mantle lithosphere. Surface heat flow is largely insensitive to variations in the heat  
767 production or thickness of the mafic lower crust and mantle lithosphere due to their heat production being ~1-2  
768 orders of magnitude lower than that of the upper crust (Hasterok and Chapman, 2011; Rudnick and Fountain,  
769 1995; Rudnick et al., 1998). The middle crustal layer can either be excluded (Hasterok and Chapman, 2011) or  
770 treated as a layer of invariable heat production (e.g. An et al., 2015, for Antarctica) due to its low heat production  
771 compared with the range of the upper crust. Lithospheric heat production can thus be defined by the heat  
772 production and relative thickness of the upper crust, or upper crustal heat producing layer (Hasterok and Chapman,  
773 2011). This can be defined by:

774 
$$Q_s = Q_b + H_{UC}D = FQ_s + H_{UC}D = H_{UC}D/(1 - F)$$

775 

Deleted: 11

776 Where  $Q_s$  is the surface heat flow,  $Q_b$  is the basal heat flow of the upper crust,  $H_{UC}$  is upper crustal heat production,  
777  $D$  is the thickness of the upper crustal heat producing layer, and  $F$  is the proportion of the surface heat flow  
778 contributed by the basal heat flow ( $Q_b$ ) (adapted from Hasterok and Chapman, 2011).

779 Rather than a simple layered model, more complex 2D or 3D models of upper crustal structure can be developed  
780 using geophysical data, and the 2D or 3D crustal units assigned heat production and conductivity values based on  
781 analyses of representative exposures. A 3D crustal model derived from gravity and aeromagnetic data was  
782 developed to map heat flow in Norway (Ebbing et al., 2006; Olesen et al., 2007). In Antarctica, this has been  
783 applied in 2D to the high heat production granites of the Ellsworth-Whitmore Mountains using airborne magnetic  
784 and gravity data and bedrock topography (Leat et al., 2018), and the Transantarctic Mountains using topography  
785 and satellite gravity data (Pappa et al., 2019b).

786 Even though variability in deep lithospheric heat production has a smaller effect on surface heat flow than  
787 variability in upper crustal heat production (Hasterok and Chapman, 2011), it is not homogenous. These  
788 thermophysical properties can be constrained from deep xenoliths (fragments of rock entrained in magma rising

Deleted: Whilst

791 from depth) (Hasterok and Chapman, 2011; Martin et al., 2014) and crustal sections (Berg et al., 1989), which  
792 can also inform on the local geothermal gradient at the time of their crystallisation.

793 To help constrain the properties of the Antarctic mantle, including its influence on Antarctic heat flow, a  
794 Geological Society of London Memoir is currently being compiled summarising the data gained from mantle  
795 xenoliths (Martin and van der Wal, in prep.). This includes a sample database, and a compilation of their grain  
796 size and water content. These xenoliths are from shallow sources, as their occurrence is biased towards areas of  
797 crustal rifting where the lithosphere is thinner, although some xenoliths are from deeper sources (e.g. from the  
798 Amery Rift and Ferrar Dolerite).

## 799 5. Glaciological inverse estimation of GHF

800 Although geothermal heat flow has a geological derivation, it can also be constrained by multiple approaches  
801 through its observable effects on the overlying ice sheet. Inverse modelling can be applied to observed  
802 glaciological properties (e.g. glacial flow and melt rates) and the required GHF calculated. We will describe in  
803 this section different methods used in glaciology to derive GHF.

### 804 5.1. Subglacial water

805 The presence of subglacial water can be detected with an ice-penetrating radar. The reflective properties of the  
806 ice-bedrock interface depend on the presence of water and, with certain caveats, radar surveys can be used to map  
807 subglacial water. In general terms, a glaciological model can then be used to estimate the values of GHF that  
808 better predict where basal temperatures reach the pressure melting point and melting occurs. We will describe in  
809 this Section examples of this approach.

810 Carter et al. (2009) modelled the dielectric loss of radar data through the ice column around Dome C in East  
811 Antarctica (Fig. 6) to infer the basal reflectivity and verify the presence of subglacial water. Because the  
812 temperature profile of the ice sheet is one parameter affecting dielectric loss, this approach required inference of  
813 the basal heat flow from temperature-depth modelling over the last 254 ka. The Shapiro and Ritzwoller (2004)  
814 GHF model was used initially (see section “4.2. Seismic estimates”), but when the calculated vertical ice velocity  
815 ( $m_w$ ) at the bed exceeded the initial melt rate ( $m_T$ ), the GHF was modified until  $m_T$  and  $m_w$  were equal. This  
816 approach identified localised high GHF anomalies, but (excepting these anomalies) they calculated that 66 % of  
817 the study area was either at or near the pressure melting point (anywhere that ice is thicker than 3500 m) without  
818 invoking enhanced GHF.

819 Schroeder et al. (2014) modelled the spatial distribution of melt beneath the ice sheet in the Thwaites Glacier  
820 catchment (Fig. 6) by mapping the relative bed echo strength of radar data in the region and modelling the water  
821 routing required to match these observations by routing alone (without heterogeneous basal melting). These  
822 routing models were based on the radar-derived ice thickness and surface slope. The 50 selected routing models  
823 were used to model the relative melt required to reproduce the observed echo strengths of each routing model.  
824 This relative melt model was in turn scaled to match the total melt water produced in an ice sheet model of the  
825 Thwaites Glacier incorporating frictional melting, horizontal advection, and an assumed uniform GHF. By  
826 subtracting the frictional and advective contributions, the GHF required to produce the remaining melt could be

**Deleted:** <#>Detrital material¶

<#>Whilst heat production can be determined for exposed bedrock, the likely heat production of the rocks beneath the Antarctic ice sheet is harder to constrain. To investigate East Antarctica, glacial clasts were sampled from moraines adjacent to the Transantarctic Mountains (Goodge, 2018). Granitic samples older than 500 Ma (Ross Orogen) were selected as likely lithologies of the interior of East Antarctica, as these are the dominant lithologies of other Precambrian cratons (>542 Ma regions of tectonically-stable continental crust; e.g. central Canada). These clasts were analysed for their HPE abundance and attributed to their likely source area (the drainage basin of their associated glaciers). A probable range of subglacial heat flow values was estimated by assuming mantle and lower crustal GHF values and a thickness for the upper crust based on other Precambrian shields. This indicates that East Antarctic heat flow is comparable to other Precambrian cratons, and comparable to geophysical models of East Antarctic heat flow (Van Liefferinge and Pattyn, 2013). However, broader application of this approach is biased towards more erosion resistant rock types, whilst less competent lithologies will not be preserved after glacial transport and deposition.¶

**Deleted:** Rather than using a forward modelling approach (i.e. determining the geological contributions and estimating their resultant heat flow), an i

**Deleted:** approach

**Deleted:** by modelling

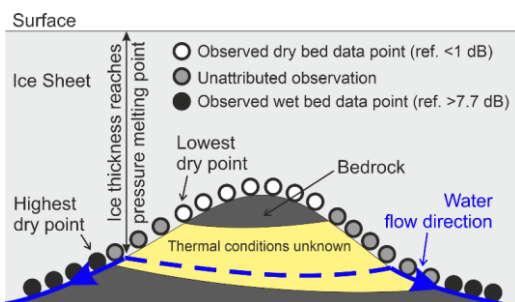
**Deleted:** ing the required heat flow

**Deleted:** A

**Deleted:** ground

859 calculated. This approach predicted very high heat flow in this region (114 to >200 mW m<sup>-2</sup>), with the highest  
860 heat flow focused around observed and inferred subglacial volcanoes.

861 With the aim of determining appropriate sites of low basal melting for old-ice drilling, Passalacqua et al. (2017)  
862 also used radar evidence for basal melting and ice sheet modelling to determine GHF around Dome C (Fig. 6).  
863 Wet and dry bed conditions were identified from radar data and ten spots were identified on bedrock topographic  
864 features marking the critical ice thickness where present basal melting becomes possible. These spots were defined  
865 as locations where the upper slopes of the bedrock topography are dry and their lee slopes are wet, with melting  
866 initiating between the two when the ice thickness passes the pressure melting point (Fig. 14). Assuming that GHF  
867 is locally homogeneous between the two bedrock elevations, heat flow was determined by increasing its value in  
868 a 1-D heat model of the local ice thickness until basal melting occurred. These point estimates were interpolated  
869 to generate an approximate map of regional heat flow and calculate basal melt rates over the last 400 ka.



871 **Fig. 14. Illustration of how the ice thickness exceeding the pressure melting point (PMP) can be identified from radar**  
872 **reflectivity data points, indicating the presence or absence of basal water beneath the ice sheet. Once the PMP is**  
873 **identified, thermal modelling can estimate the required local GHF. Between the thresholds of radar reflectivities**  
874 **representative of wet and dry basal conditions, the thermal conditions are unknown (yellow-shaded region of the**  
875 **bedrock). Adapted from Passalacqua et al. (2017).**

876 Van Liefferinge and Pattyn (2013) and Van Liefferinge et al. (2018) used steady state and transient  
877 thermodynamic modelling of the East Antarctic Ice Sheet to map the minimum heat flow required to raise the  
878 basal temperature above pressure melting point and generate basal melting. Whilst this was executed to identify  
879 possible sites for drilling the oldest ice in areas that are unlikely to have undergone basal melting in the last 1.5  
880 Ma and did not produce an estimate of absolute GHF, if this approach were combined with other evidence for  
881 basal conditions above the pressure melting point (e.g. combining thermodynamic modelling with subglacial lake  
882 locations), points of minimum heat flow could be mapped.

## 883 5.2. Subglacial lakes

884 If temperatures are sufficient for basal melting, and topography depressions are suitable, subglacial lakes can  
885 develop. Subglacial lakes exhibit radio reflectivities 10-20 dB greater than the ice-bedrock boundary, allowing  
886 the current identification of at least 402 lakes beneath the Antarctic ice sheet (Wright and Siegert, 2012).

Field Code Changed

Field Code Changed

887 Whether basal temperatures are sufficient for basal melting and preservation of subglacial lakes is dependent on  
888 ice thickness, the surface temperature and accumulation rate, heat transported through ice advection, heat  
889 produced by internal deformation and basal sliding, and the GHF. When subglacial lakes are located near ice  
890 divides, heat derived by horizontal advection, basal friction, and internal deformation is assumed to be minimal,  
891 and thus the heat required to bring the base of the ice sheet above the pressure melting point is a product of ice  
892 thickness and GHF. Thus, when subglacial lakes are located near ice divides and the accumulation rate is known  
893 (high accumulation rates cool the ice mass), point estimates of *minimum* GHF can be calculated from one-  
894 dimensional thermal models of the ice sheet temperature profile, but an assumption that water was derived locally  
895 and not routed from elsewhere must also be considered as lakes can only form in topographic depressions. The  
896 absence of a lake or basal water does not imply the bed is frozen if the water can drain away (Pattyn, 2010; Siegert  
897 and Dowdeswell, 1996).

898 Conversely, and with the same caveats regarding basal topography and drainage, where the ice sheet is known to  
899 be frozen to the bed, the *maximum* GHF can be estimated. For example, Fudge et al. (2019) used the presence of  
900 Raymond Arches to deduce where the ice was frozen to the bed at the Siple Coast ice rises to estimate maximum  
901 GHF values. Combined, maximum and minimum estimates are more useful than either alone.

### 902 5.3. Englacial stratigraphy

903 Jordan et al. (2018) identified draw down of internal ice sheet layers and increased bed reflectivity from radar data  
904 ~200 km from the South Pole (Fig. 6), indicating enhanced basal melting. Melt rates were calculated using dated  
905 radar layers, traced from the Dome C ice-core site, and a depth age model that simulates the draw-down effect of  
906 ice from subglacial melt rate. The low ice velocity ( $<1.5 \text{ m a}^{-1}$ ) indicated minimal frictional contribution to basal  
907 temperature, and a location at the top of a hydraulic catchment area indicated a low heat contribution from  
908 subglacial water. By negating these contributions to heat flow, assuming the basal temperature is at the pressure  
909 melting point (and thus could be derived from the ice thickness) and that temporal temperature variations match  
910 those of the Dome C ice core, a time-dependent heat equation was applied to the ice sheet to derive the basal GHF  
911 required to generate the enhanced melt rates.

### 912 5.4. Microwave emissivity

913 Englacial temperature profiles have been derived from satellite and airborne passive detection of high frequency  
914 L-band microwave radiation ( $\sim 1.4 \text{ GHz}$ ; Macelloni et al., 2019, 2016; Passalacqua et al., 2018); data primarily  
915 collected to investigate soil moisture and ocean salinity (Kerr et al., 2010). These wavelengths have very low  
916 absorption in ice and low scattering by particles (e.g. grainsize and ice bubbles), providing high penetration depths  
917 in dry ice.

918 Macelloni et al. (2019) derived englacial temperature profiles for the Antarctic ice sheet from 2-year averaged  
919 vertical-polarised (V) radiation collected at the “Brewster angle” ( $57.1^\circ \pm 2.6^\circ$ ; the angle of incidence at which the  
920 radiation is perfectly transmitted through the air-snow interface with no reflection, minimising the influence of  
921 surface or shallow sub-surface effects). The corrected intensity (brightness temperature,  $T_B$ ) correlates with the  
922 surface temperature of the ice, but is also affected by the ice sheet thickness (a largely inverse correlation), density  
923 profile, and grain size (Macelloni et al., 2016). As such, the ice sheet’s thermal structure at depth could be

Deleted: near

925 estimated by comparing the observed  $T_B$  and a simulated  $T_B$  derived through microwave emissivity modelling,  
926 including one-dimensional modelling of the ice sheet's temperature profile. Included in the assumed values for  
927 this modelling are the GHF and the accumulation rate; the sources of greatest uncertainty. This method only  
928 applies in areas of slow flowing ice ( $<10 \text{ m yr}^{-1}$ ), and is optimal in areas of very slow flowing ice ( $<5 \text{ m yr}^{-1}$ ) as  
929 this negates heating by horizontal ice advection and deformation-derived heat production. It is also only applicable  
930 to areas of thick ice ( $>1000 \text{ m}$ ) as the simulations used to model microwave emission do not include bedrock  
931 reflections. This is not a limitation for application to Antarctic GHF research, as it is under these conditions that  
932 heat flow has the greatest influence on ice sheet dynamics.

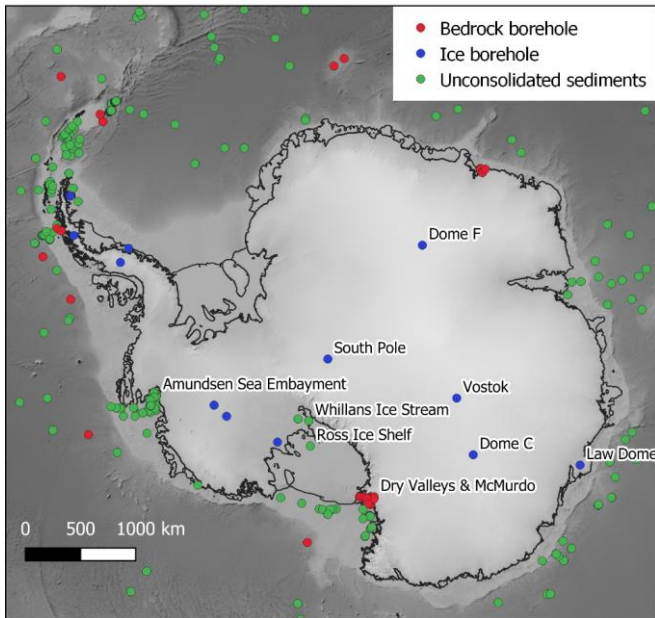
933 Comparison of the microwave-derived temperature profile and that simulated by glaciological modelling (Van  
934 Liefferinge and Pattyn, 2013) show good agreement in the upper third of the ice sheet, but diverge in their  
935 temperature estimates with depth, with the largest uncertainties close to the bedrock. This is largely due to  
936 uncertainty in the GHF, but also reflects a decrease in sensitivity of the simulated  $T_B$  to the temperature profile  
937 below 1000-1500 m (the bottom 1000-1500 m of the ice sheet contributes  $<10 \%$  to the total emission). Longer  
938 wavelength emissions (0.5 GHz) with greater sensitivity to the deeper temperature profile may provide greater  
939 accuracy at depth (Jezek et al., 2014). Deep measurements of the ice sheet's temperature profile are required to  
940 validate this method compared to the glaciological models. Although currently limited by its sensitivity to  
941 temperature at depth and the accuracy of the assumed parameters (notably accumulation rate), this approach has  
942 the potential to constrain basal heat flow though variation of the assumed GHF values used in the emissivity  
943 modelling.

## 944 6. Existing data

945 Although subglacial borehole-derived estimates of terrestrial GHF are lacking in Antarctica, estimates have been  
946 made from probes into marine sediments and boreholes into exposed bedrock. We have compiled 431 of these  
947 point estimates (Fig. 15; data available in the Supplementary Material and from  
948 <https://github.com/RicardaDziadek/Antarctic-GHF-DB>). The compiled data originates from multiple methods,  
949 and is variable in its accuracy and limitations, and so we have attempted to qualitatively grade the likely reliability  
950 of each estimate based on specific parameters (Supplementary Material). We do not include values for marine  
951 measurements compiled in the database "Global Heat Flow Data – Abbott Compilation". This database is  
952 available via GeoMapApp and completely undocumented. The labels may point to cruise reports, but not  
953 published data and the data quality remains impossible to evaluate up to this point.

Deleted: 3

Deleted: However, t



956

957 **Fig. 15. Locations of all compiled point estimates of GHF. Database available in the Supplementary Material and from**  
 958 <https://github.com/RicardaDziadek/Antarctic-GHF-DB>.

959 **6.1. Boreholes into bedrock**

960 Terrestrial, borehole-derived measurements of the geothermal gradient (12 boreholes, Supplementary Material)  
 961 are limited to the Dry Valleys and McMurdo Sound region (Fig. 15; Bucher, 1980; Decker, 1974; Decker and  
 962 Bucher, 1982; Pruss et al., 1974; Talalay and Pyne, 2017), and no subglacial terrestrial borehole measurements  
 963 have been made into the Antarctic bedrock. However, as discussed in Section 3.1., temperature gradients in  
 964 bedrock must be taken to a sufficient depth to be representative of upward conduction of the GHF rather than  
 965 downward conduction of the surface temperature. Whilst the GHF estimates from the Dry Valleys Drilling Project  
 966 (DVDP, including McMurdo Station) were taken from the 75 to >300 m deep boreholes (Bucher, 1980; Decker  
 967 and Bucher, 1982; Talalay and Pyne, 2017), the shallow 7.6 m borehole from McMurdo Station produces a much  
 968 higher GHF estimate (164 mW m<sup>-2</sup>, Risk and Hochstein, 1974). This shallow measurement should thus be  
 969 neglected in preference for the 66 mW m<sup>-2</sup> value from the 260 m deep DVDP borehole (Decker and Bucher, 1982).

970 Boreholes into submarine bedrock (34 boreholes, Supplementary Material) have been drilled and temperature  
 971 gradients measured beneath the McMurdo Sound, Amundsen Sea Embayment, and Ross Ice Shelf (Fig. 15;  
 972 Bucker et al., 2001; Decker et al., 1975; Gohl et al., 2019; McKay et al., 2018; Morin et al., 2010).

973 The US Rapid Access Ice Drill project (RAID) aims to achieve the first subglacial, borehole-derived thermal  
 974 measurements of bedrock following drilling of the overlying ice sheet and coring of ≥25 m of bedrock (Goode  
 975 and Severinghaus, 2016).

<b>Field Code Changed</b>
<b>Formatted:</b> German (Germany)
<b>Formatted:</b> German (Germany)

976 **6.2. Ice boreholes**

977 GHF estimates from ice boreholes ([15 boreholes, Supplementary Material](#)) are better distributed across the  
978 Antarctic continent than terrestrial bedrock boreholes (Fig. 15). However, not all ice boreholes drilled have been  
979 sufficiently deep or in appropriate sites for GHF estimation (i.e. the ice sheet needs to be stationary and frozen to  
980 the bed). This limits the available GHF estimates to Vostok (Salamatin et al., 1998), Law Dome (Dahl-Jensen et  
981 al., 1999), South Pole (Price et al., 2002), Marie Byrd Land (Clow et al., 2012; Engelhardt, 2004; Gow et al.,  
982 1968), and the Antarctic Peninsula (Mulvaney et al., 2012; Nicholls and Paren, 1993; Zagorodnov et al., 2012)  
983 (Fig. 15). [Dome Fuji \(Hondoh et al., 2002\) is not frozen to the bed, but provides a minimum GHF estimate.](#)

Deleted: Dome Fuji (Hondoh et al., 2002),

984 **6.3. Marine and onshore unconsolidated sediments**

985 The most abundant resource of heat flow estimates from measured temperature profiles around Antarctica comes  
986 from unconsolidated marine sediments (Fig. 15; [362 measurements south of -72° S, Supplementary Material](#)).  
987 However, the data distribution is sparse and heterogeneous, and whilst some regions are well sampled (e.g. the  
988 Amundsen Sea embayment; Dziadek et al., 2019, 2017), other regions (e.g. the Weddell Sea) remain poorly  
989 constrained (Fig. 15). In addition to the open water measurements, two shallow probes (deepest sensors at 1.4 and  
990 0.8 m below the upper sediment surface) have measured the temperature gradient in subglacial sediments below  
991 the Whillans Ice Stream (Begeman et al., 2017; Fisher et al., 2015; see section 3.3.). Two temperature gradients  
992 have also been measured beneath the Ross Ice Shelf (Foster, 1978; Morin et al., 2010), but otherwise heat flow  
993 beneath the Antarctic ice shelves remains poorly constrained regions.

994 As discussed in Section 3.3, when using these estimates it is important to consider whether the shallow (<~5 m)  
995 temperature gradient recorded by the probe is representative of the deeper GHF, or will have been perturbed by  
996 temperature variation in the overlying ice sheet or water column (e.g. Dziadek et al., 2019). Consequently, the  
997 water depth, the temperature profile of the water column, and possible sources of long-term temperature variation  
998 (e.g. variations in deep water circulation and temperature) should be considered when selecting appropriate point  
999 estimates. Similarly, whilst the shallow temperature gradients measured from Subglacial Lake Whillans (Fisher  
1000 et al., 2015), and the Whillans Ice Stream grounding zone (Begeman et al., 2017) are presented as subglacial direct  
1001 measurements of Antarctic GHF, by the nature of their location within an ice stream they are not in a thermal  
1002 steady state, and the temperature profile will have been affected by long term variation from heat advection and  
1003 shear heating. These are effects that cannot be evaluated from their very shallow temperature gradient (0.8 and  
1004 1.4 m deep), and accordingly these estimates should be used with caution.

1005 **7. Current challenges and future research directions**

1006 The collated existing data and methodologies presented above highlight our current limitations in determining the  
1007 subglacial GHF of Antarctica and allow discussion of future research.

1008 **7.1. Borehole and probe-derived estimates**

1009 The fundamental limitation for GHF estimation in Antarctica is the lack of borehole-derived estimates from  
1010 beneath the Antarctic ice sheet. Without these independent, discrete validation points, the more extensive regional  
1011 estimates cannot be accurately evaluated. Therefore, the most promising future development will be the  $\geq 25$  m

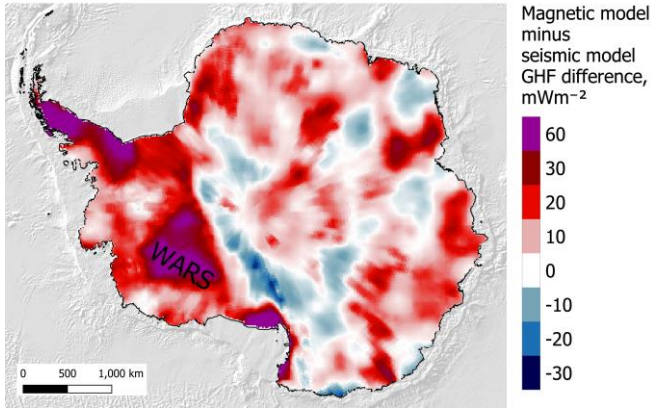


1013 deep bedrock borehole measurements of the Rapid Access Ice Drill project (RAID; Goodge and Severinghaus,  
1014 2016). However, (as noted above) local temperature gradients may not be representative of the regional heat flow,  
1015 as local geology, hydrothermal circulation, and topography can result in localised GHF variability. In response,  
1016 multiple boreholes where the basal ice is frozen to the bedrock are required to categorise the regional variation,  
1017 and topographic effects must be considered and accounted for. Topography may have significant effects on GHF  
1018 via its effects on heat diffusion pathways to the surface (Bullard, 1938; Lees, 1910) and must be considered and  
1019 investigated in GHF estimates at all scales, including those based on local temperature gradient measurements  
1020 (i.e. borehole and probe-derived estimates) and more extensive geophysical and glaciological-derived models.

1021 It is also a necessity that thermal modelling of the bedrock temperature profile for the RAID target sites is executed  
1022 prior to drilling to constrain the penetration depth of low-frequency time variation of temperature. Whilst the  
1023 RAID target bedrock borehole depth of  $\geq 25$  m is much shallower than the  $>100$  m borehole depth achieved for  
1024 exposed bedrock (Section 3.1.), the overlying ice sheet insulates the bedrock temperature profile from short  
1025 duration surface temperature variability (temperature variation penetration depth is dependent on the frequency  
1026 of the variation and thermal diffusivity of the material; Carslaw and Jaeger, 1959). However, as is considered for  
1027 GHF estimates from ice boreholes (Section 3.2.), low-frequency variation in surface temperatures, heat advection,  
1028 and shear heating will all affect the subglacial temperature profile. Consequently, low-frequency temperature  
1029 variation must be corrected for, and boreholes are best drilled where the ice is stationary and frozen to the bed (as  
1030 is applied to ice borehole selection for GHF estimation). By drilling in such sites where glaciological approaches  
1031 are most effective for GHF estimation, the RAID data will allow validation of GHF estimates for the various  
1032 englacial temperature methods applied to stationary ice at ice divides (Section 5.). These methods include borehole  
1033 temperature profiles, subglacial lakes, ice sheet models, and microwave emissivity. It is thus important that the  
1034 englacial temperature profile is measured in addition to the bedrock temperature gradient.

1035 Beyond bedrock drilling there is lot to be gained from further ice borehole drilling. Firstly, existing data must be  
1036 evaluated to ensure the methodologies of GHF modelling from borehole temperature profiles are consistent and  
1037 accurate. Future ice boreholes into stationary ice frozen to the bed has the potential to supplement the existing  
1038 borehole and probe-derived GHF estimates, particularly if the proposed methodology for shallow boreholes can  
1039 be validated (600 m depth, or the upper 20% of the ice column; Section 3.2.).

**Deleted:** This is particularly true for the Dome C borehole, for which the previously published  $49.0 \text{ mW m}^{-2}$  value (de Mendoza et al., 2016) has been retracted.



1044  
1045 **Fig. 16. Difference in heat flow values between the most recent magnetic (Martos et al., 2017) and forward-modelled**  
1046 **seismic (An et al., 2015b) heat flow models. WARS – West Antarctic Rift System.**

1047 Whilst only geophysical methods have provided continental-scale GHF estimates, their values and distribution  
1048 vary greatly (Fig. 5, Fig. 16, and Fig. 17). Probability density functions show that whilst there is better agreement  
1049 in East Antarctica (Fig. 17a), the seismically derived models estimate more variable and slightly higher GHF than  
1050 the magnetically-derived models. In West Antarctica the discrepancies between models are greater (Fig. 5g and  
1051 Fig. 17b) even when using similar techniques (compare the empirical seismically-derived estimates of Shapiro  
1052 and Ritzwoller, 2002, and Shen et al., 2020, Fig. 17b). However, none of the models of West Antarctica reflects  
1053 the GHF distribution of other better-constrained rift systems (Fig. 17c; Lucazeau, 2019), where much more  
1054 heterogeneous distributions and a greater proportion of high GHF values ( $>150 \text{ mW m}^{-2}$ ) are expected.

1055 The fundamental question thus remains: does the West Antarctic Rift System (WARS) have elevated GHF? The  
1056 magnetically-derived model of Martos et al. (2017) estimates high GHF, but the most recent forward and  
1057 empirically-derived seismic models do not (An et al., 2015b; Shen et al., 2020; Fig 5). If the seismic models are  
1058 correct, then the high GHF estimates of the magnetic model reflect thinning of the magnetic crust, but GHF has  
1059 subsequently reduced in the ~90 My since the dominant phase of WARS crustal extension in the Cretaceous  
1060 (~105-95 Ma, Siddoway, 2008; as illustrated in Fig. 9b). If the magnetic model is correct, then GHF remains  
1061 elevated in response to the younger, 43-11 Ma Cenozoic phase of crustal extension (Granot and Dymant, 2018;  
1062 e.g. Fig. 9a). Subglacial hydrological modelling (Schroeder et al., 2014) supports the high GHF estimates in the  
1063 Thwaites Glacier region of the WARS. However, high-fidelity borehole estimates, and better constraints on the  
1064 nature of the geology, lithospheric architecture, and tectonic history of the WARS are required if we are to resolve  
1065 the different estimates and use other locations as analogues for verifying the modelled GHF distribution.

Deleted: and

Deleted: (

Deleted: )

Deleted: (

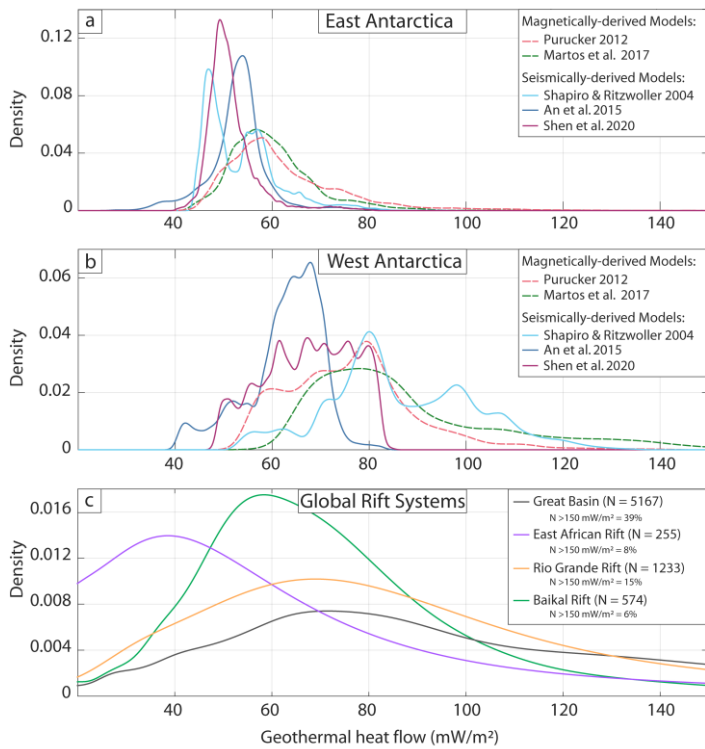
Deleted: (Lucazeau, 2019)

Deleted: high

Deleted: (

Deleted: ,

Deleted: )



075  
076 **Fig. 17. Probability density functions of the geophysically derived continental GHF datasets (Fig. 5 a – e) for a) West**  
077 **Antarctica and b) East Antarctica. Values extracted at 10 km spacing. The histograms were calculated with a bin size**  
078 **of 1 and fitted with a non-parametric distribution in the positive domain. c) GHF estimates from measured temperature**  
079 **gradients for global rift systems for comparison with West Antarctica (data from Lucazeau, 2019). Note the number of**  
080 **proportion of the data points (N) greater than 150 mW m<sup>-2</sup>.**

081 **To evaluate the accuracies of the different models, uncertainty estimates are required.** Uncertainties of <10 mW  
082 m<sup>-2</sup> for the majority of Antarctica were presented for the Curie Depth GHF model of Martos et al. (2017).  
083 However, not only are the modelled values greatly different from those derived by seismic modelling (An et al.,  
084 2015b), the calculated Curie depth is deeper than the seismically- or gravitationally-derived Moho depth for large  
085 areas of the continent (Fig. 10). **Even though** this can occur where metallic phases are present in cratonic mantle  
086 (Ferré et al., 2013; Section 4.1.), this cannot explain the full distribution, nor are these occurrences likely to be  
087 this extensive. Without being critical of the model itself, it is reasonable to dispute the accuracy of the calculated  
088 uncertainties, and suggest that **although** their calculation from the geophysical data may be logical, there may be  
089 a geological contribution to uncertainty (e.g. lithological variation in the lithosphere) that is not being considered.  
090 As GHF models are utilised by researchers in different fields to those publishing the models, they cannot be  
091 independently evaluated by the user, and so accuracy in published uncertainty values is arguably more important  
092 than the accuracy of the model itself. We recommend that future research (including geophysical, geological,  
093 glaciological, and borehole and probe-derived estimates) is careful in its presentation of uncertainty.

Formatted: Superscript

Deleted: Whilst

Deleted: whilst

1096 The largest limitations to existing geophysical-derived GHF models are uncertainties in the structure,  
1097 composition, heat production, and thermophysical properties of the unexposed crust, lithosphere, and underlying  
1098 mantle. All current continental models assume the lithosphere to be laterally homogenous in its composition and  
1099 thermophysical properties, and although seismic GHF models (e.g. An et al., 2015b) incorporate variable mantle  
1100 temperatures, its composition is assumed to be homogenous. Geophysical GHF models assume that lithospheric  
1101 heat production is focussed in the upper crust, and is orders of magnitude greater than the deeper heat production  
1102 of the middle and lower crust and the mantle. These models assume that lithospheric heat production either  
1103 exponentially decreases with depth (e.g. the Curie depth models of Fox Maule et al., 2005; Martos et al., 2017;  
1104 and Purucker, 2012), or is concentrated within a laterally homogenous layer of variable depth and constant heat  
1105 production (e.g. the seismic model of An et al., 2015a, and the thermal-isostatic model for Australia of Hasterok  
1106 and Gard, 2016). However, although the lower crust is enriched in mafic rocks (iron-rich rocks of high  
1107 crystallisation temperature, e.g. basalt) of low heat production, deep boreholes and crustal sections have shown  
1108 that whilst there is a correlation between heat production and lithology in the upper crust, there is no such  
1109 correlation with depth or metamorphic grade (Section 4.6.3.). Similarly, the assumption of laterally homogenous  
1110 heat production has been shown to be unreasonable for estimation of Antarctica's GHF, which (like all continents)  
1111 has a laterally variable geology and associated concentration of HPEs (Burton-Johnson et al., 2017; Carson et al.,  
1112 2014). The exponential decrease model of crustal heat production should thus be rejected, and attempts should be  
1113 made to derive the depth and structure of crustal heat production.

1114 The most promising approach to address the challenge of uncertainty in the contribution to GHF from the  
1115 unexposed crust and deeper lithosphere is the derivation of a three-dimensional lithospheric structure model for  
1116 Antarctica. This approach uses geophysical modelling integrating seismic, magnetic, and thermal-isostatic  
1117 evidence, and integrating into the modelling the heat production, conductivity, and petrophysical properties of  
1118 exposed lithologies and deeper crustal xenoliths or crustal sections. A similar model was developed for Norway  
1119 (Ebbing et al., 2006; Olesen et al., 2007), and an Antarctic model would build upon recent 2D and 3D  
1120 geophysically-derived models (Leat et al., 2018; Pappa et al., 2019b, 2019a). This requires an expanded database  
1121 of the geochemistry of Antarctica's rock outcrops (particularly the HPEs). Beneath the Antarctic ice sheet, where  
1122 the surface geology is unknown, the lithologies and probable heat production is best constrained by determining  
1123 the probable heat production of each drainage basin based on its detrital clasts (e.g. Goodge, 2018).

1124 The assumption of a homogenous mantle composition beneath East Antarctica is challenged by discrepancies  
1125 between the Moho depth models derived by gravity and isostatic modelling (Pappa et al., 2019b, 2019a), as this  
1126 indicates variable lithospheric mantle densities, or deeper mantle effects on topography. A review of the available  
1127 mantle xenoliths and mantle-derived basalt chemistry may be able to constrain the composition of the mantle  
1128 beneath Antarctica, and thermal-isostatic modelling may be able to identify these regions of anomalous mantle  
1129 anomalies (as in the Australian study of Hasterok and Gard, 2016). If the seismic data for Antarctica is sufficient  
1130 to determine crustal density, such a thermal isostatic model would provide an additional independent method to  
1131 determine the depth of the upper crustal heat producing layer (Hasterok and Chapman, 2011) and evaluate the  
1132 other GHF models.

**Field Code Changed**

**Deleted:** (e.g. the Curie depth models of Fox Maule et al., 2005, and Martos et al., 2017)

**Deleted:** Section

1136 Finally, it is important to compare Antarctica with its conjugate margins (e.g. Pollett et al., 2019), where GHF and  
1137 crustal structure are better constrained. This provides constraints on the GHF along the margins of East Antarctica,  
1138 as well as informing on the geology beneath the ice sheet.

1139 Beyond individual geological and geophysical approaches, a further challenge is how best to integrate different  
1140 models. Robust methods must be developed to incorporate datasets with different resolutions and uncertainty,  
1141 including techniques already used by the broader data analysis community. For example, Rezvanbehbahani et al.  
1142 (2017) applied a multi-variate regression analysis to estimate heat flow in Greenland from sparse and variable  
1143 geological and geophysical models and data.

Deleted: (

Deleted: ,

### 1144 7.3. Glaciological GHF estimates

1145 Englacial temperatures are more sensitive to GHF in areas of the interior of Antarctica where basal sliding is  
1146 negligible (Section 2.1). Out of all the methods discussed to derive GHF in the Antarctic interior, the most  
1147 promising method is to derive GHF from englacial temperatures obtained from microwave emission (Section 5.4.)  
1148 at a longer wavelength (0.5 GHz) than the currently available (~1.4 GHz). The increase in wavelength will reduce  
1149 the uncertainty in englacial temperatures below 1000-1500 m (Jezek et al., 2014). By improving the estimations  
1150 of englacial temperature near the bed, this will reduce the role of ice flow modelling required to extrapolate  
1151 temperature from the partial-depth data. Potentially, if near-the-bed englacial temperatures are known with  
1152 sufficient precision, GHF could be derived as from borehole thermometry (Section 3.2). However, the longer-  
1153 wavelength method requires the acquisition of currently unavailable satellite-derived data. The method is only  
1154 applicable in areas of thick, very slow-flowing ice, and within this area only two ice boreholes exist for validation.  
1155 Further validation of the technique to determine the origin of the differences between the temperature model  
1156 derived from emissivity data, and glaciological thermal modelling (Macelloni et al., 2019), and other spatially  
1157 variable processes affecting microwave emissivity must also be considered (e.g. wind speed, accumulation rate,  
1158 surfaces roughness, and density heterogeneities in the firn layer; Passalacqua et al., 2018).

Deleted: this

Deleted: as, despite the potential of this method, the 2018 Cryorad proposal submitted to ESA (Macelloni et al., 2018) was unsuccessful

Deleted: .

1159 Existing glaciological data, like subglacial water distribution or dated englacial layers, has been successfully used  
1160 in estimating heat flow in regions of thick, slow flowing ice near ice divides, where advection and shear heating  
1161 are minimised. To extend these regional studies to continental scale, both data and models have to be improved.  
1162 A significant challenge for radar-derived subglacial water distribution is our ability to discriminate between water  
1163 at the bed versus contrasts in the geometric properties of ice sheet and bed (Schroeder et al., 2014). However the  
1164 improvement in radar techniques and the combination with seismic surveys and direct access observations, is our  
1165 best chance to improve our observations of subglacial hydrology (Ashmore and Bingham, 2014).

1166 The inventory of subglacial lakes (Wright and Siegert, 2012) is a better constrained and expanding dataset.  
1167 Subglacial lakes can be detected also using satellite surface altimetry (Fricker et al., 2007), providing a way to  
1168 expand the coverage and to confirm dubious cases. However, as noted in Section 5.1., topography must be  
1169 considered when using evidence for subglacial lakes as they can only develop in topographic depressions, and the  
1170 absence of basal water does not imply the bed is frozen if water can drain away.

1171 Subglacial melting can also be detected in englacial stratigraphy (Section 5.3) but the required radar product  
1172 (internal radar reflective horizons) is not often available. “AntArchitecture” is a SCAR (Scientific Committee on

1180 Antarctic Research) Action Group bringing together key datasets on Antarctic internal layering from the principal  
1181 institutions and scientists who have been responsible for acquiring, processing and storing them over the last four  
1182 decades (AntArchitecture Action Group, 2017). As the coverage of Antarctic internal layers becomes widely  
1183 available, its application to infer GHF will increase in popularity.

1184 Finally, and for any of the glaciological methods described above, the glaciological models used to infer GHF  
1185 have to be improved. The current thermal models used to infer GHF can be classified in two larger groups: 1) 1D  
1186 time-dependent high-complexity models, and 2) 2D/3D steady-state low-complexity models. The first category is  
1187 generally used near ice domes or ridges, with low horizontal flow, and where horizontal heat advection can be  
1188 neglected (e.g., Passalacqua, 2017). The latter are used across the whole continent (e.g. Van Liefferinge et al.,  
1189 2018), but ignore the changes in temperature between glacial and interglacial periods despite their strong effect  
1190 on englacial temperatures (Ritz, 1989). The challenge is to develop thermal models with the required level of  
1191 complexity at a continental scale, accommodating the main physical processes. This remains a technical challenge,  
1192 and thermodynamic models remain dependant on GHF estimates.

Field Code Changed

## 1193 8. Conclusions

1194 We present state-of-the-art data and models to estimate geothermal heat flow in Antarctica and highlight the need  
1195 for a detailed continental map. We also discuss current challenges and future directions.

1196 With multiple methodologies and models for Antarctic GHF currently published, the most promising future  
1197 direction for local estimates is borehole-derived estimation of GHF beneath the Antarctic ice sheet from RAID  
1198 bedrock drilling and englacial temperatures from ice boreholes. Ideally, the latter approach will be validated by  
1199 the former to support expansion of the dataset from shallow boreholes (potentially only 600 m deep, or 20 % of  
1200 the total ice sheet thickness).

1201 The ice sheet is most sensitive to variation in GHF within the interior of Antarctica, where heat production from  
1202 sliding at the base of the ice sheet is negligible. However, it is in this region that GHF is hardest to constrain by  
1203 geophysical estimates because of the scarcity of local GHF estimates from down-hole measured temperature  
1204 gradients, geological data, and insight from conjugate margins. It is thus in the interior of Antarctica where  
1205 glaciological approaches are the most applicable. Out of the methods presented, the determination of englacial  
1206 temperatures from long-wavelength microwave emissivity is the most promising, but this data is not currently  
1207 available and requires further validation.

Deleted: slide

1208 We highlight the potential of regional estimates of GHF from subglacial meltwater inventories. Aside from the  
1209 ever expanding inventory of subglacial lakes we encourage initiatives like “AntArchitecture” that will make radar  
1210 products widely available. Also, we discuss future requirements of thermal models (either 1D or those lacking  
1211 glacial-interglacial variability) to expand the methods beyond domes in the interior of Antarctica.

1212 Geophysical methods remain the most attractive approach to estimate GHF because they are independent of ice  
1213 flow. However, they vary greatly in their estimated magnitude and distribution of GHF. The greatest uncertainty  
1214 in all the geophysical models is uncertainty in the composition and structure of the lithosphere and mantle. We  
1215 recommend ceasing to use the exponential decrease model of crustal heat production. Instead, we suggest using  
1216 geological and geophysical approaches to model the thickness, structure and composition of the crust. We also

1218 recommend the application of a thermal-isostatic approach to provide an independent estimate, and highlight  
1219 regions of anomalous isostatic elevation and probable mantle heterogeneities. The effects of topography must also  
1220 be considered in all GHF models.

1221 Finally, the greatest challenge for Antarctic GHF estimation is the necessity for multidisciplinary science and how  
1222 best to integrate the different methods. Hopefully, this paper provides a first step in communicating the approaches  
1223 and limitations of the different fields across the GHF community. We sincerely recommend the continuation and  
1224 enhancement of the international collaborations within SCAR, building on the work of the GHF sub-group of the  
1225 SERCE research programme (Solid Earth Response and influence on Cryospheric Evolution), and encourage and  
1226 appreciate SCAR's continuing support in this field of research.

#### 1227 Data availability

1228 The database of GHF point estimates (Fig. 15) is available in the Supplementary Material and from  
1229 <https://github.com/RicardaDziadek/Antarctic-GHF-DB>. The GHF mean and standard deviation maps of the  
1230 geophysical models of continental GHF (Fig. 5f and 5g) are available in the Supplementary Material.

#### 1231 Author contributions

1232 ABJ and RD conceived the project. ABJ was the lead author for all sections and the specialist in geology and  
1233 geochemistry. RD was a co-author for all sections, compiler of the supplemental GHF database, and the specialist  
1234 in geophysics. CM was a co-author for all sections and the specialist in glaciology.

#### 1235 Competing interests

1236 The authors declare that they have no conflicts of interest.

#### 1237 Acknowledgements

1238 The authors thank Brice Van Liefvering, an anonymous reviewer, and John Goodge for their helpful and thorough  
1239 reviews and comments, which have all improved this final manuscript. Alexander Robinson for his work and  
1240 comments as our handling editor, and the Copernicus team for all their assistance. This research is a contribution  
1241 to the SCAR SERCE scientific research programme, and we thank the discussions and support of this group from  
1242 the TACTical 2018 (Hobart, Australia), POLAR 2018 (Davos, Switzerland), ISAES 2019 (Incheon, Korea), and  
1243 SCAR 2020 Open Science Conference (online) meetings. We particularly thank Jacqueline Halpin (IMAS,  
1244 Hobart) for her comments on the manuscript and her work promoting and developing the Antarctic GHF  
1245 community.

#### 1246 Financial support

1247 A. Burton-Johnson and C. Martin were funded by the Natural Environment Research Council as part of the British  
1248 Antarctic Survey Polar Science for Planet Earth programme. R. Dziadek was supported by the Deutsche  
1249 Forschungsgemeinschaft (DFG) in the framework of the Priority Program 1158 "Antarctic research with  
1250 comparative investigations in Arctic ice areas" by grant GO 724/14-1. Additional funds were contributed by the  
1251 AWI Research Program PACES-II Workpackage 3.2.

Formatted: Heading 1, Indent: Left: 0 cm, Hanging: 0.63 cm

Formatted: Heading 1, Indent: Left: 0 cm, Hanging: 0.63 cm

Formatted: Heading 1, Indent: Left: 0 cm, Hanging: 0.63 cm

Formatted: Indent: Left: 0 cm, Hanging: 0.63 cm, No bullets or numbering

Deleted: A. Burton-Johnson and C. Martin were funded by the Natural Environment Research Council as part of the British Antarctic Survey Polar Science for Planet Earth programme. R. Dziadek was supported by the Deutsche Forschungsgemeinschaft (DFG) in the framework of the Priority Program 1158 "Antarctic research with comparative investigations in Arctic ice areas" by grant GO 724/14-1. Additional funds were contributed by the AWI Research Program PACES-II Workpackage 3.2.

Deleted: and

Deleted: in

Formatted: Heading 1, Indent: Left: 0 cm, Hanging: 0.63 cm

263 [Review statement](#)

264 [This paper was reviewed by Brice Van Liefvering and an anonymous reviewer. Alexander Robinson was the](#)  
265 [handling editor. John Goodge provided an additional short comment in the interactive discussion.](#)

Formatted: Heading 1, Indent Left: 0 cm, Hanging: 0.63 cm

1266 **9. References**

- 1267 Aboud, E., Salem, A. and Mekkawi, M.: Curie depth map for Sinai Peninsula, Egypt deduced from the analysis  
1268 of magnetic data, *Tectonophysics*, 506(1–4), 46–54, 2011.
- 1269 Aitken, A. R. A., Betts, P. G., Young, D. A., Blankenship, D. D., Roberts, J. L. and Siegert, M. J.: The Australo-  
1270 Antarctic Columbia to Gondwana transition, *Gondwana Research*, 29(1), 136–152, 2016.
- 1271 Alessio, K. L., Hand, M., Kelsey, D. E., Williams, M. A., Morrissey, L. J. and Barovich, K.: Conservation of deep  
1272 crustal heat production, *Geology*, 46(4), 335–338, 2018.
- 1273 Amante, C. and Eakins, B. W.: ETOPO1 Arc-Minute Global Relief Model: Procedures, Data Sources and  
1274 Analysis, National Oceanic and Atmospheric Administration Technical Memorandum NESDIS NGDC-24., 2009.
- 1275 An, M., Wiens, D. A., Zhao, Y., Feng, M., Nyblade, A. A., Kanao, M., Li, Y., Maggi, A. and L  v  que, J.-J.: S-  
1276-velocity model and inferred Moho topography beneath the Antarctic Plate from Rayleigh waves, *Journal of*  
1277 *Geophysical Research: Solid Earth*, 120(1), 359–383, 2015a.
- 1278 An, M., Wiens, D. A., Zhao, Y., Feng, M., Nyblade, A., Kanao, M., Li, Y., Maggi, A. and L  v  que, J.-J.:  
1279 Temperature, lithosphere-asthenosphere boundary, and heat flux beneath the Antarctic Plate inferred from seismic  
1280 velocities, *Journal of Geophysical Research: Solid Earth*, 120(12), 8720–8742, 2015b.
- 1281 Andr  s, J., Marz  n, I., Ayarza, P., Mart  , D., Palomeras, I., Torn  , M., Campbell, S. and Carbonell, R.: Curie point  
1282 depth of the Iberian Peninsula and surrounding margins. A thermal and tectonic perspective of its evolution,  
1283 *Journal of Geophysical Research: Solid Earth*, 123(3), 2049–2068, 2018.
- 1284 AntArchitecture Action Group: AntArchitecture: Archiving and interrogating Antarctica’s internal structure from  
1285 radar sounding. Final Report, in Workshop to establish scientific goals, working practices and funding routes.  
1286 University of Edinburgh, UK, University of Edinburgh, UK. [online] Available from:  
1287 <https://www.scar.org/library/science-4/geosciences/antarchitecture/5240-antarchitecture-workshop-2017/file>,  
1288 2017.
- 1289 Arnaiz-Rodr  guez, M. S. and Orihuela, N.: Curie point depth in Venezuela and the Eastern Caribbean,  
1290 *Tectonophysics*, 590, 38–51, 2013.
- 1291 Artemieva, I.: *Lithosphere: an interdisciplinary approach*, Cambridge University Press, Cambridge, UK., 2011.
- 1292 Artemieva, I. M. and Mooney, W. D.: Thermal thickness and evolution of Precambrian lithosphere: A global  
1293 study, *Journal of Geophysical Research: Solid Earth*, 106(B8), 16387–16414, 2001.
- 1294 Ashmore, D. W. and Bingham, R. G.: Antarctic subglacial hydrology: current knowledge and future challenges,  
1295 *Antarctic Science*, 26(6), 758–773, 2014.
- 1296 Bansal, A. R., Gabriel, G., Dimri, V. P. and Krawczyk, C. M.: Estimation of depth to the bottom of magnetic  
1297 sources by a modified centroid method for fractal distribution of sources: An application to aeromagnetic data in  
1298 Germany, *Geophysics*, 76(3), L11–L22, 2011.
- 1299 Bansal, A. R., Anand, S. P., Rajaram, M., Rao, V. K. and Dimri, V. P.: Depth to the bottom of magnetic sources  
1300 (DBMS) from aeromagnetic data of Central India using modified centroid method for fractal distribution of  
1301 sources, *Tectonophysics*, 603, 155–161, 2013.
- 1302 Barletta, V. R., Bevis, M., Smith, B. E., Wilson, T., Brown, A., Bordoni, A., Willis, M., Khan, S. A., Rovira-  
1303 Navarro, M. and Dalziel, I.: Observed rapid bedrock uplift in Amundsen Sea Embayment promotes ice-sheet  
1304 stability, *Science*, 360(6395), 1335–1339, 2018.



- 1305 Baron Fourier, J. B. J.: *Théorie analytique de la chaleur*, Chez Firmin Didot, père et fils, Paris., 1822.
- 1306 Barrett, B. E., Nicholls, K. W., Murray, T., Smith, A. M. and Vaughan, D. G.: Rapid recent warming on Rutford  
1307 Ice Stream, West Antarctica, from borehole thermometry, *Geophysical Research Letters*, 36(2), 2009.
- 1308 Bea, F.: The sources of energy for crustal melting and the geochemistry of heat-producing elements, *Lithos*, 153,  
1309 278–291, doi:10.1016/j.lithos.2012.01.017, 2012.
- 1310 Bea, F. and Montero, P.: Behavior of accessory phases and redistribution of Zr, REE, Y, Th, and U during  
1311 metamorphism and partial melting of metapelites in the lower crust: an example from the Kinzigite Formation of  
1312 Ivrea-Verbano, NW Italy, *Geochimica et Cosmochimica Acta*, 63(7), 1133–1153, 1999.
- 1313 Beamish, D. and Busby, J.: The Cornubian geothermal province: heat production and flow in SW England:  
1314 estimates from boreholes and airborne gamma-ray measurements, *Geothermal Energy*, 4(1), 4, 2016.
- 1315 Beardsmore, G. R. and Cull, J. P.: *Crustal heat flow: a guide to measurement and modelling*, Cambridge  
1316 University Press, Cambridge, UK., 2001.
- 1317 Begeman, C. B., Tulaczyk, S. M. and Fisher, A. T.: Spatially variable geothermal heat flux in West Antarctica:  
1318 evidence and implications, *Geophysical Research Letters*, 44(19), 9823–9832, 2017.
- 1319 Berg, J. H., Moscati, R. J. and Herz, D. L.: A petrologic geotherm from a continental rift in Antarctica, *Earth and  
1320 Planetary Science Letters*, 93(1), 98–108, 1989.
- 1321 Bhattacharyya, B. K. and Leu, L.-K.: Analysis of magnetic anomalies over Yellowstone National Park: mapping  
1322 of Curie point isothermal surface for geothermal reconnaissance, *Journal of Geophysical Research*, 80(32), 4461–  
1323 4465, 1975.
- 1324 Blakely, R. J.: *Potential theory in gravity and magnetic applications*, Cambridge university press, Cambridge,  
1325 UK., 1996.
- 1326 Blakely, R. J., Brocher, T. M. and Wells, R. E.: Subduction-zone magnetic anomalies and implications for  
1327 hydrated forearc mantle, *Geology*, 33(6), 445–448, 2005.
- 1328 Boden, D. R.: *Geology and Heat Architecture of the Earth's Interior*, in *Geologic Fundamentals of Geothermal  
1329 Energy*, Routledge., 2016.
- 1330 Bodorkos, S., Sandiford, M., Minty, B. R. and Blewett, R. S.: A high-resolution, calibrated airborne radiometric  
1331 dataset applied to the estimation of crustal heat production in the Archaean northern Pilbara Craton, Western  
1332 Australia, *Precambrian Research*, 128(1–2), 57–82, 2004.
- 1333 Bucher, G. J.: *Heat flow and radioactivity studies in the Ross Island-Dry Valley area, Antarctica and their tectonic  
1334 implications.*, PhD Thesis, University of Wyoming, Wyoming, USA., 1980.
- 1335 Bücker, C., Jarrard, R. D. and Wonik, T.: Downhole temperature, radiogenic heat production, and heat flow from  
1336 the CRP-3 drillhole, Victoria Land Basin, Antarctica, *Terra Antarctica*, 8(3), 151–160, 2001.
- 1337 Bullard, E. C.: The disturbance of the temperature gradient in the earth's crust by inequalities of height,  
1338 *Geophysical Supplements to the Monthly Notices of the Royal Astronomical Society*, 4(5), 360–362, 1938.
- 1339 Bullard, E. C.: The time taken for a borehole to attain temperature equilibrium, *Monthly Notices of the Royal  
1340 Astronomical Society, Geophysics Supplement*, 5, 127–130, 1947.
- 1341 Burton-Johnson, A., Halpin, J. A., Whittaker, J. M., Graham, F. S. and Watson, S. J.: A new heat flux model for  
1342 the Antarctic Peninsula incorporating spatially variable upper crustal radiogenic heat production, *Geophysical  
1343 Research Letters*, 44(11), 5436–5446, doi:10.1002/2017GL073596, 2017.

- 1344 Burton-Johnson, A., Dziadek, R. and Shen, W.: Report of the Geothermal Heat Flux Side Meeting at XIII ISAES,  
1345 2019, Incheon, Republic of Korea. [online] Available from: <https://www.scar.org/scar-library/search/science-4/research-programmes/serce/5334-ghf-meeting-report-2019/file>, 2019.
- 1347 Burton-Johnson, A., Dziadek, R., Martin, C., Halpin, J. A., Whitehouse, P. L., Ebbing, J., Martos, Y. M., Martin,  
1348 A. P., Schroeder, D. M., Shen, W., Ritz, C., Goodge, J. W., Van Liefferinge, B., Pattyn, F., Reading, A. M.,  
1349 Ferraccioli, F. and The SERCE Geothermal Heat Flow Sub-Group: Antarctic Geothermal Heat Flow: Future  
1350 research directions, SCAR-SERCE White Paper [online] Available from: <https://www.scar.org/scar-library/search/science-4/research-programmes/serce/5454-scar-serce-white-paper-on-antarctic-geothermal-heat-flow/>, 2020.
- 1353 Carlson, R. W., Pearson, D. G. and James, D. E.: Physical, chemical and chronological characteristics of  
1354 continental mantle, *Reviews in Geophysics*, 43, RG1001, doi:10.1029/2004RG000156, 2005.
- 1355 Carslaw, H. S. and Jaeger, J. C.: *Conduction of heat in solids*, Oxford: Clarendon Press, 1959, 2nd ed., 1959.
- 1356 Carson, C. J. and Pittard, M.: *A Reconnaissance Crustal Heat Production Assessment of the Australian Antarctic  
1357 Territory (AAT)*, Geoscience Australia, Canberra, Australia., 2012.
- 1358 Carson, C. J., McLaren, S., Roberts, J. L., Boger, S. D. and Blankenship, D. D.: Hot rocks in a cold place: high  
1359 sub-glacial heat flow in East Antarctica, *Journal of the Geological Society*, 171(1), 9–12, 2014.
- 1360 Carter, S. P., Blankenship, D. D., Young, D. A. and Holt, J. W.: Using radar-sounding data to identify the  
1361 distribution and sources of subglacial water: application to Dome C, East Antarctica, *Journal of Glaciology*,  
1362 55(194), 1025–1040, 2009.
- 1363 Chen, B., Haeger, C., Kaban, M. K. and Petrunin, A. G.: Variations of the effective elastic thickness reveal tectonic  
1364 fragmentation of the Antarctic lithosphere, *Tectonophysics*, 746, 412–424, 2018.
- 1365 Clauser, C., Giese, P., Huenges, E., Kohl, T., Lehmann, H., Rybach, L., Šafanda, J., Wilhelm, H., Windloff, K.  
1366 and Zoth, G.: The thermal regime of the crystalline continental crust: implications from the KTB, *Journal of  
1367 Geophysical Research: Solid Earth*, 102(B8), 18417–18441, 1997.
- 1368 Clow, G. D., Cuffey, K. M. and Waddington, E. D.: High heat-flow beneath the central portion of the West  
1369 Antarctic Ice Sheet, in *AGU Fall Meeting Abstracts.*, 2012.
- 1370 Courtney, R. C. and White, R. S.: Anomalous heat flow and geoid across the Cape Verde Rise: evidence for  
1371 dynamic support from a thermal plume in the mantle, *Geophysical Journal International*, 87(3), 815–867, 1986.
- 1372 Cuffey, K. M. and Paterson, W. S. B.: *The physics of glaciers*, 4th Edition., Elsevier, Oxford, UK., 2010.
- 1373 Cuffey, K. M., Clow, G. D., Alley, R. B., Stuiver, M., Waddington, E. D. and Saltus, R. W.: Large arctic  
1374 temperature change at the Wisconsin-Holocene glacial transition, *Science*, 270(5235), 455–458, 1995.
- 1375 Daczko, N. R., Halpin, J. A., Fitzsimons, I. C. and Whittaker, J. M.: A cryptic Gondwana-forming orogen located  
1376 in Antarctica, *Scientific reports*, 8(1), 8371, 2018.
- 1377 Dahl-Jensen, D., Morgan, V. I. and Elcheikh, A.: Monte Carlo inverse modelling of the Law Dome (Antarctica)  
1378 temperature profile, *Annals of Glaciology*, 29, 145–150, 1999.
- 1379 Dalby, C. J., Shail, R. K., Batchelor, A., Cotton, L., Gutmanis, J., Rollinson, G. K., Wall, F. and Hickey, J.: Deep  
1380 geothermal energy from the Cornubian Batholith: preliminary lithological and heat flow insights from the United  
1381 Downs Deep Geothermal Power Project, Plymouth, UK., 2020.
- 1382 Davis, E. E., Villinger, H., MacDonald, R. D., Meldrum, R. D. and Grigel, J.: A robust rapid-response probe for  
1383 measuring bottom-hole temperatures in deep-ocean boreholes, *Marine Geophysical Researches*, 19(3), 267–281,  
1384 1997.

- 1385 Decker, E. R.: Preliminary geothermal studies of the Dry Valley Drilling Project holes at McMurdo Station, Lake  
1386 Vanda, Lake Vida, and New Harbor, Antarctica, *Bulletin-Dry Valley Drilling Project (DVDP)*, 4, 22–23, 1974.
- 1387 Decker, E. R. and Bucher, G. J.: Geothermal studies in the Ross Island-Dry Valley region, *Antarct Geosci*, 4, 887–  
1388 894, 1982.
- 1389 Decker, E. R., Baker, K. H. and Harris, H.: Geothermal studies in the Dry Valleys and on Ross Island, *Antarctic  
1390 Journal*, 10(4), 176, 1975.
- 1391 Dymet, J. and Arkani-Hamed, J.: Equivalent source magnetic dipoles revisited, *Geophysical Research Letters*,  
1392 25(11), 2003–2006, 1998.
- 1393 Dziadek, R., Gohl, K., Diehl, A. and Kaul, N.: Geothermal heat flux in the Amundsen Sea sector of West  
1394 Antarctica: New insights from temperature measurements, depth to the bottom of the magnetic source estimation,  
1395 and thermal modeling, *Geochemistry, Geophysics, Geosystems*, 18(7), 2657–2672, 2017.
- 1396 Dziadek, R., Gohl, K. and Kaul, N.: Elevated geothermal surface heat flow in the Amundsen Sea Embayment,  
1397 West Antarctica, *Earth and Planetary Science Letters*, 506, 530–539, 2019.
- 1398 Ebbing, J., Lundin, E., Olesen, O. and Hansen, E. K.: The mid-Norwegian margin: a discussion of crustal  
1399 lineaments, mafic intrusions, and remnants of the Caledonian root by 3D density modelling and structural  
1400 interpretation, *Journal of the Geological Society*, 163(1), 47–59, 2006.
- 1401 Ebbing, J., Gernigon, L., Pascal, C., Olesen, O. and Osmundsen, P. T.: A discussion of structural and thermal  
1402 control of magnetic anomalies on the mid-Norwegian margin, *Geophysical Prospecting*, 57(4), 665–681, 2009.
- 1403 Elbeze, A. C.: On the existence of another source of heat production for the earth and planets, and its connection  
1404 with gravitomagnetism, *SpringerPlus*, 2(1), 1–13, doi:10.1186/2193-1801-2-513, 2013.
- 1405 Engelhardt, H.: Ice temperature and high geothermal flux at Siple Dome, West Antarctica, from borehole  
1406 measurements, *Journal of Glaciology*, 50(169), 251–256, 2004.
- 1407 Fahnestock, M., Abdalati, W., Joughin, I., Brozena, J. and Gogineni, P.: High geothermal heat flow, basal melt,  
1408 and the origin of rapid ice flow in central Greenland, *Science*, 294(5550), 2338–2342, 2001.
- 1409 Ferraccioli, F., Finn, C. A., Jordan, T. A., Bell, R. E., Anderson, L. M. and Damaske, D.: East Antarctic rifting  
1410 triggers uplift of the Gamburtsev Mountains, *Nature*, 479(7373), 388–392, 2011.
- 1411 Ferré, E. C., Friedman, S. A., Martín-Hernández, F., Feinberg, J. M., Conder, J. A. and Ionov, D. A.: The  
1412 magnetism of mantle xenoliths and potential implications for sub-Moho magnetic sources, *Geophysical Research  
1413 Letters*, 40(1), 105–110, 2013.
- 1414 Fischer, H., Severinghaus, J., Brook, E., Wolff, E., Albert, M., Alemany, O., Arthern, R., Bentley, C.,  
1415 Blankenship, D., Chappellaz, J. and others: Where to find 1.5 million yr old ice for the IPICS" Oldest-Ice" ice  
1416 core, *Climate of the Past*, 9(6), 2489–2505, 2013.
- 1417 Fisher, A. T. and Harris, R. N.: Using seafloor heat flow as a tracer to map subseafloor fluid flow in the ocean  
1418 crust, *Geofluids*, 10(1–2), 142–160, 2010.
- 1419 Fisher, A. T., Mankoff, K. D., Tulaczyk, S. M., Tyler, S. W., Foley, N. and others: High geothermal heat flux  
1420 measured below the West Antarctic Ice Sheet, *Science advances*, 1(6), e1500093, 2015.
- 1421 Flowerdew, M. J., Tyrrell, S., Boger, S. D., Fitzsimons, I. C. W., Harley, S. L., Mikhalsky, E. V. and Vaughan,  
1422 A. P. M.: Pb isotopic domains from the Indian Ocean sector of Antarctica: implications for past Antarctica–India  
1423 connections, *Geological Society, London, Special Publications*, 383(1), 59–72, 2013.
- 1424 Foster, T. D.: Temperature and salinity fields under the Ross Ice Shelf, *Antarctic Journal [of the United States]*,  
1425 13, 81–82, 1978.

- 1426 Fox Maule, C., Purucker, M. E., Olsen, N. and Mosegaard, K.: Heat flux anomalies in Antarctica revealed by  
1427 satellite magnetic data, *Science*, 309(5733), 464–467, 2005.
- 1428 Fricker, H. A., Scambos, T., Bindschadler, R. and Padman, L.: An active subglacial water system in West  
1429 Antarctica mapped from space, *Science*, 315(5818), 1544–1548, 2007.
- 1430 Frost, B. R. and Shive, P. N.: Magnetic mineralogy of the lower continental-crust, *Journal of Geophysical  
1431 Research-Solid Earth and Planets*, 91(B6), 6513–6521, 1986.
- 1432 Fudge, T. J., Biyani, S., Clemens-Sewall, D. and Hawley, B.: Constraining geothermal flux at coastal domes of  
1433 the Ross Ice Sheet, Antarctica, *Geophysical Research Letters*, 46(22), 13090–13098, 2019.
- 1434 Gard, M., Hasterok, D. and Halpin, J. A.: Global whole-rock geochemical database compilation, *Earth System  
1435 Science Data*, 11(4), 1553–1566, doi:<https://doi.org/10.5194/essd-2019-50>, 2019.
- 1436 Godey, S., Deschamps, F., Trampert, J. and Snieder, R.: Thermal and compositional anomalies beneath the North  
1437 American continent, *Journal of Geophysical Research: Solid Earth*, 109(B1), 2004.
- 1438 Goelzer, H., Robinson, A., Seroussi, H. and Van De Wal, R. S.: Recent progress in Greenland ice sheet modelling,  
1439 *Current climate change reports*, 3(4), 291–302, 2017.
- 1440 Gohl, K., Wellner, J. S., Klaus, A. and Expedition 379 Scientists: Expedition 379 Preliminary Report: Amundsen  
1441 Sea West Antarctic Ice Sheet History, *International Ocean Discovery Program*, 379,  
1442 doi:<https://doi.org/10.14379/iodp.pr.379.2019>, 2019.
- 1443 Golynsky, A., Chiappini, M., Damaske, D., Ferraccioli, F., Finn, C. A., Ishihara, T., Kim, H. R., Kovacs, L.,  
1444 Masolov, V. N., Morris, P. and others: ADMAP—a digital magnetic anomaly map of the Antarctic, in *Antarctica*,  
1445 pp. 109–116, Springer., 2006.
- 1446 Goodge, J. W.: Crustal heat production and estimate of terrestrial heat flow in central East Antarctica, with  
1447 implications for thermal input to the East Antarctic ice sheet., *Cryosphere*, 12, 491–504,  
1448 doi:<https://doi.org/10.5194/tc-12-491-2018>, 2018.
- 1449 Goodge, J. W. and Severinghaus, J. P.: Rapid Access Ice Drill: a new tool for exploration of the deep Antarctic  
1450 ice sheets and subglacial geology, *Journal of Glaciology*, 62(236), 1049–1064, 2016.
- 1451 Gow, A. J., Ueda, H. T. and Garfield, D. E.: Antarctic ice sheet: preliminary results of first core hole to bedrock,  
1452 *Science*, 161(3845), 1011–1013, 1968.
- 1453 Granot, R. and Dymment, J.: Late Cenozoic unification of East and West Antarctica, *Nature communications*, 9(1),  
1454 3189, 2018.
- 1455 Grauch, V. J. S.: Limitations on digital filtering of the DNAG magnetic data set for the conterminous US,  
1456 *Geophysics*, 58(9), 1281–1296, 1993.
- 1457 Greve, R. and Hutter, K.: Polythermal three-dimensional modelling of the Greenland ice sheet with varied  
1458 geothermal heat flux, *Annals of Glaciology*, 21(1), 8–12, 1995.
- 1459 Guimarães, S. N. P., Hamza, V. M. and Ravat, D.: Curie depths using combined analysis of centroid and matched  
1460 filtering methods in inferring thermomagnetic characteristics of Central Brazil, in *13th International Congress of  
1461 the Brazilian Geophysical Society & EXPOGEF, Rio de Janeiro, Brazil, 26–29 August 2013*, pp. 1853–1858,  
1462 Society of Exploration Geophysicists and Brazilian Geophysical Society., 2013.
- 1463 Gutenberg, B.: 6. Temperature and Thermal Processes in the Earth, in *International Geophysics*, vol. 1, edited by  
1464 B. Gutenberg, pp. 121–148, Academic Press Inc., New York., 1959.
- 1465 Haggerty, S. E.: Mineralogical constraints on Curie isotherms in deep crustal magnetic anomalies, *Geophysical  
1466 Research Letters*, 5(2), 105–108, 1978.

- 1467 Halpin, J. A. and Reading, A. M.: Report on Taking the Temperature of the Antarctic Continent (TACTical)  
1468 Workshop 21-23 March 2018, Hobart, Tasmania, Australia, Hobart, Australia., 2018.
- 1469 Halpin, J. A., Whittaker, J. M., Gard, M., Hasterok, D., Burton-Johnson, A., Staal, T., Maritati, A., Reading, A.  
1470 M., McLaren, S., Hand, M. and Raimondo, T.: Heterogenous Antarctic crustal heat production, Incheon, Republic  
1471 of Korea., 2019.
- 1472 Hasterok, D. and Chapman, D. S.: Continental thermal isostasy: 1. Methods and sensitivity, *Journal of*  
1473 *Geophysical Research: Solid Earth*, 112(B6), 2007a.
- 1474 Hasterok, D. and Chapman, D. S.: Continental thermal isostasy: 2. Application to North America, *Journal of*  
1475 *Geophysical Research: Solid Earth*, 112(B6), 2007b.
- 1476 Hasterok, D. and Chapman, D. S.: Heat production and geotherms for the continental lithosphere, *Earth and*  
1477 *Planetary Science Letters*, 307(1–2), 59–70, doi:10.1016/j.epsl.2011.04.034, 2011.
- 1478 Hasterok, D. and Gard, M.: Utilizing thermal isostasy to estimate sub-lithospheric heat flow and anomalous crustal  
1479 radioactivity, *Earth and Planetary Science Letters*, 450, 197–207, 2016.
- 1480 Hasterok, D., Gard, M., Halpin, J. A., Hand, M. P., Pollett, A., McLaren, S., Raimondo, T., Willcocks, S. and  
1481 Linke, M.: Constraining Geothermal Heat Flux Beneath Ice Sheets Using Thermal Isostasy, in AGU Fall Meeting  
1482 2019, AGU., 2019.
- 1483 Heesemann, M., Villinger, H., Fisher, A. T., Tréhu, A. M. and White, S.: Data report: testing and deployment of  
1484 the new APCT-3 tool to determine in situ temperatures while piston coring, in *Proceedings of the Integrated Ocean*  
1485 *Drilling Program*, 311, edited by M. Riedel, T. Collett, M. Malone, and the Expedition 311 Scientists, Integrated  
1486 Ocean Drilling Program Management International, Inc., Washington, DC., 2006.
- 1487 Hillenbrand, C.-D., Smith, J. A., Hodell, D. A., Greaves, M., Poole, C. R., Kender, S., Williams, M., Andersen,  
1488 T. J., Jernas, P. E. and Elderfield, H.: West Antarctic Ice Sheet retreat driven by Holocene warm water incursions,  
1489 *Nature*, 547(7661), 43, 2017.
- 1490 Hindmarsh, R. C. and Ritz, C. M.: How deep do you need to drill through ice to measure the geothermal heat  
1491 flux?, in *EGU General Assembly Conference Abstracts*, vol. 14, p. 8629., 2012.
- 1492 Hondoh, T., Shoji, H., Watanabe, O., Salamatin, A. N. and Lipenkov, V. Y.: Depth–age and temperature  
1493 prediction at Dome Fuji station, East Antarctica, *Annals of Glaciology*, 35, 384–390, 2002.
- 1494 Huang, Y., Chubakov, V., Mantovani, F., Rudnick, R. L. and McDonough, W. F.: A reference Earth model for  
1495 the heat-producing elements and associated geoneutrino flux, *Geochemistry, Geophysics, Geosystems*, 14(6),  
1496 2003–2029, 2013.
- 1497 Hughes, T.: Modeling ice sheets from the bottom up, *Quaternary Science Reviews*, 28(19–20), 1831–1849, 2009.
- 1498 Hyndman, R. D., Langseth, M. G. and Von Herzen, R. P.: Deep Sea Drilling Project geothermal measurements:  
1499 a review, *Reviews of geophysics*, 25(8), 1563–1582, 1987.
- 1500 Hyvönen, E., Turunen, P., Vanhanen, E., Arkimaa, H. and Sutinen, R.: Airborne gamma-ray surveys in Finland,  
1501 *Aerogeophysics in Finland*, 2004, 1972.
- 1502 Jaeger, J. C.: Numerical values for the temperature in radial heat flow, *Journal of Mathematics and Physics*, 34(1–  
1503 4), 316–321, 1956.
- 1504 Jaeger, J. C.: The effect of the drilling fluid on temperatures measured in bore holes, *Journal of Geophysical*  
1505 *Research*, 66(2), 563–569, 1961.
- 1506 Jaeger, J. C.: Application of the theory of heat conduction to geothermal measurements, *Terrestrial heat flow*, 8,  
1507 7–23, 1965.

- 1508 James, D. W.: The thermal diffusivity of ice and water between- 40 and+ 60° C, *Journal of Materials Science*,  
1509 3(5), 540–543, 1968.
- 1510 Jezek, K. C., Johnson, J. T., Drinkwater, M. R., Macelloni, G., Tsang, L., Aksoy, M. and Durand, M.: Radiometric  
1511 approach for estimating relative changes in intraglacier average temperature, *IEEE Transactions on Geoscience  
1512 and Remote Sensing*, 53(1), 134–143, 2014.
- 1513 Jordan, T., Martin, C., Ferraccioli, F., Matsuoka, K., Corr, H., Forsberg, R., Olesen, A. and Siegert, M. J.: Newly  
1514 discovered geothermal anomaly at South Pole ice divide; origins and implications, in *Geophysical Research  
1515 Abstracts*, vol. 20, p. 15511., 2018.
- 1516 Jordan, T. A., Riley, T. R. and Siddoway, C. S.: The geological history and evolution of West Antarctica, *Nature  
1517 Reviews Earth & Environment*, 1, 117–133, 2020.
- 1518 Kawakatsu, H. and Watada, S.: Seismic evidence for deep-water transportation in the mantle, *Science*, 316(5830),  
1519 1468–1471, 2007.
- 1520 Kerr, Y. H., Waldteufel, P., Wigneron, J.-P., Delwart, S., Cabot, F., Boutin, J., Escorihuela, M.-J., Font, J., Reul,  
1521 N. and Gruhier, C.: The SMOS mission: New tool for monitoring key elements of the global water cycle,  
1522 *Proceedings of the IEEE*, 98(5), 666–687, 2010.
- 1523 Kingslake, J., Scherer, R. P., Albrecht, T., Coenen, J., Powell, R. D., Reese, R., Stansell, N. D., Tulaczyk, S.,  
1524 Wearing, M. G. and Whitehouse, P. L.: Extensive retreat and re-advance of the West Antarctic Ice Sheet during  
1525 the Holocene, *Nature*, 558(7710), 430–434, 2018.
- 1526 Korenaga, J.: Earth's heat budget: Clairvoyant geoneutrinos, *Nature Geoscience*, 4(9), 581, 2011.
- 1527 Kuchar, J. and Milne, G. A.: The influence of viscosity structure in the lithosphere on predictions from models of  
1528 glacial isostatic adjustment, *Journal of Geodynamics*, 86, 1–9, 2015.
- 1529 Lachenbruch, A. H.: Preliminary geothermal model of the Sierra Nevada, *Journal of Geophysical Research*,  
1530 73(22), 6977–6989, 1968.
- 1531 Lachenbruch, A. H.: Crustal temperature and heat production: Implications of the linear heat-flow relation, *Journal  
1532 of Geophysical Research*, 75(17), 3291–3300, 1970.
- 1533 Lachenbruch, A. H. and Brewer, M. C.: Dissipation of the temperature effect of drilling a well in Arctic Alaska,  
1534 *United States Geological Survey Bulletin*, 1083-C, 73–109, 1959.
- 1535 Langel, R. A. and Hinze, W. J.: *The magnetic field of the Earth's lithosphere: The satellite perspective*, Cambridge  
1536 University Press, Cambridge, UK., 1998.
- 1537 Larour, E., Morlighem, M., Seroussi, H., Schiermeier, J. and Rignot, E.: Ice flow sensitivity to geothermal heat  
1538 flux of Pine Island Glacier, Antarctica, *Journal of Geophysical Research: Earth Surface*, 117(F4), 2012.
- 1539 Leat, P. T., Jordan, T. A., Flowerdew, M. J., Riley, T. R., Ferraccioli, F. and Whitehouse, M. J.: Jurassic high heat  
1540 production granites associated with the Weddell Sea rift system, Antarctica, *Tectonophysics*, 722, 249–264, 2018.
- 1541 Lees, C. H.: On the shapes of the isotherms under mountain ranges in radio-active districts, *Proceedings of the  
1542 Royal Society of London. Series A, Containing Papers of a Mathematical and Physical Character*, 83(563), 339–  
1543 346, 1910.
- 1544 Li, C.-F., Lu, Y. and Wang, J.: A global reference model of Curie-point depths based on EMAG2, *Scientific  
1545 reports*, 7, 45129, 2017.
- 1546 Llubes, M., Lanseau, C. and Rémy, F.: Relations between basal condition, subglacial hydrological networks and  
1547 geothermal flux in Antarctica, *Earth and Planetary Science Letters*, 241(3), 655–662, 2006.
- 1548 Lowrie, W.: *Fundamentals of geophysics*, 2nd ed., Cambridge University Press, Cambridge., 2007.

- 1549 Lucazeau, F.: Analysis and mapping of an updated terrestrial heat flow dataset, *Geochemistry, Geophysics, Geosystems*, 20(8), 4001–4024, 2019.  
1550
- 1551 Macelloni, G., Leduc-Leballeur, M., Brogioni, M., Ritz, C. and Picard, G.: Analyzing and modeling the SMOS spatial variations in the East Antarctic Plateau, *Remote sensing of environment*, 180, 193–204, 2016.  
1552
- 1553 Macelloni, G., Leduc-Leballeur, M., Montomoli, F., Brogioni, M., Ritz, C. and Picard, G.: On the retrieval of internal temperature of Antarctica Ice Sheet by using SMOS observations, *Remote Sensing of Environment*, 233, 111405, 2019.  
1554  
1555
- 1556 Mareschal, J. C. and Jaupart, C.: Radiogenic heat production, thermal regime and evolution of continental crust, *Tectonophysics*, 609, 524–534, doi:10.1016/j.tecto.2012.12.001, 2013.  
1557
- 1558 Martin, A. P. and van der Wal, W., Eds.: *The Antarctic Mantle*, The Geological Society, London, UK., in prep.
- 1559 Martin, A. P., Cooper, A. F. and Price, R. C.: Increased mantle heat flow with on-going rifting of the West Antarctic rift system inferred from characterisation of plagioclase peridotite in the shallow Antarctic mantle, *Lithos*, 190, 173–190, 2014.  
1560  
1561
- 1562 Martos, Y. M., Catalán, M., Jordan, T. A., Golynsky, A., Golynsky, D., Eagles, G. and Vaughan, D. G.: Heat flux distribution of Antarctica unveiled, *Geophysical Research Letters*, 44(22), 11–417, 2017.  
1563
- 1564 Martos, Y. M., Jordan, T. A., Catalán, M., Jordan, T. M., Bamber, J. L. and Vaughan, D. G.: Geothermal heat flux reveals the Iceland hotspot track underneath Greenland, *Geophysical Research Letters*, 45(16), 8214–8222, 2018.  
1565
- 1566 Maus, S.: Magnetic field model MF7. Retrieved August 28, 2018, from [www.geomag.us/models/MF7.html](http://www.geomag.us/models/MF7.html), 2010.  
1567
- 1568 Mayhew, M. A.: Inversion of satellite magnetic anomaly data, *Journal of Geophysics*, 45(1), 119–128, 1979.
- 1569 McDonough, W. F. and Sun, S. s.: The composition of the Earth, *Chemical Geology*, 120(3–4), 223–253, doi:10.1016/0009-2541(94)00140-4, 1995.  
1570
- 1571 McKay, R., De Santis, L., Kulhanek, D. K. and Expedition 374 Scientists: International Ocean Discovery Program Expedition 374 Preliminary Report: Ross Sea West Antarctic Ice Sheet History, International Ocean Discovery Program, 374, doi:<https://doi.org/10.14379/iodp.pr.374.2018>, 2018.  
1572  
1573
- 1574 McKenzie, D., Jackson, J. and Priestley, K.: Thermal structure of oceanic and continental lithosphere, *Earth and Planetary Science Letters*, 233(3–4), 337–349, 2005.  
1575
- 1576 Morgan, J. P., Rüpke, L. H. and White, W. M.: The Current Energetics of Earth’s Interior: A Gravitational Energy Perspective, *Frontiers in Earth Science*, 4(May), 1–28, doi:10.3389/feart.2016.00046, 2016.  
1577
- 1578 Morin, R. H., Williams, T., Henrys, S. A., Magens, D., Niessen, F. and Hansraj, D.: Heat flow and hydrologic characteristics at the AND-1B borehole, ANDRILL McMurdo Ice Shelf Project, Antarctica, *Geosphere*, 6(4), 370–378, 2010.  
1579  
1580
- 1581 Mulder, J. A., Halpin, J. A., Daczko, N. R., Orth, K., Meffre, S., Thompson, J. M. and Morrissey, L. J.: A Multiproxy provenance approach to uncovering the assembly of East Gondwana in Antarctica, *Geology*, 47(7), 645–649, 2019.  
1582  
1583
- 1584 Müller, C., Usbeck, R. and Miesner, F.: Temperatures in shallow marine sediments: Influence of thermal properties, seasonal forcing, and man-made heat sources, *Applied Thermal Engineering*, 108, 20–29, 2016.  
1585
- 1586 Mulvaney, R., Abram, N. J., Hindmarsh, R. C., Arrowsmith, C., Fleet, L., Triest, J., Sime, L. C., Alemany, O. and Foord, S.: Recent Antarctic Peninsula warming relative to Holocene climate and ice-shelf history, *Nature*, 489(7414), 141–144, 2012.  
1587  
1588

- 1589 Mulvaney, R., Martin, C., Massam, A., Rix, J. and Ritz, C.: Estimating geothermal heat flux from ice sheet  
1590 borehole temperature measurements, in XIII International Symposium on Antarctic Earth Sciences, Incheon,  
1591 Republic of Korea., 2019.
- 1592 Nicholls, K. W. and Paren, J. G.: Extending the Antarctic meteorological record using ice-sheet temperature  
1593 profiles, *Journal of climate*, 6(1), 141–150, 1993.
- 1594 Obande, G. E., Lawal, K. M. and Ahmed, L. A.: Spectral analysis of aeromagnetic data for geothermal  
1595 investigation of Wikki Warm Spring, north-east Nigeria, *Geothermics*, 50, 85–90, 2014.
- 1596 Okubo, Y., Graf, R. J., Hansen, R. O., Ogawa, K. and Tsu, H.: Curie point depths of the island of Kyushu and  
1597 surrounding areas, Japan, *Geophysics*, 50(3), 481–494, 1985.
- 1598 Olesen, O., Balling, N., Barrère, C., Breiner, N., Davidsen, B., Ebbing, J., Elvebakk, H., Gernigon, L., Koziel, J.,  
1599 Lutro, O. and others: KONTIKI final report, continental crust and heat generation in 3D, NGU Report, 42, 2007.
- 1600 Pappa, F., Ebbing, J., Ferraccioli, F. and van der Wal, W.: Modeling satellite gravity gradient data to derive  
1601 density, temperature, and viscosity structure of the Antarctic lithosphere, *Journal of Geophysical Research: Solid  
1602 Earth*, 124, 12053–12076, 2019a.
- 1603 Pappa, F., Ebbing, J. and Ferraccioli, F.: Moho Depths of Antarctica: Comparison of Seismic, Gravity, and  
1604 Isostatic Results, *Geochemistry, Geophysics, Geosystems*, 20(3), 1629–1645, 2019b.
- 1605 Passalacqua, O., Ritz, C., Parrenin, F., Urbini, S. and Frezzotti, M.: Geothermal flux and basal melt rate in the  
1606 Dome C region inferred from radar reflectivity and heat modelling, *The Cryosphere*, 11, 2231–2246,  
1607 doi:<https://doi.org/10.5194/tc-11-2231-2017>, 2017.
- 1608 Passalacqua, O., Picard, G., Ritz, C., Leduc-Leballeur, M., Quiquet, A., Larue, F. and Macelloni, G.: Retrieval of  
1609 the Absorption Coefficient of L-Band Radiation in Antarctica From SMOS Observations, *Remote Sensing*,  
1610 10(12), 1954, 2018.
- 1611 Paterson, W. S. B.: *The physics of glaciers*, Third Edition., Elsevier, Oxford, UK., 1994.
- 1612 Pattyn, F.: Antarctic subglacial conditions inferred from a hybrid ice sheet/ice stream model, *Earth and Planetary  
1613 Science Letters*, 295(3), 451–461, 2010.
- 1614 Pfender, M. and Villinger, H.: Miniaturized data loggers for deep sea sediment temperature gradient  
1615 measurements, *Marine Geology*, 186(3–4), 557–570, 2002.
- 1616 Phaneuf, C. and Mareschal, J.-C.: Estimating concentrations of heat producing elements in the crust near the  
1617 Sudbury Neutrino Observatory, Ontario, Canada, *Tectonophysics*, 622, 135–144, 2014.
- 1618 Pittard, M. L., Galton-Fenzi, B. K., Roberts, J. L. and Watson, C. S.: Organization of ice flow by localized regions  
1619 of elevated geothermal heat flux, *Geophysical Research Letters*, 43(7), 3342–3350, 2016a.
- 1620 Pittard, M. L., Roberts, J. L., Galton-Fenzi, B. K. and Watson, C. S.: Sensitivity of the Lambert-Amery glacial  
1621 system to geothermal heat flux, *Annals of Glaciology*, 57(73), 56–68, 2016b.
- 1622 Pollack, H. N. and Chapman, D. S.: Mantle heat flow, *Earth and Planetary Science Letters*, 34(2), 174–184, 1977.
- 1623 Pollack, H. N., Hurter, S. J. and Johnson, J. R.: Heat flow from the Earth's interior: Analysis of the global data  
1624 set, *Reviews of Geophysics*, 31(3), 267–280, doi:[10.1029/93RG01249](https://doi.org/10.1029/93RG01249), 1993.
- 1625 Pollard, D., DeConto, R. M. and Nyblade, A. A.: Sensitivity of Cenozoic Antarctic ice sheet variations to  
1626 geothermal heat flux, *Global and Planetary Change*, 49(1), 63–74, 2005.
- 1627 Pollett, A., Hasterok, D., Raimondo, T., Halpin, J. A., Hand, M., Bendall, B. and McLaren, S.: Heat flow in  
1628 southern Australia and connections with East Antarctica, *Geochemistry, Geophysics, Geosystems*, 20(11), 5352–  
1629 5370, 2019.



- 1630 Popov, Y. A., Pevzner, S. L., Pimenov, V. P. and Romushkevich, R. A.: New geothermal data from the Kola  
1631 superdeep well SG-3, *Tectonophysics*, 306(3–4), 345–366, 1999.
- 1632 Price, P. B., Nagornov, O. V., Bay, R., Chirkin, D., He, Y., Miocinovic, P., Richards, A., Woschnagg, K., Koci,  
1633 B. and Zagorodnov, V.: Temperature profile for glacial ice at the South Pole: Implications for life in a nearby  
1634 subglacial lake, *Proceedings of the National Academy of Sciences*, 99(12), 7844–7847, 2002.
- 1635 Pruss, E. F., Decker, E. R. and Smithson, S. B.: Preliminary temperature-measurements at DVDP holes 3, 4, 6,  
1636 and 8, *Antarctic Journal of the United States*, 9(4), 133–134, 1974.
- 1637 Purucker, M.: Geothermal heat flux data set based on low resolution observations collected by the CHAMP  
1638 satellite between 2000 and 2010, and produced from the MF-6 model following the technique described in Fox  
1639 Maule et al. (2005), available at: [http://webserv.cs.umt.edu/isis/images/c/c8/Antarctica\\_heat\\_flux\\_5km.nc](http://webserv.cs.umt.edu/isis/images/c/c8/Antarctica_heat_flux_5km.nc), 2012.
- 1640 Purucker, M. and Whaler, K.: Crustal magnetism, edited by M. Kono, *Treatise on Geophysics*, 5, 195–237, 2007.
- 1641 Ravat, D., Pignatelli, A., Nicolosi, I. and Chiappini, M.: A study of spectral methods of estimating the depth to  
1642 the bottom of magnetic sources from near-surface magnetic anomaly data, *Geophysical Journal International*,  
1643 169(2), 421–434, 2007.
- 1644 Rémy, F. and Legresy, B.: Subglacial hydrological networks in Antarctica and their impact on ice flow, *Annals  
1645 of Glaciology*, 39, 67–72, 2004.
- 1646 Rezvanbehbahani, S., Stearns, L. A., Kadivar, A., Walker, J. D. and van der Veen, C. J.: Predicting the geothermal  
1647 heat flux in Greenland: A machine learning approach, *Geophysical Research Letters*, 44(24), 12–271, 2017.
- 1648 Risk, G. F. and Hochstein, M. P.: Heat flow at arrival heights, Ross Island, Antarctica, *New Zealand Journal of  
1649 Geology and Geophysics*, 17(3), 629–644, 1974.
- 1650 Ritz, C.: Time dependent boundary conditions for calculation of temperature fields in ice sheets, in *The Physical  
1651 Basis of Ice Sheet Modelling (Proceedings of the Vancouver Symposium, August 1987)*, vol. IAHS Publ. no. 170,  
1652 pp. 207–216, Vancouver, Canada., 1987.
- 1653 Ritz, C.: Interpretation of the temperature profile measured at Vostok, East Antarctica, *Annals of glaciology*, 12,  
1654 138–144, 1989.
- 1655 Rix, J., Mulvaney, R., Hong, J. and Ashurst, D.: Development of the British Antarctic Survey Rapid Access  
1656 Isotope Drill, *Journal of Glaciology*, 65(250), 288–298, 2019.
- 1657 Rogozhina, I., Hagedoorn, J. M., Martinec, Z., Fleming, K., Soucek, O., Greve, R. and Thomas, M.: Effects of  
1658 uncertainties in the geothermal heat flux distribution on the Greenland Ice Sheet: An assessment of existing heat  
1659 flow models, *Journal of Geophysical Research: Earth Surface*, 117, F02025, doi:doi:10.1029/2011JF002098,  
1660 2012.
- 1661 Ross, H. E., Blakely, R. J. and Zoback, M. D.: Testing the use of aeromagnetic data for the determination of Curie  
1662 depth in California, *Geophysics*, 71(5), L51–L59, 2006.
- 1663 Roy, R. F., Blackwell, D. D. and Birch, F.: Heat generation of plutonic rocks and continental heat flow provinces,  
1664 *Earth and Planetary Science Letters*, 5, 1–12, 1968.
- 1665 Rudnick, R. and Fountain, D.: Nature and composition of the continental crust: a lower crustal perspective,  
1666 *Reviews of Geophysics*, (95), 267–309, 1995.
- 1667 Rudnick, R. L., McDonough, W. F. and O’Connell, R. J.: Thermal structure, thickness and composition of  
1668 continental lithosphere, *Chemical Geology*, 145(3–4), 395–411, 1998.
- 1669 Rybach, L.: Amount and significance of radioactive heat sources in sediments, *Collection colloques seminaires*,  
1670 44, 311–322, 1986.

- 1671 Salamatin, A. N., Lipenkov, V. Y., Barkov, N. I., Jouzel, J., Petit, J. R. and Raynaud, D.: Ice core age dating and  
1672 paleothermometer calibration based on isotope and temperature profiles from deep boreholes at Vostok Station  
1673 (East Antarctica), *Journal of Geophysical Research: Atmospheres*, 103(D8), 8963–8977, 1998.
- 1674 Salem, A., Green, C., Ravat, D., Singh, K. H., East, P., Fairhead, J. D., Mogren, S. and Biegert, E.: Depth to Curie  
1675 temperature across the central Red Sea from magnetic data using the de-fractal method, *Tectonophysics*, 624, 75–  
1676 86, 2014.
- 1677 Sandiford, M. and Hand, M.: Controls on the locus of intraplate deformation in central Australia, *Earth and  
1678 Planetary Science Letters*, 162(1–4), 97–110, 1998.
- 1679 Sandiford, M. and McLaren, S.: Tectonic feedback and the ordering of heat producing elements within the  
1680 continental lithosphere, *Earth and Planetary Science Letters*, 204(1), 133–150, 2002.
- 1681 Schroeder, D. M., Blankenship, D. D., Young, D. A. and Quartini, E.: Evidence for elevated and spatially variable  
1682 geothermal flux beneath the West Antarctic Ice Sheet, *Proceedings of the National Academy of Sciences*, 111(25),  
1683 9070–9072, 2014.
- 1684 Sclater, J., Jaupart, C. and Galson, D.: The heat flow through oceanic and continental crust and the heat loss of  
1685 the Earth, *Reviews of Geophysics*, 18(1), 269–311, 1980.
- 1686 Shapiro, N. M. and Ritzwoller, M. H.: Monte-Carlo inversion for a global shear-velocity model of the crust and  
1687 upper mantle, *Geophysical Journal International*, 151(1), 88–105, 2002.
- 1688 Shapiro, N. M. and Ritzwoller, M. H.: Inferring surface heat flux distributions guided by a global seismic model:  
1689 particular application to Antarctica, *Earth and Planetary Science Letters*, 223(1), 213–224, 2004.
- 1690 Shen, W., Wiens, D., Lloyd, A. and Nyblade, A.: A Geothermal heat flux map of Antarctica empirically  
1691 constrained by seismic structure, *Geophysical Research Letters*, e2020GL086955, 2020.
- 1692 Siddoway, C. S.: Tectonics of the West Antarctic Rift System: new light on the history and dynamics of distributed  
1693 intracontinental extension, *Antarctica: A Keystone in a Changing World*, 91–114, 2008.
- 1694 Siegert, M. J.: Antarctic subglacial lakes, *Earth-Science Reviews*, 50(1), 29–50, 2000.
- 1695 Siegert, M. J. and Dowdeswell, J. A.: Spatial variations in heat at the base of the Antarctic ice sheet from analysis  
1696 of the thermal regime above subglacial lakes, *Journal of Glaciology*, 42(142), 501–509, 1996.
- 1697 Slagstad, T.: Radiogenic heat production of Archaean to Permian geological provinces in Norway., *Norwegian  
1698 Journal of Geology/Norsk Geologisk Forening*, 88(3), 2008.
- 1699 Spector, A. and Grant, F. S.: Statistical models for interpreting aeromagnetic data, *Geophysics*, 35(2), 293–302,  
1700 1970.
- 1701 Stein, C. A. and Stein, S.: A model for the global variation in oceanic depth and heat flow with lithospheric age,  
1702 *Nature*, 359(6391), 123, 1992.
- 1703 Stein, C. A. and Stein, S.: Mantle plumes: heat-flow near Iceland, *Astronomy & Geophysics*, 44(1), 1–8, 2003.
- 1704 Suárez, F., Dozier, J., Selker, J. S., Hausner, M. B. and Tyler, S. W.: Heat transfer in the environment:  
1705 development and use of fiber-optic distributed temperature sensing, *INTECH Open Access Publisher Rijeka*,  
1706 2011.
- 1707 Swanberg, C. A.: Vertical distribution of heat generation in the Idaho batholith, *Journal of Geophysical Research*,  
1708 77(14), 2508–2513, 1972.
- 1709 Talalay, P. G. and Pyne, A. R.: Geological drilling in McMurdo Dry Valleys and McMurdo Sound, Antarctica:  
1710 Historical development, *Cold Regions Science and Technology*, 141, 131–162, 2017.

- 1711 Tanaka, A., Okubo, Y. and Matsubayashi, O.: Curie point depth based on spectrum analysis of the magnetic  
1712 anomaly data in East and Southeast Asia, *Tectonophysics*, 306(3–4), 461–470, 1999.
- 1713 Taylor, S. R. and McLennan, S. M.: *The continental crust: its composition and evolution*, Blackwell Publishing,  
1714 Oxford, UK., 1985.
- 1715 Trifonova, P., Zhelev, Z., Petrova, T. and Bojadgieva, K.: Curie point depths of Bulgarian territory inferred from  
1716 geomagnetic observations and its correlation with regional thermal structure and seismicity, *Tectonophysics*,  
1717 473(3–4), 362–374, 2009.
- 1718 Turcotte, D. L. and Schubert, G.: *Geodynamics*, Cambridge University Press, Cambridge, UK., 2014.
- 1719 Ukil, A., Braendle, H. and Krippner, P.: Distributed temperature sensing: review of technology and applications,  
1720 *IEEE Sensors Journal*, 12(5), 885–892, 2011.
- 1721 Van Liefveringe, B. and Pattyn, F.: Using ice-flow models to evaluate potential sites of million year-old ice in  
1722 Antarctica, *Climate of the Past*, 9(5), 2335–2345, 2013.
- 1723 Van Liefveringe, B., Pattyn, F., Cavitte, M. G., Karlsson, N. B., Young, D. A., Sutter, J. and Eisen, O.: Promising  
1724 Oldest Ice sites in East Antarctica based on thermodynamical modelling, *The Cryosphere*, 12(8), 2773–2787,  
1725 2018.
- 1726 Veikkolainen, T. and Kukkonen, I. T.: Highly varying radiogenic heat production in Finland, Fennoscandian  
1727 Shield, *Tectonophysics*, 750, 93–116, 2019.
- 1728 Viel, G.-M. L., Martin, C., Hindmarsh, R. C. A. and Lüthi, M. P.: Basal freeze-on generates complex ice-sheet  
1729 stratigraphy, *Nature communications*, 9(1), 1–13, 2018.
- 1730 Vitorello, I. and Pollack, H. N.: On the variation of continental heat flow with age and the thermal evolution of  
1731 continents, *Journal of Geophysical Research: Solid Earth*, 85(B2), 983–995, 1980.
- 1732 Vosteen, H.-D. and Schellschmidt, R.: Influence of temperature on thermal conductivity, thermal capacity and  
1733 thermal diffusivity for different types of rock, *Physics and Chemistry of the Earth, Parts A/B/C*, 28(9–11), 499–  
1734 509, 2003.
- 1735 van der Wal, W., Barnhoorn, A., Stocchi, P., Gradmann, S., Wu, P., Drury, M. and Vermeersen, B.: Glacial  
1736 isostatic adjustment model with composite 3-D Earth rheology for Fennoscandia, *Geophysical Journal  
1737 International*, 194(1), 61–77, 2013.
- 1738 van der Wal, W., Whitehouse, P. L. and Schrama, E. J.: Effect of GIA models with 3D composite mantle viscosity  
1739 on GRACE mass balance estimates for Antarctica, *Earth and Planetary Science Letters*, 414, 134–143, 2015.
- 1740 Wangen, M.: *Physical principles of sedimentary basin analysis*, Cambridge University Press, Cambridge, UK.,  
1741 2010.
- 1742 Wasilewski, P. J. and Mayhew, M. A.: The Moho as a magnetic boundary revisited, *Geophysical Research Letters*,  
1743 19(22), 2259–2262, 1992.
- 1744 Winsborrow, M. C., Clark, C. D. and Stokes, C. R.: What controls the location of ice streams?, *Earth-Science  
1745 Reviews*, 103(1), 45–59, 2010.
- 1746 Wright, A. and Siegert, M.: A fourth inventory of Antarctic subglacial lakes, *Antarctic Science*, 24(6), 659–664,  
1747 2012.
- 1748 Zagorodnov, V., Nagornov, O., Scambos, T. A., Muto, A., Mosley-Thompson, E., Pettit, E. C. and Tyufin, S.:  
1749 Borehole temperatures reveal details of 20th century warming at Bruce Plateau, Antarctic Peninsula, *The  
1750 Cryosphere*, 6(3), 675–686, 2012.

1751